JET

Journal of ENERGY TECHNOLOGY

University of Maribor Press

VOLUME 19
NUMBER 1
JULY 2026

JET

Editor-in-chief Jurij Avsec
(University of Maribor, Slovenia)

Co-editors Amor Chowdhury
(University of Maribor, Slovenia)

Brigita Ferčec
(University of Maribor, Slovenia)

Matej Fike
(University of Maribor, Slovenia)

Miralem Hadžiselimović
(University of Maribor, Slovenia)

Gorazd Hren
(University of Maribor, Slovenia)

Zdravko Praunseis
(University of Maribor, Slovenia)

Sebastijan Seme
(University of Maribor, Slovenia)

Bojan Štumberger
(University of Maribor, Slovenia)

Peter Virtič
(University of Maribor, Slovenia)

Technical editors Jan Perša
(University of Maribor, University of Maribor Press, Slovenia)

Sonja Krajnc
(University of Maribor, Slovenia)

Lecturer in english Shelagh Margaret Hedges

Founding editor Andrej Predin
(University of Maribor, Slovenia)

Cover designer Jan Perša
(University of Maribor, University of Maribor Press, Slovenia)

Cover graphics Photo: Jurij Avsec, 2026

Graphics material Sources are own unless otherwise noted.

Publication type E-publication

EDITORIAL BOARD

Antun Barac (University of Slavonski Brod, Croatia) • Miloš Bekovič (University of Maribor, Slovenia) • Anton Bergant (Litostroj Power d.d., Slovenia) • Marinko Barukčić (Josip Juraj Strossmayer University of Osijek, Croatia) • Goga Cvetkovski (Ss. Cyril and Methodius University in Skopje, Macedonia) • Nenad Cvetković (University of Nis, Serbia) • Damir Dović (University of Zagreb, Croatia) • Željko Hederić (Josip Juraj Strossmayer University of Osijek, Croatia) • Dalibor Igrec (Margento R&D d.o.o., Slovenia) • Marko Jesenik (University of Maribor, Slovenia) • Eva Klemenčič (University of Maribor, Slovenia) • Ivan Aleksander Kodeli (Jožef Stefan Institute, Slovenia) • Ankica Kovač (University of Zagreb, Croatia) • Marjan Kromar (Jožef Stefan Institute, Slovenia) • Igor Medved

(Slovak University of Technology in Bratislava, Slovakia) • Matej Mencinger (University of Maribor, Slovenia) • Franjo Pranjić (University of Maribor, Slovenia) • Anita Praprotnik Brdnik (University of Maribor, Slovenia) • Dušan Strušnik (Energetika Ljubljana d.o.o., Slovenia) • Klemen Sredenšek (University of Maribor, Slovenia) • Urška Lavrenčič Štangar (University of Ljubljana, Slovenia) • Gorazd Štumberger (University of Maribor, Slovenia) • Anton Trnik (Constantine the Philosopher University in Nitra, Slovakia) • Mykhailo Zagirnyak (Kremenchuk Mykhailo Ostrohradskyi National University, Ukraine) • Marija Živić (University of Slavonski Brod, Croatia)

EDITORIAL OFFICE ADDRESS
University of Maribor
Faculty of Energy Technology
Hočevarjev trg 1, 8270 Krško, Slovenia
Koroška cesta 62a, 3320 Velenje, Slovenia
e-mail: jet@um.si
https://www.fe.um.si

PUBLISHED BY
University of Maribor
University of Maribor Press
Slomškov trg 15, 2000 Maribor, Slovenia
e-mail: zalozba@um.si, zalozba.journals@um.si
https://press.um.si/, https://journals.um.si

University of Maribor

Faculty of Energy Technology

ISSN 1855-5748 (printed)
ISSN 2463-7815 (electronic)

The **Journal of Energy Technology** is a peer-reviewed journal published by University of Maribor Press and issued by University of Maribor, Faculty of Energy Technology (Slovenia). The journal is indexed and abstracted in databases INSPEC©, EBSCO and Proquest. For more information, please visit our website at https://journals.um.si/index.php/jet

© University of Maribor, University Press
/ *Univerza v Mariboru, Univerzitetna založba*

Text © Authors, 2026

This journal is licensed under the Creative Commons Attribution 4.0 International License.

This license allows reusers to distribute, remix, adapt, and build upon the material in any medium or format, so long as attribution is given to the creator. The license allows for commercial use.

Any third-party material in this journal is published under the book's Creative Commons licence unless indicated otherwise in the credit line to the material. If you would like to reuse any third-party material not covered by the journals's Creative Commons licence, you will need to obtain permission directly from the copyright holder.

https://creativecommons.org/licenses/by/4.0

Journal of Energy Technology is co-funded by Slovenian Research and Innovation Agency

Journal of Energy Technology

Volume 18 Number 1 July 2026

ARTICLES

JOURNAL OF ENERGY TECHNOLOGY
Vol. 19, No. 1, July 2026

Dear Readers of the Journal of Energy Technology (JET)

JURIJ AVSEC
Editor-in-chief of JET

Hybrid Energy Storage Systems (HESS) are becoming one of the key technologies of modern power systems, as they enable the efficient integration of renewable energy sources, enhance the reliability of electricity supply, and increase the flexibility of power grids. Their principal advantage lies in combining different energy storage technologies, Driven by the rapid expansion of renewable energy sources and the global transition toward low-carbon energy systems, hybrid energy storage systems are increasingly being developed and deployed across Europe, the United States, China, and many other regions of the world, where they represent an essential building block of future smart and sustainable energy systems. Among their most important applications are the integration of renewable energy sources, power system stabilization, peak shaving, microgrids, industrial energy management, and the provision of backup power for critical infrastructure.

Hydrogen and methanol technologies are also becoming an important component of modern hybrid energy storage systems, enabling the long-term storage of surplus electrical energy through its conversion into chemical energy. Hydrogen produced by water electrolysis can be used directly in fuel cells or as a feedstock for methanol synthesis. Owing to its easier storage, transportation, and compatibility with existing fuel infrastructure, methanol represents a promising energy carrier for sectors where direct electrification remains technically or economically challenging.

Heat pumps are playing an increasingly important role in the global energy sector. According to the latest available estimates, they have become one of the fastest-growing heating technologies worldwide. However, the vast majority are still installed in residential and commercial buildings, while their use in industrial applications remains significantly less widespread. It is estimated that nearly 400 million heat pumps are currently in operation worldwide, of which approximately 28 million are installed in Europe.

Most heat pumps are used for domestic hot water production, space heating, and cooling. At the same time, the application of heat pumps in industry is attracting growing interest. Industrial processes predominantly require high-temperature heat pumps, which are increasingly being adopted to provide process heat, improve energy efficiency, and reduce greenhouse gas emissions.

The current issue of the journal presents several interesting contributions related to these topics, offering insights into recent advances and future perspectives in hybrid energy storage technologies. I wish you an enjoyable and inspiring reading experience reading this issue.

Spoštovani bralci revije Journal of Energy Technology (JET)

Hibridni sistemi za shranjevanje energije (HESS) postajajo ena izmed ključnih tehnologij sodobnega elektroenergetskega sistema, saj omogočajo učinkovito vključevanje obnovljivih virov energije, večjo zanesljivost oskrbe in večjo prilagodljivost elektroenergetskega omrežja. Njihova osnovna prednost je združevanje različnih tehnologij shranjevanja energije. Zaradi hitrega razvoja obnovljivih virov in potrebe po razogljičenju energetike se hibridni sistemi za shranjevanje energije vse pogosteje razvijajo in uvajajo v Evropi, ZDA, na Kitajskem in drugih delih sveta, kjer predstavljajo pomemben gradnik prihodnjih nizkoogljičnih in pametnih energetskih sistemov. Med najpomembnejšimi primeri uporabe so: integracija obnovljivih virov energije, stabilizacija elektroenergetskega omrežja in pokrivanje koničnih obremenitev.

Pomemben del sodobnih hibridnih sistemov za shranjevanje energije predstavljajo tudi vodikove in metanolove tehnologije, ki omogočajo dolgoročno shranjevanje presežkov električne energije s pretvorbo v kemijsko energijo. Vodik, proizveden z elektrolizo, se lahko neposredno uporabi v gorivnih celicah ali kot surovina za sintezo metanola, ki zaradi enostavnejšega skladiščenja, transporta in obstoječe infrastrukture predstavlja obetaven energent za sektorje, kjer je neposredna elektrifikacija otežena.

Tudi toplotne črpalke imajo vedno večji pomen v svetovni energetiki. Po zadnjih razpoložljivih ocenah so toplotne črpalke postale ena najhitreje rastočih tehnologij za ogrevanje, vendar je velika večina še vedno namenjena stavbam (stanovanjskim in poslovnim), medtem ko je industrijska uporaba bistveno manj razširjena. Po ocenah je v svetu v uporabi blizu 400 milijonov toplotnih črpalk, v Evropi pa približno 28 milijonov. Večina toplotnih črpalk se uporablja za ogrevanje sanitarne vode, ogrevanje prostorov in hlajenje. Vedno bolj zanimiva pa je uporaba toplotnih črpalk tudi v industriji, kjer se večinoma uporabljajo visokotemperaturne toplotne črpalke. Na ta način se lahko zmanjša ogljični odtis in hkrati poveča učinkovitost energetskih naprav.

Nekaj zanimivih informacij, povezanih s predstavljenimi tematikami, lahko najdemo v tej številki revije. Želim vam zanimivo branje.

JOURNAL OF ENERGY TECHNOLOGY
Vol. 19, No. 1, pp. 5–30, July 2026

Original Scientific Article

RESULTS OF THE HESS PROJECT – HYBRID ENERGY STORAGE SYSTEM IN POST-MINING INFRASTRUCTURE

SERGEJ JAMNIKAR,[1] AGATA CZARDYBON,[2] PIOTR MATUSIAK,[3] DANIEL KOWOL,[3] MARCIN LUTYNSKI,[4] JAKUB OCHMANN,[4] KONRAD KOŁODZIEJ,[4] ZBYSZEK SZELIGA,[5] GREGOR JEROMEL,[1] JANEZ ROŠER[1]

[1] Premogovnik Velenje, Velenje, Slovenija
sergej.jamnikar@rlv.si, gregor.jeromel@rlv.si, janez.roser@rlv.si
[2] ITPE, Zabrze, Poland
aczardybon@itpl.pl
[3] KOMAG, Gliwice, Poland
pmatusiak@komag.eu, dkowol@komag.eu
[4] Politechnika Slaska, Gliwice, Poland
marcin.lutynski@polsl.pl, jakub.ochmann@polsl.pl, konrad.kolodziej@polsl.pl
[5] VSB – TU Ostrava, Ostrava, Czechia
zbyszek.szeliga@vsb.cz

CORRESPONDING AUTHOR
sergej.jamnikar@rlv.si

Submitted
9. 6. 2026

Accepted
26. 6. 2026

Published
15. 7. 2026

Abstract The project`s aim was to develop a Hybrid Energy Storage System (HESS) consisting of three different energy storage systems: Pumped Storage Hydroelectricity (PSH), Compressed Gas – Air/CO2 Energy Storage (CAES) and Thermal Energy Storage (TES) using a post-mining infrastructure. The possibility of using geothermal energy and the use and potential storage of CO2 were also included in the research. The assumed total energy storage capacity in the HESS project was in the range of 30 MWh. On the basis of the energy demand of each HESS component, a method of thermal and mechanical integration of the entire system was investigated and developed, together with an algorithm for the mutual interaction between the elements of the energy storage system. The optimal cooperation of the various elements of the HESS was decided to be supervised by an energy router. The router also manages energy exchanges with the national power grid for the intake of low-cost green energy and peak energy production. The single HESS energy router system should take into account the possibility of the cooperation of multiple HESS systems working in a distributed system.

Keywords
energy storage, post-mining infrastructure, pumped storage hydroelectricity, compressed gas – air/CO2 energy storage, thermal energy storage, RFCS Project HESS

https://doi.org/10.18690/jet.19.1.5-30.2026
CC-BY, text © Jamnikar et al. 2026
This work is licensed under the Creative Commons Attribution 4.0 International License.
This license allows reusers to distribute, remix, adapt, and build upon the material in any medium or format, so long as attribution is given to the creator. The license allows for commercial use. https://creativecommons.org/licenses/by/4.0

University of Maribor Press

1 Introducton

European countries have declared a »coal exit« in the coming years, and, consequently, the remaining coal mines will have to shift from production to closure. Mine closure is a demanding process, which requires a great deal of financial resources, trained personnel and a well- prepared time line, which must be prepared in accordance with the environmental, ecological and geomechanical requirements. All three key aspects must be studied carefully in order to avoid or minimise impacts on the surface area and underground features below the allowed measures. Some of the mine closure practices showed different approaches towards the process. However, in some cases, alternatives have been introduced, tested and accessed for possible post-mining use as an integration into energy production or a storage solution.

Coal mining usually required a great amount of underground access and approach infrastructure for its effective operation. Construction was done under increased stability criteria, with an emphasis on a long-time life span of these objects. Support generally included the installation of elements and materials that represented a strong lining along shafts, drifts and main access to the mine network. In most cases, the support consisted of prefabricated concrete panels, strong closed steel arch systems, anchoring, reinforced poured concrete, cement (or other material) injection and a combination of the given options.

After the coal production stops the closure sequence follows, from the active mining areas of the coal mine towards the access objects, what leaves the structurally and geometrically favoured objects as a potential for alternative, post mining use.
Slovenia joined the EU-wide programme of coal exit after the Integrated National Energy and Climate Plan was signed in 2020. In accordance with similar plans across the EU, a completely new approach towards mining infrastructure occurred, and therefore the EU Commission's Research Fund for Coal and Steel added research of the potential post-mining infrastructure into the funding scheme.

In 2022, a consortium of partners (the Institute of Energy and Fuel Processing Technology (Poland), the Silesian University of Technology (Poland), the Institut Techniki Gorniczej (Poland), the Technical University of Ostrava (Czech Republic), and Premogovnik Velenje (Slovenia)) submitted a HESS (Hybrid Energy Storage

System in post-mining infrastructure) research project and succeeded in gaining the positive review together with fundings in 2023.

The project frame consisted of seven work packages, in which a coherent review of technologies, objects and other key factors were assessed for multiple locations. Over the project a decisive protocol was introduced and tested, in order to achieve the optimal, or near-to-optimal variants of the proposed solutions.

2 HESS Project objectives

The main aim of the project was the development of a Hybrid Energy Storage System (HESS) consisting of three different energy storage systems: a pumped storage hydroelectricity (PSH), compressed gas – air/CO_2 energy storage (CAES / CCES) and thermal energy storage (TES) using a post-mining infrastructure. The assumed total energy storage capacity was a min. of 30 MWh (10 MWh for each system).

The objective of the HESS project was to determine the feasibility of using post-mining shafts (and access the underground infrastructure), by identifying the structure of the shaft and rock layers (determining storage volume of the mine shaft and its permeability), in order to use all three considered types of energy storage systems.

To achieve this objective (Identification of a post-mining infrastructure for use in the Hybrid Energy Storage System), an analysis and assessment was carried out of the possibilities of using the underground and surface mine infrastructure for HESS development in Poland, the Czech Republic and Slovenia. An extensive database of coal mining shafts was created containing around 200 records. The hydrological and geological requirements were determined for the most optimal use for the underground pumped storage hydroelectricity, compressed gas energy storage and thermal energy storage. Minimum requirements have been defined for the implementation of HESS in the mining area. The locations for the implementation of HESS must match the detailed criteria, specified in the multi-criteria assessment, with a minimum storage capacity of 10 MWh and a cubic capacity of 10.000 m3.

The specific objective for the project is to ensure the tightness of the tanks in the pumped storage hydroelectricity system for a minimum of 10 years. The materials for the construction of water tanks in the PSH system were analysed and selected as part of this task. Corrosion and erosion, as well as water and brine permeability tests were carried out for each construction material. On the basis of the results, the minimum thickness of the tank walls was determined, ensuring their operation for at least 10 years. The results obtained, combined with the economic analysis, directed the selection of the tank construction material.

Another specific objective for the HESS project is achieving the working pressure ~ 80 bar for the air and ~ 20 bar for the CO_2 in the Compressed Gas Energy Storage System. The pressure losses in the sealed mining shaft should be less than 5% of the maximum pressure (during one cycle of CGES operation).

The further research was related to the development of the Compressed Air and CO_2 Energy Storage system. As part of the implementation, extensive thermodynamic modelling was carried out using in-house computational codes. The subject of the study were adiabatic energy storage systems in compressed air (CAES) and in compressed carbon dioxide (CCES). The work resulted in a multi-variant analysis, based on which the variants of the studied systems were recommended for further work. The focus was that the identified variants should be characterised by acceptable operating parameters, energy indicators and the possibility of integration with an energy router.

The specific objective for the project is to ensure an energy storage temperature up to 500°C, and to achieve an energy recovery capacity of at least 1,5 MWt for at least 2 hours.

As part of the research, an extensive analysis of the available solid, liquid and phase change materials dedicated to heat storage was performed, in accordance with the project's objectives. Materials for storage were selected that can be used at three temperature levels: 100°C, 300°C, 500°C. In addition, experimental tests were performed using solid ceramic materials. These materials have demonstrated favourable thermophysical performance with regard to heat storage; however, their elevated cost does not currently allow them to be used on an industrial scale. Experimental studies are also being conducted with the thermal energy storage tank, with the objective of investigating the potential for heat storage in natural rock materials and providing experimental data for the validation of numerical models.

Another objective of the HESS project is the creation of the energy router concept for measurements, data acquisition and performance integration of all the HESS modules, energy storage management and cooperation with the National Power System.

At the present time, work is being carried out on the integration concept and the calculation model of the HESS configuration. The exchange, collection and analysis of data from previous research tasks is ongoing. The initial installation works have been completed, the control cabinet has been adapted, a server for network communication and a controller with an operator panel have been installed, and the system components have been integrated into a cohesive infrastructure. After the installation, the basic system functions were tested, enabling the launch of its key elements. Work has also begun on a computer application for managing the energy router, which will coordinate the system, process data and present the parameters in a graphical format. Additionally, work is ongoing on visualisation tools to monitor the system in real time.

An important final aim of the project is to conduct a technical, economic and environmental assessment of the Hybrid Energy Storage System. These assessments are based on the information obtained at earlier stages of the project. The techno-economic assessment of HESS in the post-mining infrastructure is in the stage of preparation in the form of a Pre-feasibility Study confirming the technological and economic feasibility. The technical, economic and environmental analyses carried out will be the basis for determining the possibilities of industrial implementation of the HESS technology.

3 Methodology

3.1 Site selection

The site selection and related analysis were focused on issues related to the adaptation of post-mining infrastructure for the purposes of energy storage purposes in the Hybrid Energy Storage System (HESS). Particular attention was paid to the analysis of the technological and structural conditions that determine the potential use of mine workings and shafts in the context of modern energy storage systems. A key aspect was identifying the existing engineering solutions and their potential integration with hydroelectric and compressed air systems, enabling efficient management of the energy surpluses in the context of the energy transition.

During the research, the identification, classification and technical assessment were carried out of objects that could be adapted for the new function. A detailed analysis was conducted on the physical parameters such as depth, diameter and the condition of the structural lining, as well as the functionality and further usability of the given infrastructure. Interdisciplinary aspects were considered, including the rock mass mechanics, mining engineering, hydrogeology and energy system modelling, which allowed for the development of criteria for evaluating and selecting the most suitable locations.

The research also attempted to determine the potential benefits of transforming the post-mining infrastructure into energy storage systems. The impact was analysed of the geotechnical and hydrogeological conditions on the long-term stability and efficiency of the planned solutions. Issues related to the durability of the structural lining, the potential for rock mass deformation, and the risk of mine water migration were considered, allowing for the identification of key factors affecting the safety and functionality of the system.

3.2 Identification of Shaft Infrastructure as a Potential Base for Energy Storage

As part of the conducted research, a key issue was the identification of the shaft infrastructure as a potential base for implementing energy storage systems. The undertaken actions included a comprehensive inventory of the shafts, with particular emphasis on their current operational status, geometric parameters, and previous function within the mine structure in Poland, the Czech Republic and Slovenia. Both shafts in operation and those designated for decommissioning were considered, allowing for the creation of an up-to-date database of objects that could be adapted for energy storage systems.

A detailed classification of the infrastructure was carried out, dividing the shafts based on their affiliation with mining enterprises and their geographical distribution. The acquired data were verified through an analysis of the technical documentation and consultations with the mining institutions, enabling precise characterisation of each object. Information regarding the depth, diameter, and the current technical condition of the shaft lining was considered, as well as the operational functions such as material transport, ventilation and the mine drainage.

The analysis covered not only the basic parameters of the shafts, but also the hydrogeological and structural aspects that could impact their future use within energy storage systems significantly. Special attention was paid to the conditions arising from the geological factors and the potential integration of the shafts with the existing power infrastructure. The conducted research allowed for an assessment of the potential limitations resulting from the decommissioning processes, which, in some cases, may prevent the adaptation of shafts for new functions.

The acquired data enabled the assessment of potential locations in terms of their suitability for implementing energy storage systems. Particular attention was paid to structures with an appropriate depth and diameter that could serve as underground water reservoirs or chambers for storing compressed gases. In the next stages of analysis, the selected shafts will undergo a more detailed evaluation regarding their structural stability and their potential integration with the existing power infrastructure.

The use of geoinformatics methods and mathematical modelling tools allowed for preliminary simulations related to the potential operation of energy storage systems within the analysed shafts.

3.3 Characteristics of mine shafts and suitability assessment

The development of an infrastructure suitability assessment system enabled the prioritisation of the analysed objects in terms of their potential application. The introduction of a multi-criteria assessment methodology allowed for an objective classification and identification of locations that meet the technical requirements and can be subjected to further, more detailed research. This approach provided a comprehensive foundation for future design work, facilitating the selection of the most optimal solutions.

The conducted analyses provided valuable insights into the possibilities of repurposing post-mining infrastructure in the context of the energy transition. It was demonstrated that these facilities could serve as valuable assets in the development of energy storage systems, opening up prospects for their further adaptation to the needs of a sustainable power system. The research laid the groundwork for the subsequent project stages, which will include in-depth technical analyses and feasibility assessments of the selected concepts under real operational conditions.

3.4 A Multi-Criteria system for the assessment of mine shafts and underground workings

As part of the conducted research, a multi-criteria assessment system was developed for evaluating the mining shafts and underground workings to determine their potential suitability for implementing energy storage systems. The developed methodology considered a wide range of technical, geological and economic parameters, which were analysed to create a comprehensive evaluation tool.

The assessment system was based on several key parameters analysed in the context of their potential adaptation. Shaft depth was considered a crucial technical parameter determining storage capacity and the ability to utilise elevation differences for energy generation in pumped storage systems. Deeper shafts were preferred, due to their higher energy accumulation efficiency. The shaft diameter influenced the feasibility of installing the technological infrastructure, including pipes for transporting water or other storage media. Wider shafts allowed for more flexible engineering solutions.

The availability of surface infrastructure was also analysed, including the existing energy installations, access roads and the possibility of integration with the power grid. Shafts located near power transmission infrastructure were more favourable for energy storage implementation. The hydrogeological conditions considered the presence and characteristics of the mine water, potential risks to shaft stability, and the possibility of using underground water as a storage medium. High water infiltration could require additional sealing systems.

The shaft lining stability was assessed in terms of its technical condition, applied materials, and the degree of degradation. Shafts with well-preserved linings had greater implementation potential, whereas those with weakened structures might require costly modernisation. The risk associated with coal seam exploitation included the threat of land deformation, seismic activity and potential rock mass movements. The stability of the shaft's surroundings was crucial for its long-term use as an energy storage facility.

The presence and characteristics of mine water were also significant, as water could be both beneficial, enabling its use as a storage medium, and problematic, requiring sealing and potentially impacting the shaft structure. A detailed chemical and physical analysis of the water was essential to assess the corrosion risks and contamination levels.

The developed assessment model employed multi-criteria analysis methods, including hierarchical analysis and scoring methods, enabling an objective classification of the shafts and underground workings. The evaluation results identified the most promising sites for implementation and outlined the necessary modernisation measures for efficient adaptation.

The findings demonstrated that the application of a multi-criteria assessment system identifies locations with the best adaptation parameters effectively, making it a crucial element in planning energy storage strategies in post-mining infrastructure.

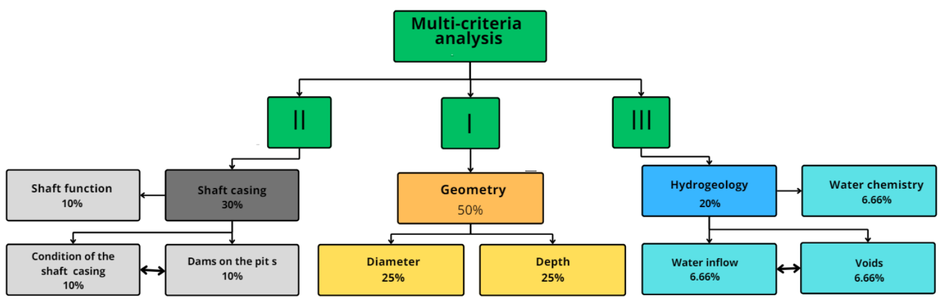

Figure 1: Distribution of weights in multi-criteria analysis
Source: HESS Technical Report

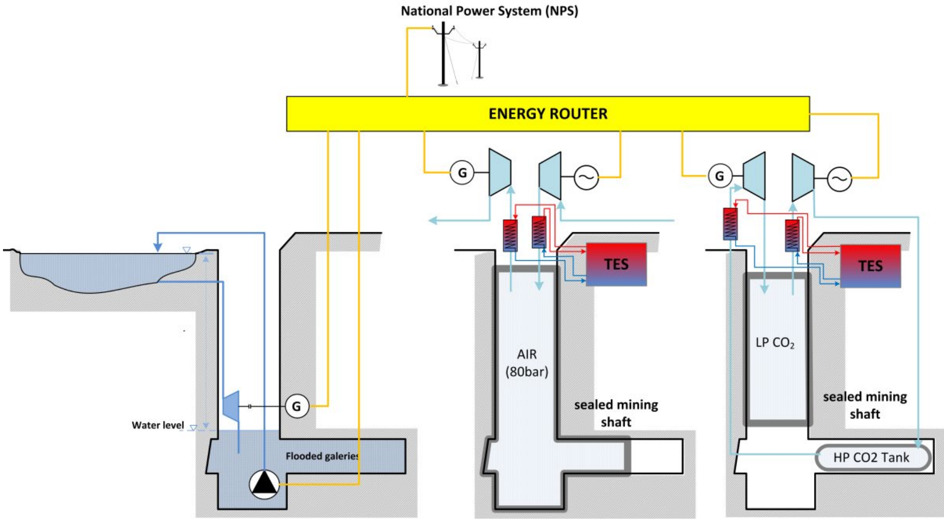

Figure 2: Three different types of energy storage in the HESS system
Source: HESS Technical Report

3.5 Description of the optimal shaft configuration for compressed air/CO_2 energy storage - Energy storage in compressed gas systems

The study also included an attempt to determine the suitability of compressed air technology for the geological conditions of post-mining shafts. It was indicated that CAES systems could be an effective solution to address energy supply instability from renewable sources such as wind and solar power. The fundamental principles of the technology were discussed, including the geological structure requirements and the necessary modifications to the existing shafts, such as lining sealing, water outflow management, and adapting the infrastructure to withstand high air pressure.

A classification and evaluation of mining shafts in the three countries were conducted, to determine their suitability for CAES adaptation. The assessment considered the geometric parameters, depth, diameter, structural integrity of the shaft lining, and availability of the energy infrastructure. It was found that the shafts in Poland, particularly in the Upper Silesian region, have the greatest implementation potential, due to their number, depth and well-developed supporting infrastructure. In contrast, the available infrastructure in the Czech Republic and Slovenia is more limited, and the shafts tend to be smaller in size, posing challenges for implementing this technology.

The collected data identified key challenges related to adapting shafts for energy storage functions. The fundamental issues included ensuring high structural tightness, controlling the impact of mine water, and geomechanical risks arising from potential rock mass instability. Additionally, the regulatory constraints were discussed, emphasising the need for detailed feasibility studies for specific locations.

The conducted analysis provided comprehensive insights into the potential for transforming the post-mining infrastructure for energy storage applications and serves as a foundation for further in-depth research and future investment planning in CAES technology in Poland, the Czech Republic and Slovenia.

Generally, the objects must require conditions comparable to Pumped Storage Power Plant shaft installations, however, the most important factor is the structural integrity of the casing in order to prevent leakage of the compressed media.

In the research, comprehensive thermodynamic models of two energy storage systems were performed: in compressed air and in compressed carbon dioxide. The energy storage systems considered are based on the storage of energy in the potential of compressed gas, which, at the discharge stage of the system (electricity generation) is directed to an expander that drives a generator. A key element of these systems are compressed gas reservoirs, which can be tanks, salt caverns, or underground spaces such as a post-mining infrastructure. The models were based on the characteristic parameters of the reference post-mining infrastructure, which have been determined by requirements in other systems. In the planning stage of the analytical boundary conditions, the previous operating experience of CAES systems was identified, which are used in the United States and Germany successfully. The thermodynamic models were enhanced with detailed maps of the operational parameters of the machines – compressors and expanders. This feature enhances the precision of the calculations by considering the impact of parameters such as the pressure in the compressed gas reservoir, or the degree of charge of the heat tank on the efficiency of the machines. The models created are distinguished by their capacity to assess multiple variants of each analysed system while preserving the stability of the calculations.

A commonality among all the systems analysed was the utilisation of a post-mining shaft as a compressed gas reservoir. During the charging phase, air is pumped into the shaft space, while carbon dioxide is pumped into tanks located in the mine shaft. Additionally, it was planned that a heat reservoir would be constructed in the mine shaft, which would engender a number of advantages, such as the possibility of building a thin-walled TES tank, consequently leading to a reduction in financial expenditure.

The work analysed the following configurations of the systems under study:

- Adiabatic CAES with a single-stage air compressor and a single-stage expander - at the stage of evaluation of the energy indicators, this system achieved the highest energy efficiency of the energy storage cycle at around 70%. This system also allows the storage of heat with the highest temperature potential (around 1000 K), as the air compressor was not sectioned, resulting in the absence of a cooler. However, due to the design assumptions of the energy router, this configuration was excluded from further research work, as thermal integration into the router is impossible due to the lack of a cooler (heat exchanger). In addition, the achieved compressed air temperatures far exceeded the boundary conditions for the defined heat accumulator.
- Adiabatic CAES with a two-stage air compressor and single-stage expander, and adiabatic CAES with a three-stage air compressor and single-stage expander have been demonstrated to exhibit energy cycle efficiencies of approximately 65%, due to the lower temperature potential of the stored heat. The employment of multi-stage air compressors facilitates the selection of compression ratios for each stage, enabling the achievement of the desired heat storage temperature within the TES tank. Moreover, the utilisation of multi-stage compressors allows for the incorporation of intercoolers (heat exchangers), thereby integrating the heat of the CAES system into the planned energy router. The utilisation of heat with a lower temperature potential (up to 570 K) not only facilitates the implementation of additional processes within the energy router, but also supports the district heating system, thereby offering a distinct advantage of the proposed energy storage systems.
- The adiabatic CCES with a single-stage compressor and carbon dioxide expander is a closed-loop system in which carbon dioxide circulates, depending

on the system cycle stage, between a low-pressure and a high-pressure CO2 reservoir. The multivariate analysis was based on varying the pressure of CO2 storage in the low-pressure reservoir, which allowed the configuration to be selected as designed, i.e., with a capacity of approximately 80 MWh. The energy efficiency of the energy storage system cycle was, depending on the variant studied, between about 50% and about 67%. Systems characterised by an LPT tank pressure variation parameter of 0 and 1 were recommended for further work within the energy router.

3.6 Underground object's casing material tests

The aim of the underground object's casing material tests was the assessment of the functional and physicochemical properties of the construction materials of the underground water reservoirs in terms of chemical and mechanical resistance. The selection of construction materials for the pumped storage tanks will be performed based on the test results obtained, in order to ensure the tightness of the tanks in the PSH.

The scope of the work included carrying out tests of the selected construction materials for underground water reservoirs in PSH in order to determine:

– corrosivity: chloride corrosion, sulphate corrosion, magnesium corrosion, acid corrosion
– erosivity
– permeability
– leaching.

For the preliminary tests with design partners, two basic building materials were selected, which were concrete class C20/25 and concrete class C35/45, prepared in accordance with the PN-EN12390-2:2019-7 Standard. These are some of the most commonly used concrete classes, which are used to build various types of foundations, building structures or construction materials. Concrete class C35/45 has a higher mechanical strength.

3.7 Heat storage in post-mining infrastructure

As part of the Heat storage in post-mining infrastructure research, a key assessment of the potential heat storage techniques was carried out from the perspective of implementing the planned energy router. This assessment involved the extensive identification of storage techniques and materials, which will enable the planning of how the planned energy storage systems can be interconnected and optimised to achieve satisfactory energy capacity, self-consumption and power system balancing at a subsequent stage of the work. The work proceeded by defining the advantages and disadvantages of the various heat transfer and storage techniques, as well as the main obstacles to the implementation of each technique. This was achieved by drawing upon the experience of the authors and other research groups that have published data on heat storage operation widely. The expected values were also defined of the parameters to be met by potential storage materials. The work was divided into two parts: experimental research and extensive literature analysis.

Experimental studies: the present section investigated the fundamental thermophysical parameters (i.e., thermal conductivity coefficient, specific heat capacity) of a ceramic storage material in the form of spherical elements with a diameter of approximately 16 mm, which are utilised for heat storage in a packed bed. The rationale for conducting this research was the innovativeness of the proposed material, given that ceramic materials are only just gaining popularity for heat storage.

A comparative analysis of two types of heat storage material was conducted, distinguished by their colour, which indicated their structural composition. The research demonstrated that the material exhibited consistency in its performance as a heat storage material. This is evidenced primarily by the low value of the thermal conductivity coefficient, which preserves the temperature potential of the stored energy and limits its natural dissipation. Furthermore, the material exhibited no evidence of internal structural degradation during cyclic heating and cooling from 40°C to 1030°C. A notable drawback of the material under investigation is its cost; however, the increasing popularity of ceramic materials as heat accumulators may lead to a reduction in their cost, and, consequently, mitigate the negative economic implications associated with these solutions.

4 Results

4.1 Site selection and infrastructure decision criteria

A selection of mining shafts with the highest potential for adaptation to energy storage systems was carried out as part of the conducted research. The selection process was based on the results of a multi-criteria analysis, in which the key technical, geological, and infrastructural parameters were assessed. The analysis included the shafts with the highest structural stability, appropriate depth, and favourable hydrogeological conditions.

Most of the shafts that match the given criteria were in Poland, followed by the Czech Republic, whereas Slovenia's shafts were excluded due to their shallower depths.

According to the given criteria, the II KWK Budryk shaft (Poland) represents the best choice from reviewed shafts. Its current function is a ventilation shaft, which means no additional equipment was installed in the shaft. The shaft reached a depth of 1157,45 metres with a diameter of 9,0 metres. The upper part of the shaft is situated at an elevation of 292,60 metres above sea level and does not have a headframe. Currently, the fan station is equipped with two main fans. The given situation represents a limited amount of additional modification operations and allows use transformation without significant additional investments.

4.2 Construction and Equipment of the Shaft Casing

The shaft was sunk in a single concrete casing with a thickness ranging from 0,55 m to 0,6 m, thickened to 0,75 m or 0,8 m in areas with coal seams and their immediate vicinity. Partially, the shaft was sunk in a masonry casing with a thickness from 0,51 m to 1,03 m, along with a foundation thickness ranging from 2,0 m to 0,52 m, a concrete casing of 0,8 m thickness, and a double casing – masonry and concrete with a concrete liner, with a total thickness of 0,99 m, as well as a double concrete casing with waterproofing, with a total thickness ranging from 1,0 m to 1,2 m. A concrete plug of 0,5 m thickness was installed at the bottom of the shaft, beneath the concrete casing.

Generally, the shaft configurations with depths above 1000 m, diameters of 7,5 m or larger, solid, water-proof casing and overall good conditions, should match the given conditions. The number of optimal shafts is reduced according to the given criteria.

4.3 Pumped storage power plant

The given parameters allow the use of the shaft for a pumped storage power plant. According to the other assumptions and performance based chosen equipment (Pelton turbine), the energy produced would be 23 MWh, which is twice the initially assumed 10 MWh. In such a case, filling half of the lower reservoir would ensure the expected 10 MWh.

Additional data analysis and calculations proved that the system could be applied to shallower shafts, with a smaller diameter, as in the case of Velenje Coal Mine, where the depths reach 416,42 m (NOP Shaft) and 390,70 m (NOP II Shaft). In limited depths, the existing underground reservoir capacity (>12.000 m^3) is of great importance in the existing roadway network. These facilities must all have water-proof casing and good stability conditions.

Normally, during a pumping operation, the pumped storage power plant will pump water from the lower reservoir in the shaft to the upper reservoir located on the mine site. Based on the analysis of the situational plan of the infrastructure elements on the mine site, possible locations (variants) were determined for such a reservoir.

In the optimal variant, the reservoir is located directly next to the shaft. Its surroundings include the dense surface infrastructure of the mine, which would need to be demolished to achieve the desired reservoir volume. The advantage of this location is the minimisation of losses resulting from water transport on horizontal sections on the surface and the costs of such an installation. The danger associated with this reservoir location (close to the shaft) is related to the load on the terrain that such a reservoir entails and its impact on the stability of the shaft structure. Due to the cyclic filling and emptying of the reservoir, such a load will vary over time.

The described criteria serve as a foundation for further detailed studies and feasibility assessments, which will determine the final list of locations designated for adaptation. The next phase of analysis will consider environmental aspects, investment costs and integration with the national power grid.

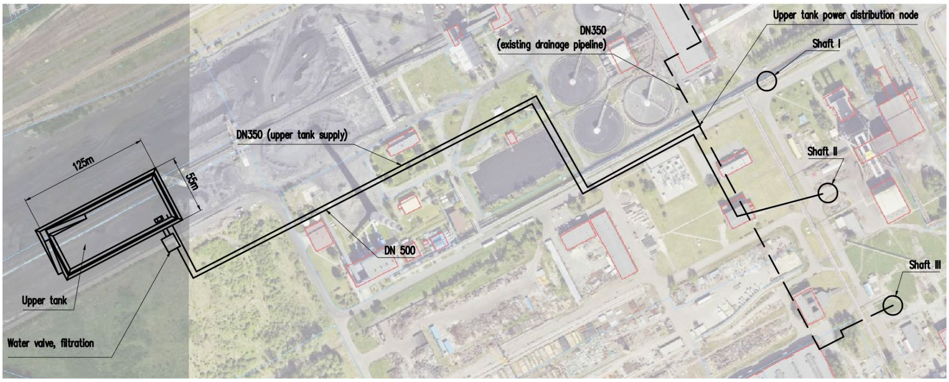

Figure 3: Presentation of Budryk coal mine area with marked facilities for a pumped storage power plant
Source: HESS Technical Report

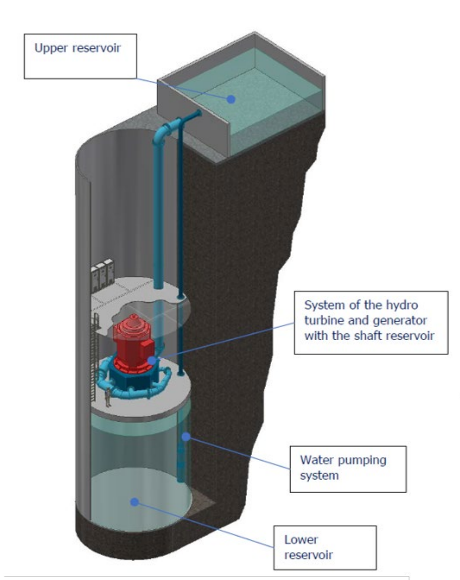

Figure 4: System of the hydro turbine and generator with the shaft reservoir
Source: HESS Technical Report

4.4 Compressed Air/CO2 storage in an underground structure

An extensive, multivariate thermodynamic analysis was conducted, which yielded recommendations for compressed gas energy storage systems utilising post-mining infrastructure. The primary focus of the analysis was the impact of the TES tank diameter on the pressure drop of the compressed air. It was demonstrated that the minimum diameter of a mine shaft should permit the construction of a tank with an internal diameter of at least 5 metres, as, below this value, the pressure loss causes a drastic reduction in the capacity of the energy storage system. The calculations indicated that, for a mine shaft with a diameter of 9 metres, a mine shaft with a minimum length of 750 metres is necessary to achieve an energy storage system with a capacity of 80 MWh.

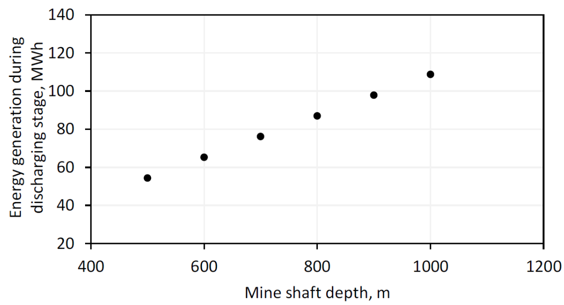

Figure 5: Dependence of the energy capacity of the CAES system on the depth of the mine shaft, assuming an internal diameter of 9 metres
Source: HESS Technical Report

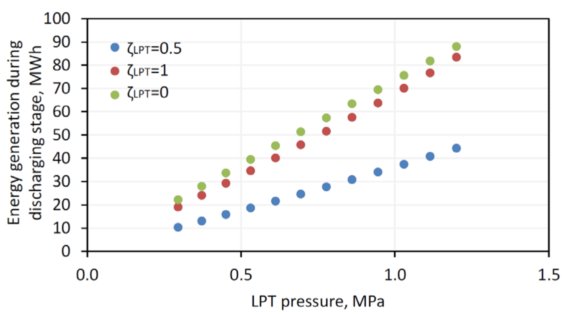

Figure 6: Dependence of the energy capacity of the CCES system on the carbon dioxide pressure in the low-pressure tank
Source: HESS Technical Report

4.5 Heat storage in post-mining infrastructure

Experimental studies were also conducted using an existing laboratory-scale heat tank. The stand includes a heat tank filled with basalt and the heat transfer fluid is air heated by an electric air heater. The design of the heat storage tank is comparable to that of a large-scale TES in a mine shaft; however, the laboratory tank is considerably slenderer than the systems documented in the existing literature. The multivariate experimental investigations are based primarily on changes in the mass flow values of the air and maximum inlet air temperatures. In addition, the design of the laboratory bench allows for bi-directional airflow through the TES, which also corresponds to the operational characteristics of the potential large-scale system.

Figure 7: Thermal energy storage tank in a variant without thermal insulation
Source: HESS Technical Report

In accordance with the objectives of the project, a range of storage materials was selected for three types of heat storage: solid materials, liquid materials and phase change materials. It was hypothesised that, within the energy router, heat storage and transfer could occur at three temperature levels: 100°C, 300°C and 500°C. These temperature ranges were utilised as the input, with 500°C representing the limiting temperature for an adiabatic CAES. As illustrated in the Figures below, the collected data are presented on the range of applicability of the different solid, liquid and different phase-change materials used for heat storage.

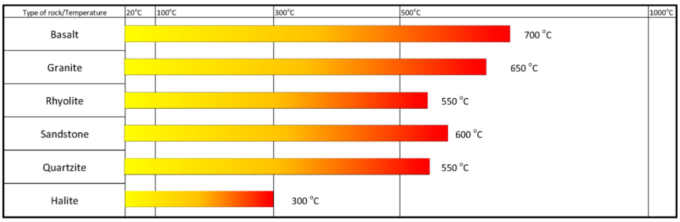

Figure 8: Range of temperature applicability of solid materials for heat storage
Source: HESS Technical Report

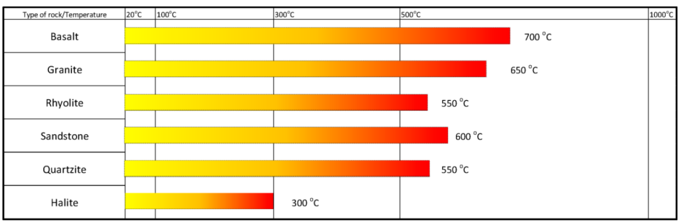

Figure 9: Range of temperature applicability of liquid materials for heat storage
Source: HESS Technical Report

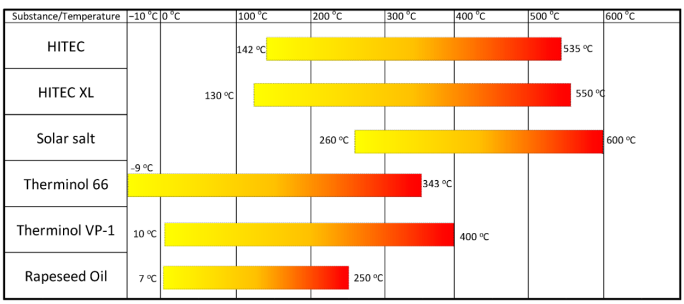

Figure 10: Range of temperature applicability of phase-change materials for heat storage
Source: HESS Technical Report

5 Conclusions - HESS system adaptations for the Velenje Coal Mine

According to the given research work and with consideration of the limitations, an assessment was prepared of the HESS system for the case of the Velenje Coal Mine. It is assumed that, after the mining, only stable objects (mine shafts, access roadway network, pumping station) will remain. All these objects match the HESS project criteria, except for the shaft dimensions, where, as a compensation factor, a wide range of underground roadways is used as a supplement.

5.1 Surface features and surface water reservoirs

According to the HESS project, the potential use of post-mining infrastructure included the research and assessment of the existing Velenje mine shafts and access infrastructure for energy generation and storage purposes.

In the case of the Velenje Coal Mine shafts, the mine infrastrucure does not match the HESS project criteria in secions of the shaft's dimensions (depth, diameter). After a secondary review, the overall setting (Figure 11) could represent the potential of energy generation.

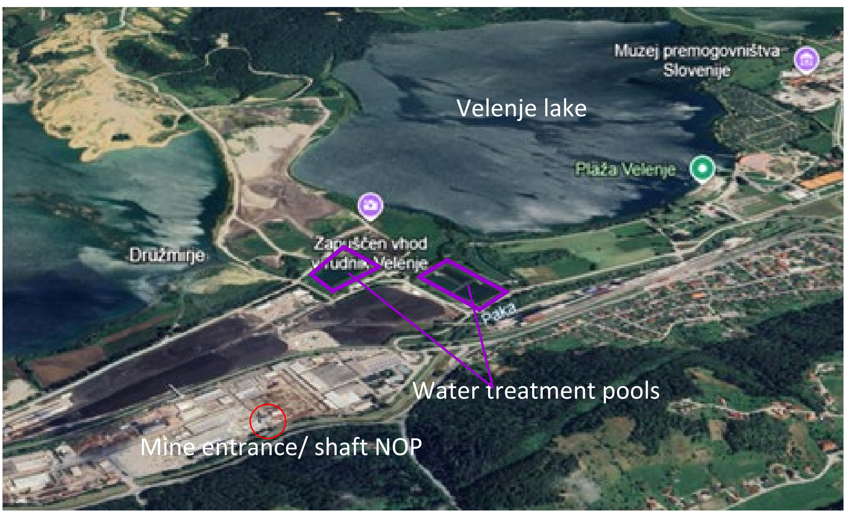

Figure 11: Surface area above Velenje Coal Mine showing subsidence lakes and water treatment pools

Source: Google Maps

Due to vicinity of lakes and/or existing surface water reservoirs, which were used in the past for waste water treathent and are no longer in use, the potential is accessed with additional input data.

As shown in Figure 11, the Velenje lake or water treatment pools could be used as surface reservoirs. Velenje lake represents an infinite water source, whereas the water treatment pools designs provide approximately 70.000 m^3 of potential water storage reservoir. In both cases, the access to the water is free, and the height difference in both cases allows gravitational flow towards the mine shaft (the average height difference is about 10 m).

5.2 Mine infrastructure for HESS system adaptation

The main Velenje Coal Mine shaft shows less favourable dimensions, with a total depth of 416,42 m and diameter of 7,20 m. The two-sided two-level cage system is in use for staff, material and equipment transport. The NOP shaft will also remain for the mine closure activities, as it represents the most effective mine supply facility.

The underground reservoirs and mine pumping station are located in the section of the mine which will remain until the end of the closure works and, optionally, after the closure works will be completed.

The location of the pumping station, -41,5, is in relative vicinity of the shaft NOP (distance 770 m), and since the pumping station is active, all the equipment is already installed, therefore any additional costs are reduced by the given value.

The combination shaft NOP – roadway "Severna talninska zveza" and mine pumping station represent a potential for water driven energy generation with the possibility of pumping water to the surface.

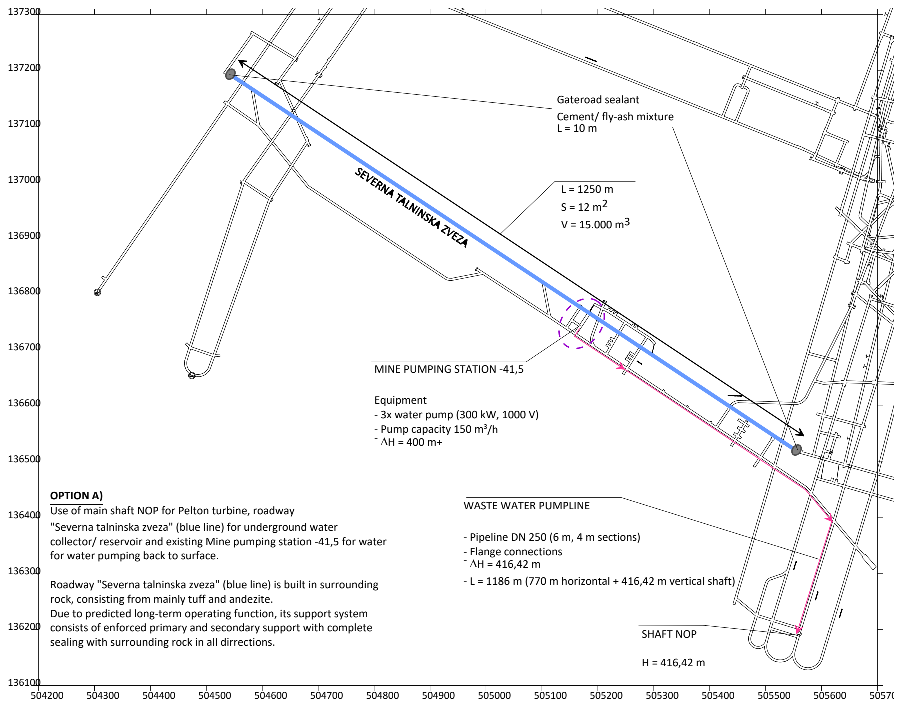

Figure 12: Locations of mine objects "Severna talninska zveza" roadway, mine pumping station -41,5, shaft NOP with the main parameters. The roadway "Severna talninska zveza" is characterised as an underground water reservoir with a storage capacity of 15.000 m3
Source: own

Among the existing shafts, the mine closure plans predict that the ventilation shafts will remain operational until mine closure. As the shafts and access roadway network designs included a reinforced support system despite the favourable geologic and geomechanical conditions, the lifespan of the given objects is estimated to be long after mine closure.

According to the HESS project tasks, the assessment of post-mining object for energy storage by CO_2 or air compression matches the object properties.

Given the data of the shaft`s properties, the shaft`s lining and roadway support, the further analysis is justified of the objects` suitability for energy storage.

If a reservoir volume of approximately 13.500–14.000 m³ or more could be achieved, a possible energy storage of 10 MWh is predicted.

The most effective approach towards the given option is determination of a reservoir volume of 12.000 m³, to develop a roadway-based storage system as an alternative to the shaft-based solution, with a capacity of approximately 9.1 MWh.

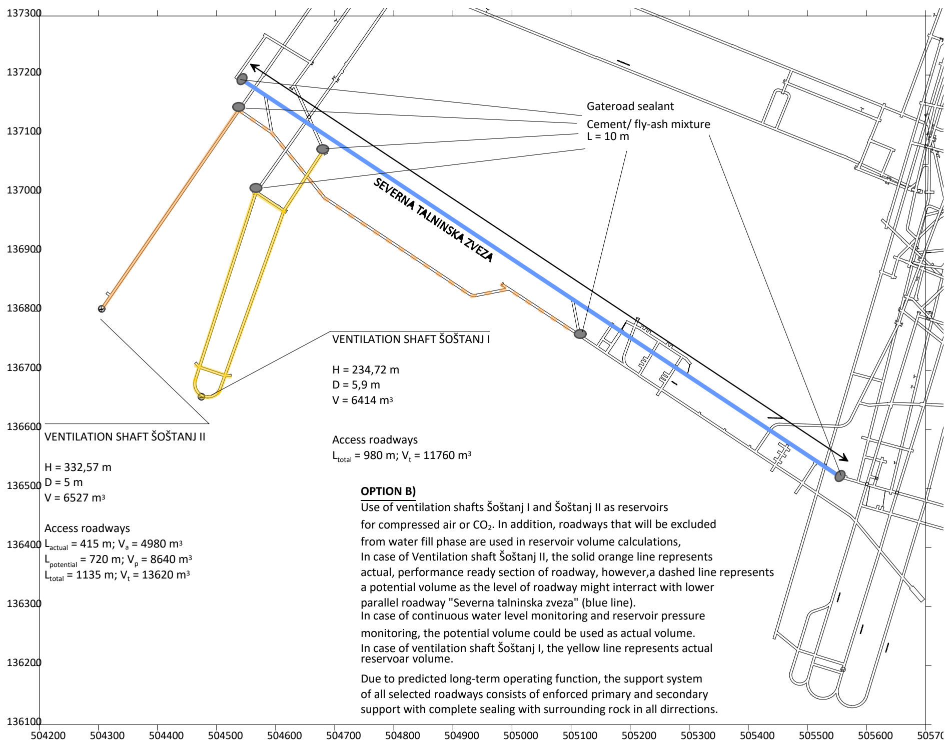

Figure 13: Section of the mine outline with marked objects for possible compressed air or CO2 underground storage reservoirs (energy storage). The measured objects dimensions and calculated values show theoretical volumes of the optionally chosen object combinations: Shaft Šoštanj I with auxiliary objects 18.174 m3, shaft Šoštanj II with auxiliary objects from 11.507 m3 to 20.147m3

Source: own

“The work presented in this paper was carried out within the framework of the HESS project (Hybrid Energy Storage System Using Post-Mining Infrastructure), Grant No. 101112380, supported by the EU Research Fund for Coal and Steel

(RFCS). The project is co-financed by the Polish Ministry of Education and Science under the 'International Projects Co-financed' programme."

References

HESS, Hybrid energy storage system using post-mining infrastructure, Project Number 101112380, Technical Report (Part B), 01.07.2023 – 31.12.2024

Jurczyk, M.; Spietz, T.; Czardybon, A.; Dobras, S.; Ignasiak, K.; Bartela, Ł.; Uchman, W.; Ochmann, J. Review of Thermal Energy Storage Materials for Application in Large-Scale Integrated Energy Systems–Methodology for Matching Heat Storage Solutions for Given Applications. Energies 2024, 17, 3544, doi:10.3390/en17143544.

Povzetek v slovenskem jeziku

Rezultati projekta HESS – Hibridni sistem shranjevanja energije v post-rudarski infrastukturi. Cilj projekta je bil razviti hibridni sistem za shranjevanje energije (HESS), ki ga sestavljajo trije različni sistemi za shranjevanje energije: črpalna hidroelektrarna (PSH), shranjevanje energije s stisnjenim plinom – zrakom/CO2 (CAES) in shranjevanje toplotne energije (TES) z uporabo infrastrukture po rudarjenju. V raziskavo je bila vključena tudi možnost uporabe geotermalne energije ter uporaba in potencialno shranjevanje CO2. Predpostavljena skupna zmogljivost shranjevanja energije v projektu HESS je bila v območju 30 MWh.

Na podlagi potreb po energiji vsake komponente HESS je bila raziskana in razvita metoda toplotne in mehanske integracije celotnega sistema, skupaj z algoritmom za medsebojno interakcijo med elementi sistema za shranjevanje energije. Za optimalno povezovanje različnih elementov HESS je bil izbran kontrolnik - usmerjevalnik energije. Usmerjevalnik upravlja tudi izmenjave energije z nacionalnim elektroenergetskim omrežjem za prevzem nizkocenovne zelene energije in konic energije. Enotni sistem usmerjevalnika energije HESS mora upoštevati možnost sodelovanja več sistemov HESS, ki delujejo v povezanem sistemu.

JOURNAL OF ENERGY TECHNOLOGY
Vol. 19, No. 1, pp. 31–54, July 2026

Original Scientific Article

STOCHASTIC MODELLING OF A LOW VOLTAGE DISTRIBUTION NETWORK OPERATION

Submitted
9. 6. 2026

Accepted
17. 6. 2026

Published
15. 7. 2026

MICHAL BAHERNÍK, MAREK HÖGER
University of Žilina, Faculty of Electrical Engineering and Information Technology, Žilina, Slovakia
michal.bahernik@feit.uniza.com, marek.hoger@uniza.com

CORRESPONDING AUTHOR
michal.bahernik@feit.uniza.com

Abstract Modelling a low-voltage network operation is becoming increasingly challenging. In the past, deterministic methods adopted from sub-transmission and transmission network analysis were sufficient for operators to assess the operating conditions. However, changes in customer behaviour, household appliance structure, and the growing penetration of residential photovoltaics, EV charging, heat pumps, and air conditioning are altering operating conditions in low voltage networks significantly. Given the strongly stochastic nature of individual customer consumption and generation, deterministic methods are becoming less suitable for proper grid operation analysis and development planning. This article presents a simple method for stochastic modelling of a network operation, where customer behaviour is described using a system of histograms. The presented approach enables in-depth investigation of operating conditions in low voltage networks, identifying potential operational extremes that compromise safety of operation, while also quantifying the frequency and probability of such events. Application of the method is demonstrated for a typical rural network.

Keywords
stochastic modelling,
low voltage network,
probability density,
histogram,
load flow,
development planning

https://doi.org/10.18690/jet.19.1.31-54.2026
CC-BY, text © Baherník, Marek Höger. 2026
This work is licensed under the Creative Commons Attribution 4.0 International License.
This license allows reusers to distribute, remix, adapt, and build upon the material in any medium or format, so long as attribution is given to the creator. The license allows for commercial use. https://creativecommons.org/licenses/by/4.0

University of Maribor Press

1 Introducton

The rapid development of new technologies at both the consumer and industrial levels has driven significant changes in consumer behaviour and introduced new challenges for distribution system operators (DSOs). The growing penetration of residential photovoltaic (PV) installations is transforming consumers into prosumers. In addition, the increasing use of air conditioning and heat pumps, together with the expansion of the residential electric vehicle (EV) charging infrastructure, is altering typical load profiles and transforming operating conditions in low-voltage (LV) networks rapidly (Damianakis, 2025).

To address these challenges, DSOs must analyse network conditions carefully, identify potential weak points, and develop measures to mitigate the negative impacts of these emerging technologies. Accurate modelling of the operating conditions in low-voltage networks is a key component of such analyses. However, modelling the operation of LV networks remains highly challenging, due primarily to the strongly stochastic nature of consumer behaviour.

Several stochastic approaches to modelling consumer behaviour have been proposed, ranging from highly detailed simulations of appliance usage in individual households (Jang, 2016) to various regression-based methods (Yildirim, 2024), neural network-based approaches (Martellotta, 2017), and advanced mathematical frameworks such as copulas (Nelsen, 2006). Each of these methods has a well-defined scope of application in which it performs effectively. However, as in almost every field of science and engineering, there is no such thing as a free lunch (Wolpert, 1997), and from the DSO perspective, these methods each carry inherent practical limitations.

Bottom-up approaches that model appliance usage in detail are extremely complex and difficult to apply at the network scale. Moreover, parameterising such models is highly demanding, making this approach more suitable for the simulation of individual entities, particularly in power quality studies.

Regression-based methods rely on a well-established mathematical framework; however, they require careful tuning and validation of the regression coefficients. Artificial neural network (ANN)-based models can uncover hidden relationships in the underlying data, but their training and validation are often time-consuming. Furthermore, the resulting models are essentially black boxes, making them difficult to interpret directly. Copula-based methods provide an elegant mathematical framework for describing complex dependencies between variables, but they rely on relatively advanced mathematics, and, like regression-based models, require careful parameter tuning with results that are similarly difficult to interpret.

A common drawback shared by ANN, copula and regression-based methods is the need for parameter tuning or model retraining. When the input dataset changes, rebuilding the model typically requires extensive recalibration. This reduces their practicality for industrial applications, where models must be updated regularly to reflect local conditions within the analysed portion of the distribution system.

The purpose of this work is to develop a stochastic modelling framework that enables the construction of statistical models from real-world measurement data with minimal fine-tuning requirements. The framework is designed to support frequent, automated model updates, while remaining easily interpretable and adaptable to represent different customer types.

The proposed model employs a system of histograms to describe the probability density of power consumption for different customer types, while preserving the temporal variability of load throughout the day. The Monte Carlo simulation framework used to generate loading scenarios from these histograms follows the standard principles described in (Kalos, 2008). The performance and usability of the method are demonstrated on a rural low-voltage network. Three scenarios with different customer type compositions are investigated, and the resulting operating conditions are analysed – nodal voltages and line currents. These case studies demonstrate the ability of the proposed method to identify potential violations of operational limits and to quantify the probability of such events.

It should be noted that the current version of the methodology does not preserve the temporal correlation of the generated power samples. As a consequence, the proposed modelling technique is not suitable for tasks involving time integrals of voltages, currents, or powers – for example, the optimisation of the location and sizing of battery energy storage systems (BESS). A different approach must be adopted for such applications (e.g., Beláň, 2022).

This article extends the work presented in (Bahernik, 2026) and (Höger & Bracinik, 2026), providing a more detailed description of the methodology and more comprehensive case studies, including a discussion of the known limitations of the proposed approach.

The rest of the article is organised as follows: Section 2 presents the proposed modelling methodology, Section 3 demonstrates the approach through different case studies, and Section 4 discusses the results, benefits and known limitations of the proposed methodology.

2 Methodology

When assessing current and future operating conditions in distribution networks (both medium and low voltage), the assessment is typically based on load flow calculations, in which the simulation model is parameterised according to the known or expected composition of the customers and their grid connection parameters (reserved capacity, tariff, historical consumption). Historically, such analyses followed the methodology adopted from the sub-transmission and transmission levels. Calculations were performed as deterministic analyses, with the temporal variability of the power profiles represented by typical load curves constructed for different consumer types, usually at an hourly time resolution. This approach was adequate when sufficient safety margins existed to absorb the occasional operational extremes, and when the analysis could focus on the typical, most probable operating scenarios.

However, the growing penetration of residential PV installations, air conditioning units, heat pumps and electric vehicles is eroding these safety margins while increasing the volatility of power profiles. Deterministic methods are no longer sufficient for LV network operation analysis. The main challenge is therefore to develop an assessment method that is both straightforward to implement and capable of providing the required insight into real operating conditions with a suitable level of confidence.

The method must allow as much automation as possible. The stochastic model must be based on existing or easily obtainable data sources, and, given the dynamic changes ongoing in the power sector, must also support frequent and easy model updates. With these requirements in mind, the proposed methodology uses simple histograms to describe the probability density of all the relevant variables and their relationships. This approach avoids the complex retraining required by ANN-based models and the fine-tuning demanded by regression or copula-based solutions, and can be managed by engineers without specialist knowledge of higher mathematics or artificial intelligence. Moreover, histograms are human-readable and directly interpretable, providing transparency at all stages of the simulation process, and facilitating backtracking, debugging and interpretation of the results. To capture the temporal and other relationships between the model variables, the histograms are organised into stacks forming multi-dimensional structures.

2.1 Data preparation and stochastic model

The framework can be implemented using either power profiles or current loading profiles, depending on the modelling approach preferred by the DSO. Measured power or current profiles can be obtained from the existing AMI/IMS infrastructure, or through dedicated measurement equipment installed at selected customer premises. The methodology can accommodate data from sources with different time resolutions; however, to capture the dynamics of real network events, a resolution of 15 minutes or finer is recommended. Sub-minute resolutions are possible but not recommended, as they increase the complexity of the underlying data structures and the number of load flow scenarios that must be solved substantially. A resolution of one or five minutes is currently considered a good balance between model complexity and the ability to capture the relevant network dynamics.

Raw data obtained from different sources must be validated and checked for timing inconsistencies, missing values and data errors. Because the method is not intended to generate time series data, occasional missing samples do not need to be filled artificially, provided the overall dataset contains enough samples to construct a statistically significant model. Data cleaning and re-timing can be performed using the standard tools available in environments such as Python or MATLAB.

After cleaning, the data must be categorised into separate groups according to the consumption type represented by the profile (e.g., standard household, household with a heat pump, household with residential EV charging). Each group is processed separately into a dedicated statistical model. Because the consumption of most consumer types is season-dependent, a separate model must be constructed for each season of interest. The model must also distinguish between workdays and weekends or public holidays, as these categories typically exhibit significantly different behaviour. Depending on the modelling strategy – which may vary considerably with the task and voltage level – the input data can be normalised with respect to the reserved or installed capacity, or, in the case of medium-voltage networks, with respect to the number of customers. In low-voltage networks, normalisation is often unnecessary, and the model can work directly with the absolute values obtained from the measurement system.

The statistical model describes the probability density of the current or power amplitude for each time interval of the day. The consumption data for a given customer type are therefore first divided into time-interval categories according to the required time granularity (e.g. a granularity of 5 minutes yields 288 categories representing a full day). When working with total three-phase loading, samples from different phases of a polyphase measurement system can be aggregated into a single dataset. For each time category, a separate histogram is constructed from the pre-processed dataset. The individual histograms are then stacked together, and, when uniform bin spacing is used across the stack, the system of histograms can be represented as a 2D array, which can be visualised effectively as a heat map. All the histograms are normalised with respect to the total number of samples, so that each histogram value represents a relative frequency in the range 0–100 %, forming a proper probability mass function over the bins. An example of such a model, representing a household with a heat pump during the winter period, is shown in Figure 1.

The framework additionally allows modelling of further relationships – for example, the power factor or reactive power loading as a function of the active power. A similar approach could be applied to other power quality parameters, such as the harmonic content. An example of a P/Q relationship model represented as a heat map is shown in Figure 2.

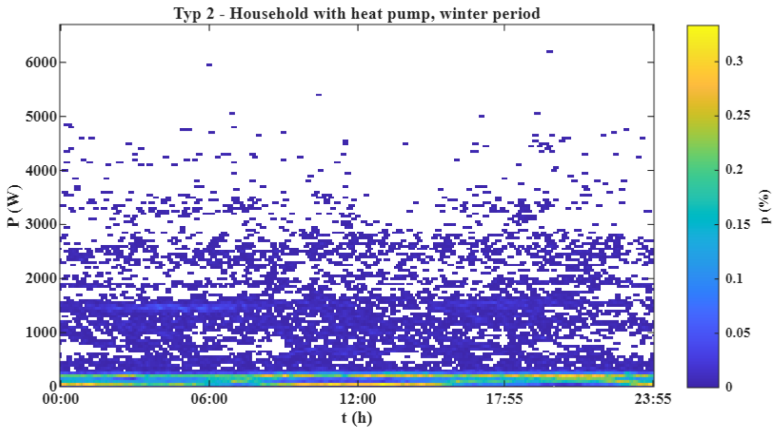

Figure 1: Heatmap representing a statistical model of a household with a heat pump

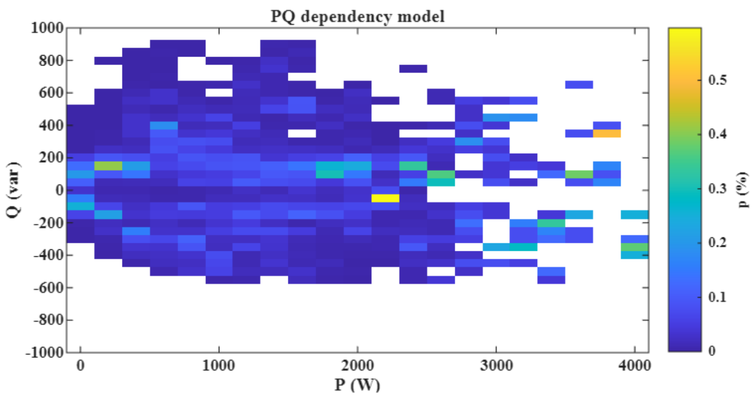

Figure 2: Heatmap representing the relation between the active and reactive power of the load

2.2 Simulation framework

The simulation framework is based on the Monte Carlo methodology (Kalos, 2008). The operating conditions are analysed statistically from the results of a large set of simulated loading scenarios. To enable temporal analysis of the network conditions, the simulation is repeated separately for each time interval at the required granularity. This allows critical time intervals to be identified, and supports tariff management decisions for customers on multi-tariff programmes or subject to mass remote control.

For each time interval, the appropriate histogram is selected from the stochastic load model – corresponding to a single column of the 2D structure – for each consumer type present in the network. A random value of active power or current is then generated for each consumer based on the selected histogram. The flow chart of the proposed framework is shown in Figure 3.

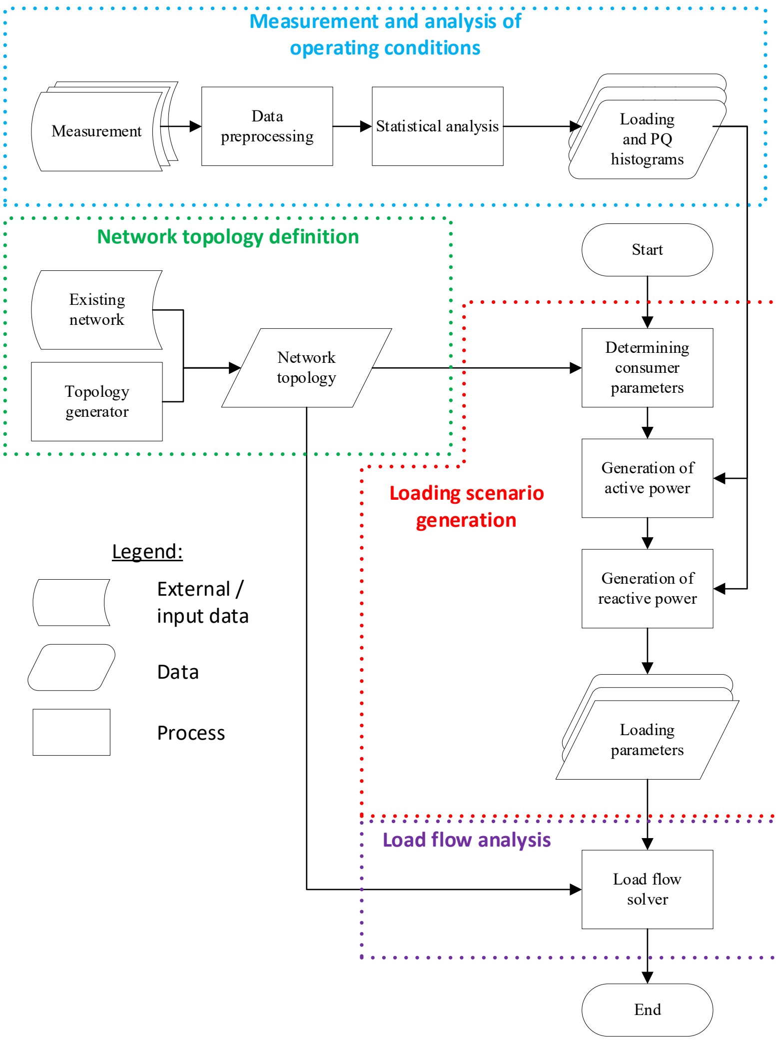

Figure 3: Flow chart of the proposed simulation framework
Source: Baherník et al., 2026

Once the active power for each consumer has been generated, the corresponding reactive power component is determined using the P/Q stochastic model. Based on the generated active power value, the appropriate partial histogram is selected from the P/Q 2D structure, and a reactive power value is sampled from it. This process yields a complex apparent power value for each consumer, together forming a single loading scenario.

Random power values are generated from the histograms using inverse transform sampling applied to the cumulative distribution function (Devroye, 1986), which maps the uniform distribution provided by the built-in random number generator to the desired probability density function describing load behaviour. One inherent limitation of histogram-based generation is the discrete spectrum of generated values; this can be mitigated partially through interpolation between the bin edges.

Each scenario is then solved using a standard load flow solver. For radial LV networks of the type considered here, the Backward-Forward Sweep (BFS) method is particularly well-suited; Gauss-Seidel is a common alternative. The Newton-Raphson method is generally less suitable for medium- and low-voltage networks, due to convergence difficulties arising from the low X:R ratio typical of these systems (Stagg, 2019). For large-scale Monte Carlo simulations requiring the solution of several hundred thousand scenarios, a more computationally efficient implementation based on a GPU-accelerated Jacobi method was developed to support the proposed framework; this solver is described in detail in the referenced work (Höger & Bahernik, 2026).

The number of scenarios required to obtain a statistically significant assessment varies with the network size and customer composition, but is typically in the range of several hundred to several thousand. The framework is therefore computationally intensive, and requires a high degree of algorithmic optimisation, particularly of the load flow solver. Because the individual scenarios are independent, parallel computing techniques can reduce the solution times substantially, with GPU-based implementations offering the best performance.

3 Case study

The introduced methodology was tested on a model of a rural low-voltage network based on a real network from a village located in the northern part of Slovakia. The network has a simple radial structure with two main side branches. The trunk section is 660 m long and the overall length of the network is 1,200 m. The network has 28 nodes and serves 56 customers. To reduce the computational complexity of the model, all the customers are modelled as connected directly to the main part of the network (the customer connection lines are neglected). This simplification reduced the number of nodes in the system from 84 to 28. The network is fed from a 22/0.4 kV distribution transformer (DTS). The single line diagram of the network is shown in Figure 4.

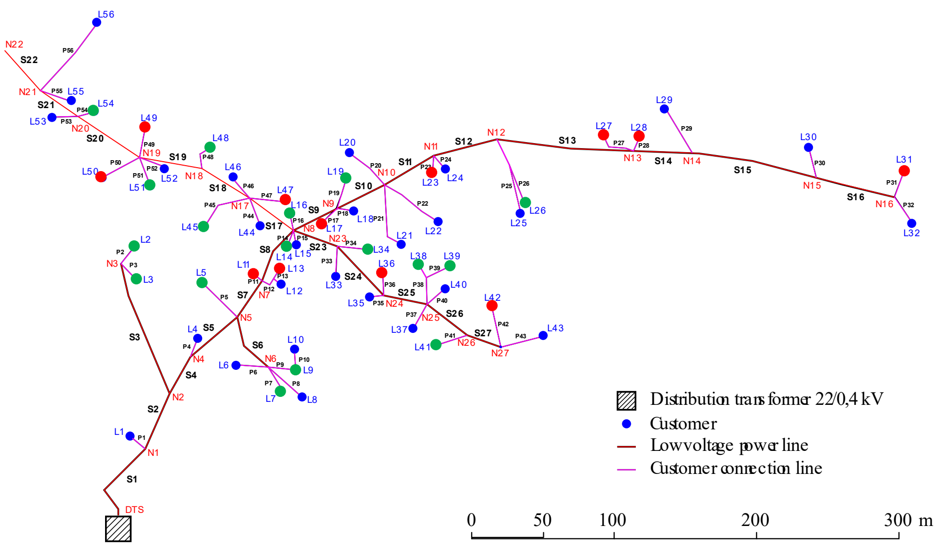

Figure 4: Single line diagram of the low voltage network used for the case study

It should be noted that the node indices used in the results are shifted by +1 relative to the node labels in the single line diagram: node index 1 corresponds to the DTS, so N1 in the diagram corresponds to index 2, N2 to index 3, and so on. Three different kinds of customers were considered:

- Type 1 – regular customers using only small electrical appliances, with no electrical heating or EV charging; this is the reference type,

- Type 2 – customers using a heat pump for space heating and hot water preparation,
- Type 3 – customers using direct electric heating and residential EV charging.

In the single line diagram, an example customer composition is shown, where Type 1 customers are marked in blue, Type 2 customers in green and Type 3 customers in red. The customer composition can be user-specified; the node assignments are generated randomly.

Figure 5 shows heat maps representing the probability distributions of consumption for Type 1 and Type 3 customers. It should be noted that the models represent the early autumn period, during which electric heating is used only sparingly.

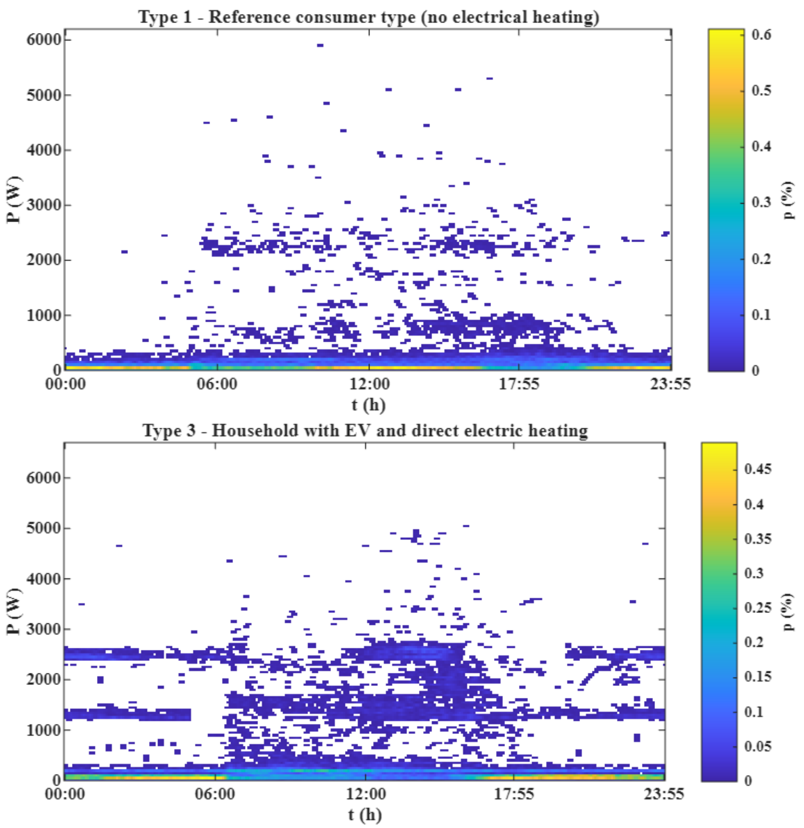

Figure 5: Examples of heat maps representing the probability distribution of consumption for type 1 (top) and type 3 (down) customers for the early autumn period

The histogram system represented by the heat maps was used to generate a loading scenario for each customer randomly. To obtain statistically significant results, a sensitivity analysis was performed by increasing the number of solved operational scenarios gradually while monitoring the spectra of voltages and currents at each node and line section of the network. The analysis showed that at least 1,000 different loading scenarios must be solved for each time interval to achieve statistically significant results. Since the network operation is modelled with a time resolution of 5 minutes, this means that 288,000 different load flow calculations must be solved in total. A highly optimised Jacobi method exploiting massive parallelism and simultaneous solution of multiple scenarios was implemented to support the modelling framework (Höger & Bahernik, 2026). Using a mid-range state-of-the-art GPU (RTX 5070Ti), the solver can complete all 288,000 nonlinear load flow scenarios in under 10 seconds.

Three scenarios were selected to illustrate the potential of the proposed network operation modelling method:

- Reference scenario – all the customers are modelled as Type 1; this scenario reflects the current state of the network,
- Scenario 2 – a customer composition of 50 % Type 1, 30 % Type 2 and 20 % Type 3, autumn period; this represents a scenario close to the operational limits of the network,
- Scenario 3 – a customer composition of 50 % Type 1, 30 % Type 2 and 20 % Type 3, winter period; this represents a scenario in which the operational limits are violated severely due to extensive use of direct electric heating.

3.1 Case 1 – Reference scenario

The reference scenario represents the current state of the network, in which virtually all the customers use gas or solid-fuel heating and hot water preparation. Since the operational limits are never violated in this scenario regardless of the season, a detailed analysis is not presented here. The conditions are illustrated by the histograms of all the nodal voltages and line section currents shown in Figure 6. The voltages are normalised with respect to the nominal voltage; the currents are normalised with respect to the ampacity of each section.

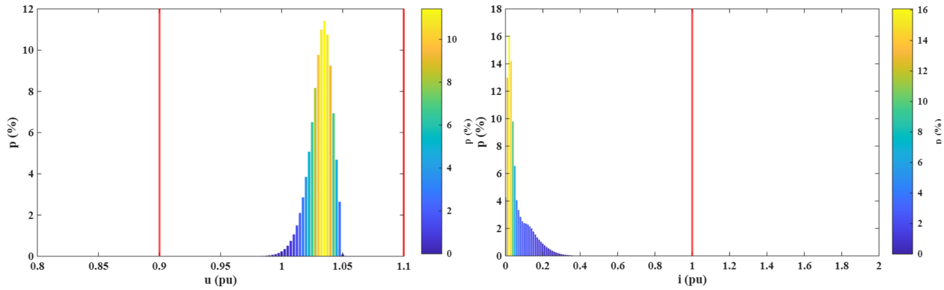

Figure 6: Spectrum of nodal voltages (left) and section currents (right)

As can be seen in Figure 6, neither voltages nor currents violate the operational limits, and a significant safety margin is maintained. The network can therefore be declared safe under any standard operating conditions in this scenario.

3.2 Case 2 – network conditions close to the operational limits

In this case, the customer composition was changed to 50 % Type 1, 30 % Type 2 and 20 % Type 3. The early autumn period was selected for this scenario, so the impact of heat pump and direct electric heating use is relatively limited. The composition was chosen deliberately to demonstrate a network operation close to its operational limits, including occasional violations.

As in the previous case, the analysis begins with a global view of the voltages and currents. The normalised voltage and current spectra are shown in Figure 7.

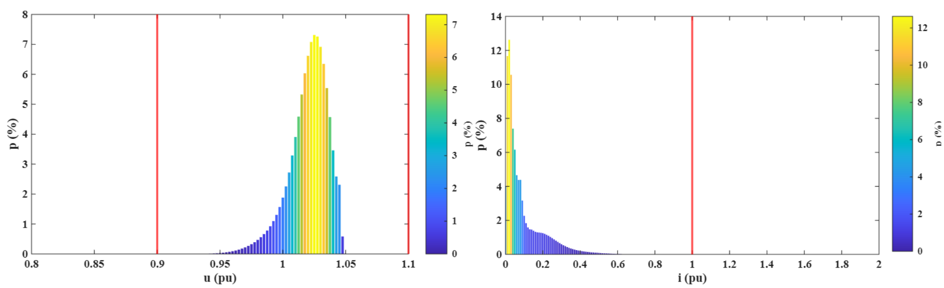

Figure 7: Spectrum of the nodal voltages (left) and section currents (right) for case 2

Compared to the reference scenario, the spectrum of values is wider; however, at first glance there still appears to be a reasonable safety margin. This global view can, however, conceal local anomalies easily. Because the total number of voltage and current samples is very large, with the majority of values well within the limits, the occasional violations are obscured completely. The global view therefore has limited informational value, and a per-element approach is significantly more useful.

In this approach, the voltage and current results are first grouped by the associated network element (node or line section). A separate histogram is then computed for each group. The histograms can be evaluated individually, or, when homogeneous bin spacing is used, stacked to form a 2D structure that can be visualised as a heat map –the stochastic load model is constructed in the same way. This approach allows potentially problematic elements to be identified immediately. The visualisation is configured to display any non-zero probability for a given voltage or current loading category.

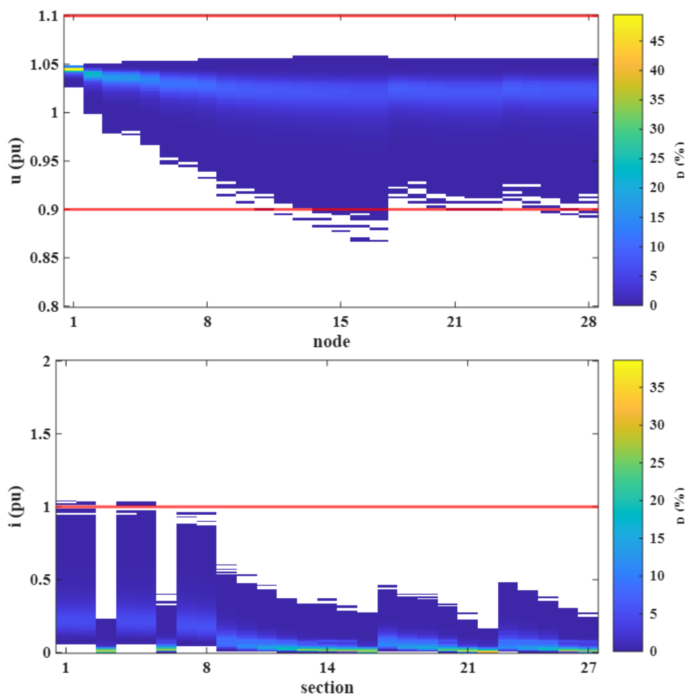

Figure 8: Spectrum of the nodal voltages (top) and section currents (down) for each individual element of the network

From Figure 8 it can be seen that voltage violations of the lower limit were observed at nodes 12–17 and 26–28, with node 17 being the most problematic. These results are consistent with the network topology: node 17 (N16) is located at the end of the trunk, while node 28 (N27) is located at the end of the lower side branch.

A similar situation is observed for the current loading: sections 1, 2, 4 and 5 can be overloaded occasionally and slightly (up to 1.04 pu). The most heavily loaded sections are those at the beginning of the feeder, which supply the majority of the network load (with section 1 carrying the total loading current).

For a network operator, however, the critical information is not merely the existence of possible limit violations, but the ability to quantify their expected frequency and probability. An occasional violation of voltage or current limits may be acceptable from the operator's perspective, not warranting costly network reinforcement. The key benefit of the proposed stochastic modelling technique is precisely this ability to quantify the probability of voltage and current extremes, enabling informed decisions on how to mitigate potential problems.

In this scenario, 9 of the 1,000 simulated daily scenarios contain at least one undervoltage event – that is, at least one node in the network falls below the voltage limit during at least one of the 288 time intervals comprising the simulated day. This corresponds to a probability of 0.9 % per day. Similarly, 3 of the 1,000 simulated scenarios contain at least one overcurrent event anywhere in the network.

The frequency and amplitude of these events are sufficiently low that no immediate network reinforcement is necessary, although the results do indicate that further changes in the customer mix could require a network upgrade within a reasonable time horizon.

Furthermore, because the modelling technique accounts for the time-varying behaviour of consumers throughout the day, it is also possible to analyse the spectrum of voltage and current amplitudes at selected elements across individual time intervals of the day. Figure 9 shows the 24-hour voltage amplitude spectrum for node 17 (N16) and the relative current loading spectrum for line section 1.

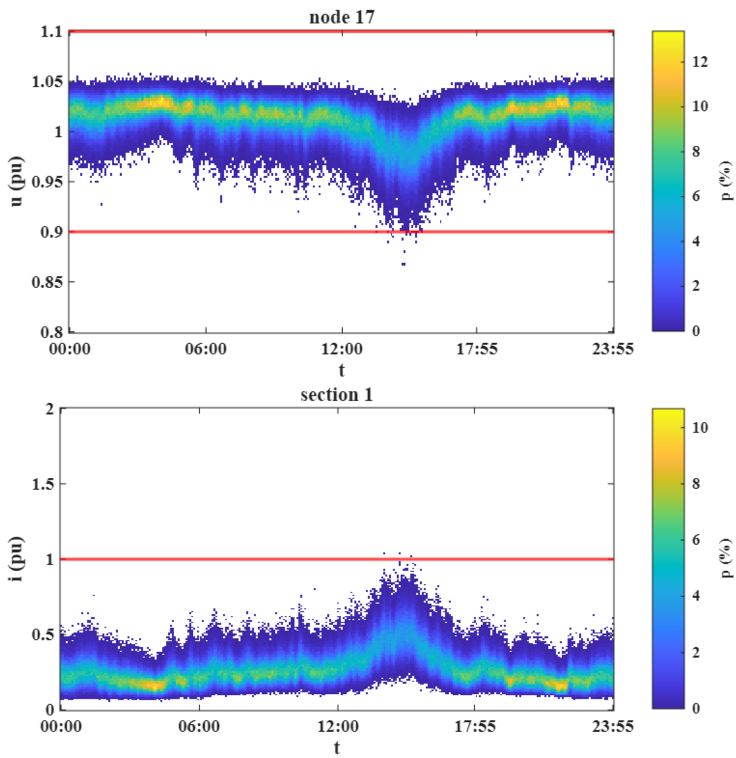

Figure 9: Spectrum of the voltage amplitudes for node 17 (top) and relative current loading for section 1 (down) for individual time intervals of a day

It can be seen that the undervoltage and overcurrent events are concentrated in a limited time window at around 15:00. This consumption peak is caused primarily by Type 3 customers returning home from work, typically between 14:00 and 16:00, and connecting their vehicles to a wall box charger.

This example demonstrates that the proposed methodology enables both spatial and temporal analysis of network operating conditions, including the quantification of the probability and frequency of operational extremes.

3.3 Case 3 – Extensive use of electric heating

The final case uses the same customer composition as Case 2, but simulates operation during the winter season. In this case, both Type 2 and Type 3 customers exhibit significantly increased consumption due to extensive use of electrical heating. As a result, frequent violations of the operational limits are expected.

As shown in Figure 10, a significant number of undervoltage events can be observed, with voltages falling as low as 0.80–0.85 pu; the lowest simulated value was 0.72 pu. A notable number of overcurrent events are also visible, with relative loading reaching 1.4 pu (while some rare events, not visible in the histogram, can reach up to 1.9 pu). Following the same definition as in Case 2, the probability that at least one undervoltage event occurs anywhere in the network during a simulated day is 6 %, while the corresponding probability for an overcurrent event is approximately 2.5 %. Given such high incidence rates, a significant portion of the network is affected – not only the most distant nodes and the first line sections.

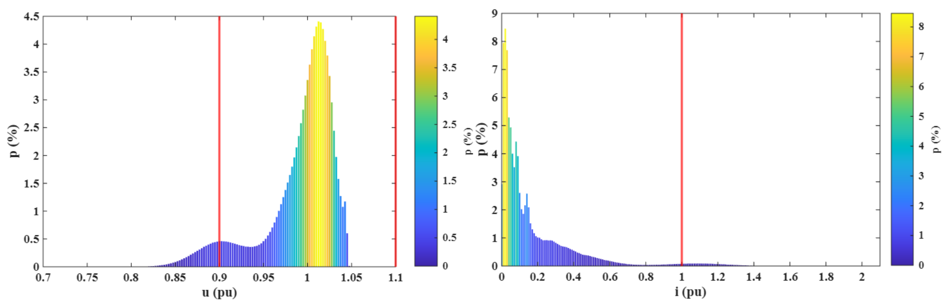

Figure 10: Spectrum of the nodal voltages (left) and section currents (right) for case 3

As shown in Figure 11, most of the network, with the exception of the first five nodes, experiences undervoltage events of varying depth and frequency.

Figure 12 shows that overloading is expected throughout the entire frontal section of the network up to the central junction of the side branches, including the first section of the upper side branch. The most critical elements remain node 17 (N16) and the first section (S1).

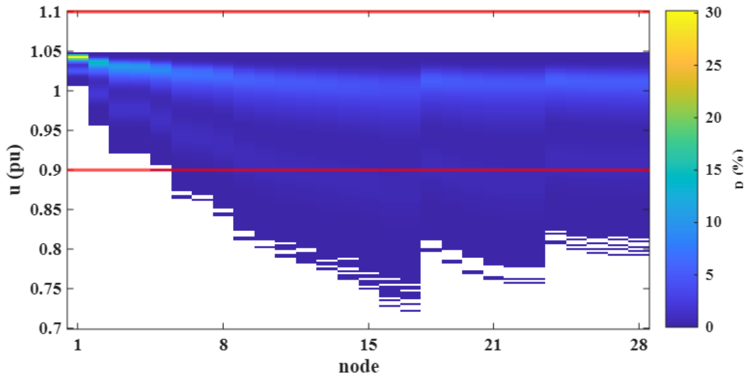

Figure 11: Spectrum of the nodal voltages for each individual element of the network

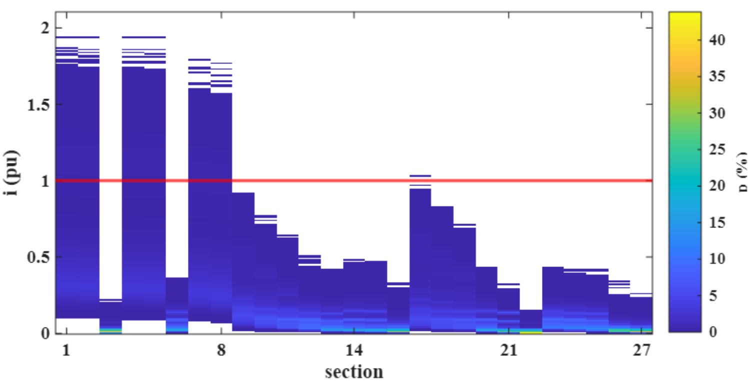

Figure 12: Spectrum of the section currents for each individual element of the network

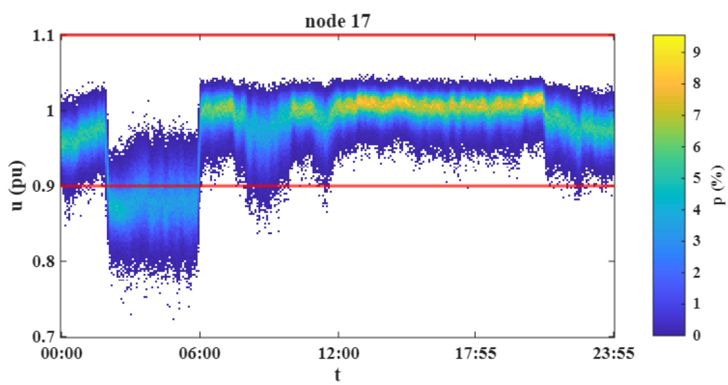

Figure 13: Spectrum of the voltage amplitudes for node 17 for individual time intervals of a day

The temporal analysis is even more revealing in this case. From the heat map in Figure 13, it can be seen that most critical events are concentrated in the interval between 01:00 and 06:00.

A sudden and steep increase in the overall loading causes a significant voltage drop during this interval. The underlying cause is straightforward: the simultaneous activation of the low electricity tariff triggers the start of heat pumps, boilers and direct heaters, which are typically blocked during the high-tariff period. At 06:00, the low tariff ends, shifting the household heating activity to off-peak hours. A similar pattern can be observed in the current loading spectrum shown in Figure 14.

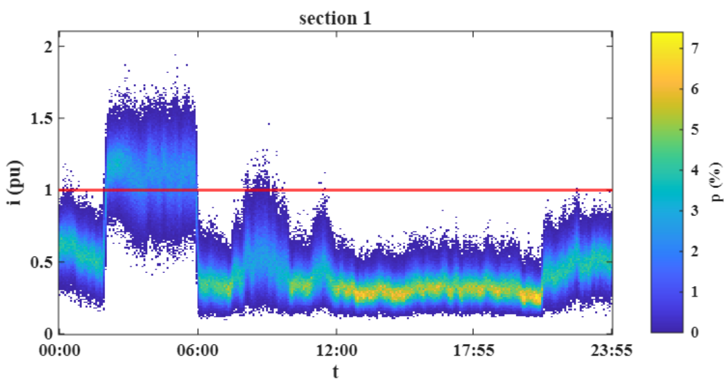

Figure 14: Spectrum of the relative current loading of section 1 for individual time intervals of a day

During this night-time interval, the relative loading of section 1 is between 1.0 and 1.5 pu for most of the period. Under such conditions the network cannot be operated reliably, and the DSO must either limit the number of customers with electrical heating, reinforce the network significantly, or implement a coordination strategy that prevents the simultaneous activation of thermal appliances within the same interval.

In response to these trends, the DSO has already decided to increase the network capacity by splitting the network into two sections: the first covering nodes N1–N16, and the second covering the side branches with nodes N17–N27, connected to the DTS via an aerial bundled cable (ABC) line. This solution increases both the network capacity and security of supply. While this upgrade was not part of the present study, it illustrates that the DSO is aware of the trends identified by the proposed analysis method and has begun implementing preventive measures. Notably, the proposed methodology could also be used directly to evaluate the effectiveness of such upgrades prior to their implementation.

4 Discussion

While the results illustrate the potential of the proposed methodology, an important question is whether the results are consistent with the operation of a real network. A full performance validation would require substantial cooperation with a distribution system operator to obtain detailed customer specifications and access to the infrastructure needed for field measurements. Such field validation is planned for the future; however, no agreement with a DSO for this purpose is currently in place.

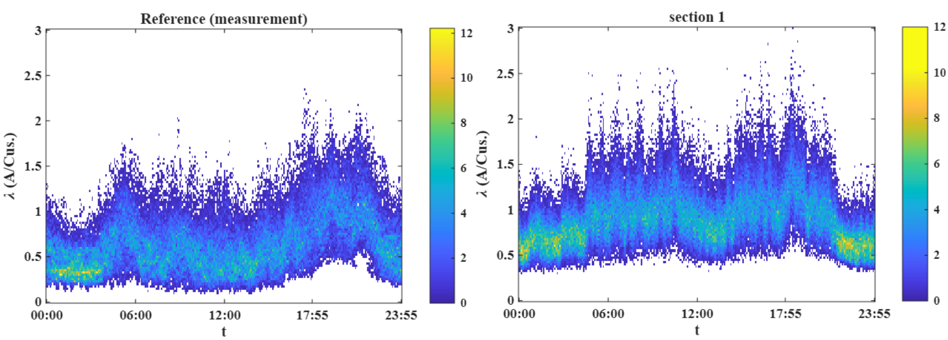

Figure 15: Spectrum of loading factor values for a real distribution transformer (left) and simulation according to Case 1 (right)

Some partial verification of the obtained results is nevertheless possible. To compare the behaviour of a real network with the simulation results, an older dataset of measurements acquired from the secondary side of several 22/0.4 kV distribution transformers can be used, originally collected during a power quality monitoring campaign focused on the power factor and voltage imbalance in low-voltage networks. Because the transformers fed low-voltage feeders with different numbers of consumers, the measured current and power profiles were normalised with respect to the total number of consumers in the corresponding network. This allows the spectrum of loading amplitude to be analysed in a manner similar to that presented in this study (Figure 5), although the analysed variable is not the per-unit current relative to line ampacity, but a loading factor λ related to the number of consumers in the network, with units of A/customer. By recalculating the current loading results for section S1 in terms of this loading factor, the measured and simulated current loading spectra can be compared directly as heat maps.

A direct quantitative validation of the simulated results against measurement data is not possible in this case, as the exact customer composition of the measured network is unknown. A qualitative comparison between the measured relative loading spectrum at the distribution transformer low-voltage output and the simulated spectrum for section 1 is, however, possible. Despite the uncertainty in customer composition, the two heat maps exhibit a comparable overall structure: similar daily loading envelopes, probability density concentration in a similar relative range, and similar scatter characteristics in the upper loading region. This supports the plausibility of the proposed modelling approach, even though precise quantitative agreement cannot be established at this stage.

Beyond this partial verification, the presented case studies demonstrate further the potential of the proposed methodology to analyse operating conditions in the investigated network, and to estimate the impact of changes in consumer behaviour on network performance. The methodology provides both a spatial and a temporal view of network conditions, and allows the probability of technical limit violations to be quantified.

The methodology is based on standard tools of statistical analysis, and does not require the training and verification procedures associated with AI-based models, the mathematical complexity of copula-based or regression models, or the detailed configuration effort of bottom-up approaches based on individual appliance usage modelling.

There are, however, known limitations of the proposed method in its current form. First, the methodology is unable to generate temporally correlated time series. Although the generated dataset resembles a collection of time series superficially, there is no temporal correlation between the individual samples. If the sequence of generated values were treated as a time series, the resulting collection would not exhibit the statistical properties of a real power profile – with the exception of the marginal value spectrum. As a consequence, the methodology is not suitable for problems where the time integral of voltages or currents plays a critical role, such as the dimensioning of battery energy storage systems or the calculation of the thermal loading of equipment. This limitation also has a direct bearing on the interpretation of the violation probabilities reported in Section 3. Although each simulated scenario spans a full day comprised of 288 time intervals, the values generated for these intervals are statistically independent: there is no temporal correlation linking consecutive intervals within a scenario. The reported "per day" probabilities should therefore be understood as the probability that at least one violation occurs somewhere within an independently sampled set of 288 time intervals representing one day rather than as a description of the duration, timing pattern, or sequential persistence of violation events. The probability that a violation occurs at a specific node or section during a specific time interval is unaffected by the absence of temporal correlation, since it depends only on the marginal distribution of that interval; what cannot be inferred from the model is whether, or for how long, a violation might persist once it occurs.

Second, the methodology is currently implemented only for symmetrical (balanced) load flow analysis. In practice, however, the operation of low-voltage networks is typically significantly unbalanced. An extension supporting asymmetric load modelling is currently under development; it will allow the generation of per-phase power profiles that reflect the asymmetry patterns observed in the measured data. This extension was not completed at the time of writing, and will be the subject of a future publication.

Because the method is based on a Monte Carlo approach, it requires an efficient implementation of the load flow solver. Using modern hardware, however, very short solution times are achievable, even for extremely large numbers of scenarios. A nonlinear solver based on the Jacobi method, implemented to exploit GPU computing, can solve several hundred thousand load flow scenarios in a short time. To illustrate the hardware accessibility of the approach: solving all 288,000 scenarios for the investigated network configuration took approximately 70 seconds on a Quadro K2200, an entry-level professional GPU from 2014. On a current mid-range GPU (RTX 5070Ti), the same task is completed in under 10 seconds.

5 Conclusion

Stochastic modelling of low-voltage networks is essential for understanding the current and future bottlenecks in distribution systems, and can support the network planning and decision-making processes of distribution system operators significantly. The presented methodology offers a straightforward, easy-to-implement solution based on a system of histograms describing the probability density distribution of power consumption profiles, including modelling of the power factor. The framework is extensible, with ongoing work targeting the representation of load asymmetry and other power quality parameters.

The primary limitation of the methodology is that it provides only a spectrum of temporally uncorrelated samples, and is therefore not suitable for problems requiring proper time series data, such as battery sizing or thermal analysis. Future work will focus on addressing this limitation, alongside the completion of the asymmetric load flow extension.

Nevertheless, the method is capable of identifying possible violations of operational limits, quantifying the probability and frequency of such events, and providing both spatial and temporal analysis of their occurrence. In this respect it outperforms the traditional deterministic approaches currently used for modelling low-voltage network operation substantially, while remaining accessible to practitioners without specialist expertise in statistical modelling or machine learning.

Acknowledgment

The authors acknowledge the use of an AI-based tool (Claude Sonnet 4.6) for language editing and grammatical correction. No generative AI tools were used in the development of the scientific content, analysis, or conclusions of this article.

Nomenclature

ABC	Aerial Bundled Cable	EV	Electric Vehicle
AMI	Advanced Metering Infrastructure	GPU	Graphical Processing Unit
ANN	Artificial Neural Networks	IMS	Intelligent Metering System
BESS	Battery Energy Storage System	LV	Low Voltage
CDF	Cumulative Distribution Function	PDF	Probability Density Function
DSO	Distribution System Operator	PV	Photovoltaics
DTS	Distribution Transformer Station		

References

Bahernik, M., Höger, M., Petrik, F. (2026) Stochastic Modelling of Low-Voltage Distribution Feeder Operation. *Proceeding of the 26th International Conference on Electric Power Engineering EPE2026*, Opole, Poland

Beláň, A, et al. (2022). Stochastic Analysis of Battery Storage Systems Integration to the Real Distribution Network with Variable Penetration Levels of PV Systems. *Proceedings of International Conference on Smart Systems and Technologies SST 2022*, Osijek, Croatia, pp. 237-242, doi: 10.1109/SST55530.2022.9954873

Damianakis, N., Mouli, G.R.C, Bauer, P. (2025) Grid impact of photovoltaics, electric vehicles and heat pumps on distribution grids – An overview, *Applied Energy*, vol. 380, doi:10.1016/j.apenergy.2024.125000

Devroye, L. (1986). *Non-uniform random variate generation*, Springer, New York, USA, doi:10.1007/978-1-4613-8643-8

Höger, M., Bahernik, M., Petrik, F. (2026) Modified Jacobi Method for Efficient Multi-Scenario Load Flow Analysis, *Advanced Power Systems Conference 2026*, Cluj-Napoca, Romania

Höger, M., Bracinik, P., Bahernik, M. (2026) Stochastic modelling of low voltage distribution networks. *7th International Scientific Conference Energy and Responsibility EnRe*, Velenje, Slovenia

Jang, H., Kang, J. (2016) A stochastic model of integrating occupant behaviour into energy simulation with respect to actual energy consumption in high-rise apartment buildings, *Energy and Buildings*, vol. 121, doi: 10.1016/j.enbuild.2016.03.037

Kalos, M.H., Whitlock, P.A. (2008) *Monte Carlo Methods*, 2nd ed., Wiley-VCH

Martellotta, F., Stefanizzi, A. U., Sacchetti, A., Riganti, G. (2017) On the use of artificial neural networks to model household energy consumptions, *Energy Procedia,* vol. 126, pp. 250-257, doi: 10.1016/j.egypro.2017.08.149

Nelsen, R. B.(2006) An Introduction to Copulas, Springer Nature

Stagg, G.W., El-Abiad, A.H. (2019) *Computer Methods in Power System Analysis*, Medtech, ISBN:9388716159

Wolpert, D. H., & Macready, W. G. (1997). No free lunch theorems for optimization. *IEEE Transactions on Evolutionary Computation*, 1(1), 67-82. https://doi.org/10.1109/4235.585893

Yildirim, F., Arslan, H. (2024), Energy Consumption Forecasting Using Time Series Analysis Methods, *International Conference on Science, Engineering Management and Information Technology SEMIT 2023*, Ankara, Turkey, doi: 10.1007/978-3-031-72287-5_9

Povzetek v slovenskem jeziku

Stohastično modeliranje obratovanja nizkonapetostnega distribucijskega omrežja. Modeliranje obratovanja nizkonapetostnega distribucijskega omrežja postaja vse zahtevnejše. V preteklosti so za ocenjevanje obratovalnih razmer zadostovale deterministične metode, povzete iz analiz srednjenapetostnih in prenosnih elektroenergetskih omrežij. Vendar pa spremembe v vedenju odjemalcev, strukturi gospodinjskih električnih naprav ter vse večja razširjenost sončnih fotonapetostnih sistemov, polnjenja električnih vozil, toplotnih črpalk in klimatskih naprav pomembno spreminjajo obratovalne razmere v nizkonapetostnih omrežjih. Ker sta poraba in proizvodnja posameznih odjemalcev izrazito stohastični, deterministične metode postajajo vse manj primerne za ustrezno analizo obratovanja omrežja in načrtovanje njegovega razvoja.

V prispevku je predstavljena preprosta metoda stohastičnega modeliranja obratovanja omrežja, pri kateri je vedenje odjemalcev opisano s sistemom histogramov. Predstavljeni pristop omogoča poglobljeno analizo obratovalnih razmer v nizkonapetostnih omrežjih, prepoznavanje potencialnih obratovalnih ekstremov, ki lahko ogrozijo varno obratovanje omrežja, ter hkrati določa pogostost in verjetnost pojava takšnih dogodkov. Uporaba metode je prikazana na primeru tipičnega podeželskega distribucijskega omrežja.

JOURNAL OF ENERGY TECHNOLOGY
Vol. 19, No. 1, pp. 55–68, July 2026

Original Scientific Article

USING A HIGH-TEMPERATURE HEAT PUMP FOR HEATING GREENHOUSES

Submitted
4. 6. 2026

Accepted
26. 6. 2026

Published
15. 7. 2026

ALMINA SARAJLIĆ, JURIJ AVSEC, URŠKA NOVOSEL
University of Maribor, Faculty of Energy Technology, Krško, Slovenia
almina.sarajlic@um.si, jurij.avsec@um.si, urska.novosel@um.si

CORRESPONDING AUTHOR
almina.sarajlic@um.si

Abstract Greenhouse heating is associated with high energy consumption and operating costs, particularly during winter conditions. This study investigates the application of a geothermal high-temperature heat pump for greenhouse heating in northeastern Slovenia. A case study greenhouse used for rose cultivation was analysed, to determine heat losses, heating demand and economic feasibility. The heat loss calculations were performed using the greenhouse geometry, the thermal properties of double-wall polycarbonate panels, and the minimum outdoor temperatures recorded between October 2023 and April 2024. The results showed that the maximum heating demand reached 91.31 kW, exceeding the capacity of the existing 80 kW electric heater. Consequently, a Thermeco2 HHR180 high-temperature heat pump was selected, with a heating capacity of 130 kW and a coefficient of performance (COP) of 4.78. An economic analysis indicated annual savings of €29,143.07 and a payback period of 6.55 years. The findings confirm that high-temperature heat pumps represent a technically feasible and economically viable solution for improving energy efficiency and sustainability in greenhouse production.

Keywords
geothermal high-temperature heat pump,
greenhouse heating,
greenhouse,
heat losses,
renewable energy sources

https://doi.org/10.18690/jet.19.1.53-68.2026
CC-BY, text © Sarajlić, Avsec, Novosel, 2026
This work is licensed under the Creative Commons Attribution 4.0 International License.
This license allows reusers to distribute, remix, adapt, and build upon the material in any medium or format, so long as attribution is given to the creator. The license allows for commercial use. https://creativecommons.org/licenses/by/4.0

University of Maribor Press

1 Introducton

Agricultural production is challenged increasingly by rising energy costs and environmental requirements. Greenhouse cultivation enables year-round production of flowers, vegetables and other high-value crops by providing controlled environmental conditions. However, maintaining the required indoor temperature during colder periods results in substantial energy consumption and operational costs.

Conventional greenhouse heating systems are commonly based on direct electric heating, natural gas, fuel oil, or biomass. Although these systems are capable of maintaining the desired thermal conditions, they often exhibit low energy efficiency, or generate considerable greenhouse gas emissions. Consequently, there is a growing interest in alternative heating technologies, that can reduce energy consumption while maintaining stable climatic conditions.

High-temperature heat pumps have emerged as a promising solution for applications requiring elevated supply temperatures. Unlike conventional heat pumps, these systems can produce water temperatures exceeding 80 °C while maintaining relatively high efficiency. Recent developments in refrigerants, compressor technologies and system integration have expanded their applicability in industrial processes, district heating systems and agricultural facilities significantly (Cox & T. L. J., 2023; Sun et al., 2023).

Previous studies have demonstrated that heat pump systems can reduce energy consumption in greenhouse applications significantly. Improved energy performance and reduced operating costs were reported when geothermal heat pumps were implemented in greenhouse heating systems (Anifantis et al., 2016). Furthermore, the integration of renewable heat sources contributes to lower greenhouse gas emissions and the improved sustainability of agricultural production.

The objective of this study is to evaluate the technical and economic feasibility of implementing a geothermal high-temperature heat pump for greenhouse heating. A case study greenhouse was analysed, used for rose cultivation in northeastern Slovenia. The research includes the determination of thermal losses, calculation of the required heating capacity, selection of a suitable heat pump and assessment of the investment costs and payback period.

2 Materials and Methods

2.1 Case Study Description

The investigated greenhouse is located in the vicinity of Maribor, Slovenia, and is used for commercial rose cultivation, as shown in Figure 1. The greenhouse consists of a steel structure covered with 10 mm double-wall polycarbonate panels. Due to the relatively high thermal transmittance of greenhouse covering materials compared with conventional buildings, the heating demand remains substantial during winter conditions.

Figure 1: Greenhouse used for rose cultivation in the case study
Source: own

The greenhouse dimensions were determined according to published greenhouse design guidelines (Nemali, 2021). The greenhouse width is 11 m, the length is 36 m and the sidewall height is 2.3 m.

The total envelope area was determined according to the greenhouse geometry using Equation (1):

$$A = 2ac + 2bc + (\pi ab/2) + (\pi a^2/4) \quad (1)$$

where A represents the total greenhouse envelope area (m²), a is the greenhouse width (m), b is the greenhouse length (m), and c denotes the sidewall height (m). The calculated total envelope area equals 933 m².

The target indoor temperature during the heating season was set to 16 °C, which corresponds to the typical cultivation requirements for roses.

2.2 Climatic Data

The thermal calculations were based on meteorological data obtained from the Slovenian Environment Agency (Agencija Republike Slovenije za okolje [ARSO], 2024). The analysis considered the minimum recorded monthly temperatures between October 2023 and April 2024, representing the heating season relevant for greenhouse operation.

The minimum temperatures were:

– October: –2.3 °C
– November: –6.5 °C
– December: –11.0 °C
– January: –15.2 °C
– February: –13.7 °C
– March: –7.8 °C
– April: –2.9 °C

These values were used to determine the maximum temperature difference between the indoor and outdoor conditions for each month.

2.3 Heat Loss Calculation

The heat losses through the greenhouse envelope were calculated using the standard heat transfer equation (2):

$$Q_{env} = U_{env} \times A_{env} \times \Delta T \quad (2)$$

where Q_{env} is the heat loss through the greenhouse envelope (W), U_{env} is the thermal transmittance coefficient of the envelope (W/m²K), A_{env} is the envelope area (m²), and ΔT represents the temperature difference between the indoor and outdoor environments (K). For the 10 mm double-wall polycarbonate panels, a thermal transmittance coefficient of 2.5 W/m²K was adopted according to manufacturer`s specifications (Akripol, 2014).

The ground heat losses were determined using Equation (3):

$$Q_g = U_g \times A_g \times \Delta T \quad (3)$$

where Q_g denotes the heat loss through the ground (W), U_g is the ground thermal transmittance coefficient (W/m²K), and A_g is the greenhouse floor area (m²). A ground thermal transmittance coefficient of 1.5 W/m²K was adopted, based on the published thermal property data (Engineering ToolBox, 2024).

The total required heating capacity was obtained as the sum of the envelope and ground heat losses, as shown in Equation (4):

$$Q = Q_{env} + Q_g \quad (4)$$

where (Q) represents the total heating capacity required to maintain the desired indoor temperature within the greenhouse.

2.4 Heat Pump Selection

A suitable high-temperature heat pump was selected following the determination of the peak heating load. The selection criteria included:

- the heating capacity,
- the coefficient of performance (COP),
- the operating temperature range,
- compatibility with the groundwater heat sources,
- economic feasibility.

A Thermeco2 HHR180 geothermal high-temperature heat pump was selected based on the calculated peak heating demand, (ENGIE, 2024) .

3 Results

3.1 Heat Loss Analysis

Table 1 presents the calculated heat losses and heating requirements during the analysed heating season.

Table 1: Monthly heat losses and required heating capacity

Month	Minimum temperature (°C)	Ground losses (kW)	Envelope losses (kW)	Heating demand (kW)
October	-2.3	10.87	42.68	53.55
November	-6.5	13.37	52.48	65.85
December	-11.0	16.04	62.98	79.02
January	-15.2	18.53	72.77	91.31
February	-13.7	17.64	69.28	86.92
March	-7.8	14.14	55.51	69.65
April	-2.9	11.23	44.08	55.31

The variation in the heating demand throughout the heating season is illustrated in Figure 2.

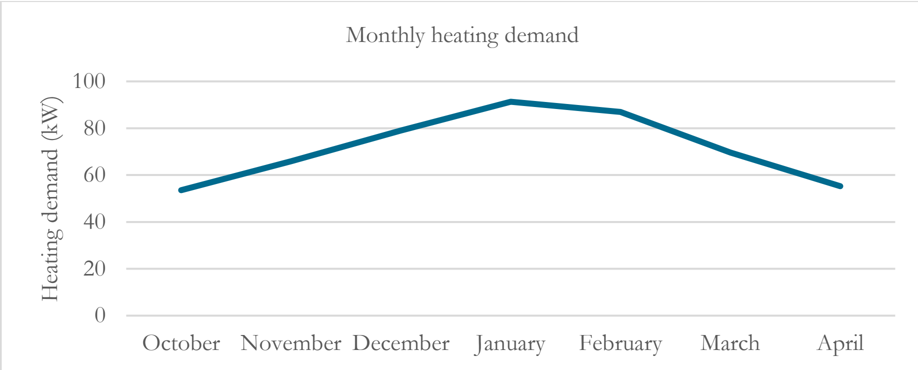

Figure 2: Monthly heating demand of the greenhouse during the heating season
Source: own

The results indicate that the heating demand depends strongly on outdoor temperature. The maximum heating load occurred during January and reached 91.31 kW. The existing electric heater installed in the greenhouse has a nominal capacity of 80 kW. Consequently, the existing system is unable to maintain the desired indoor temperature under the most demanding winter conditions.

3.2 Heat Pump Selection Results

Based on the calculated peak heating demand, The Thermeco2 HHR180 heat pump was selected based on the calculated peak heating demand. The main technical characteristics are summarised in Table 2.

Table 2: Main technical characteristics of the selected heat pump

Parameter	Value
Heating capacity	130 kW
Cooling capacity	85 kW
Maximum electrical power consumption	60 kW
COP	4.78
Refrigerant	CO_2
Maximum outlet temperature	90 °C

The selected heat pump provides sufficient reserve capacity above the calculated peak demand, ensuring reliable operation during extreme weather conditions.

Although the calculated peak heating demand of the greenhouse was 91.31 kW, the selected heat pump has a nominal heating capacity of 130 kW. This difference is related primarily to the limited range of commercially available units offered by the manufacturer, as no intermediate model with a capacity closer to the calculated demand was available. Therefore, the next larger unit was selected, to ensure reliable operation under extreme weather conditions.

According to the manufacturer's technical documentation, the coefficient of performance (COP) of the selected heat pump depends on the operating conditions, particularly the heat source temperature and the heating water supply temperature. The reported COP value of 4.78 corresponds to the operating conditions specified by the manufacturer, and was therefore adopted for the purposes of this study (ENGIE, 2024).

In addition, the selected capacity provides opportunities for future expansion of the heating system. A residential building located in the immediate vicinity of the greenhouse could potentially be connected to the same heat pump system for space heating and domestic hot water preparation. Consequently, the additional capacity increases the flexibility of the installation, and may improve the overall utilisation of the heat pump throughout the year.

4 Economic Analysis

The estimated investment cost includes the heat pump unit, installation works and groundwater wells required for the water-to-water system configuration.

The total investment cost was estimated at €190,000. The investment costs for the groundwater wells were estimated according to the published market price data (Daibau International, 2024). The greenhouse is currently heated using electric resistance heating. Based on the annual heat demand and published electricity prices, the annual heating cost was estimated at €36,854.94 (GEN-I, 2023).

The annual heating cost of the existing electric resistance heater was calculated according to Equation (5):

$$C_{EH} = Q_{annual} \times c_e \tag{5}$$

Substituting the calculated values gives:

$$C_{EH} = 196{,}332 \times 0.18776 = 36{,}854.94 \text{ €}$$

where C_{EH} is the annual heating cost (€), Q_{annual} is the annual heating demand (196,332 kWh), and c_e is the electricity price (0.18776 €/kWh).

After the implementation of the heat pump the annual electricity consumption was reduced significantly due to the high COP value.

The annual electricity consumption of the heat pump was determined from the annual heating demand and the coefficient of performance (COP):

$$E_{HP} = \frac{Q_{annual}}{COP} \tag{6}$$

where E_{HP} is the annual electricity consumption of the heat pump (kWh).
Substituting the calculated values:

$$E_{HP} = \frac{196{,}332}{4.78} = 41{,}073 \text{ kWh/year}$$

The annual operating cost of the heat pump was then calculated as:

$$C_{HP} = E_{HP} \times c_e \tag{7}$$

which resulted in

$$C_{HP} = 41{,}073 \times 0.18776 = 7{,}711.87 \text{ €}$$

A comparison of the annual heating costs for the existing electric heater and the proposed heat pump system is presented in Figure 3.

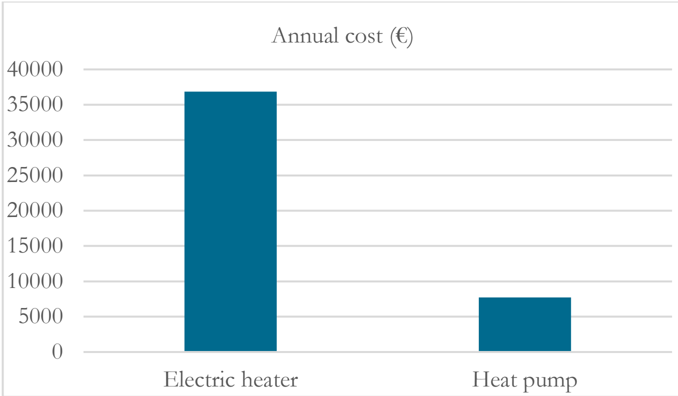

Figure 3: Comparison of the annual heating costs for the existing electric heater and the proposed heat pump system

Source: own

The annual savings were determined as the difference between the annual heating costs of the existing electric heater and the proposed heat pump system:

$$S = C_{EH} - C_{HP} \tag{8}$$

where S represents the annual savings (€).

Substituting the calculated values gives:

$$S = 36{,}854.94 - 7{,}711.87 = 29{,}143.07\ €$$

The simple payback period was calculated using Equation (9):

$$PB = \frac{I}{S} \tag{9}$$

where PB is the payback period (years), I is the investment cost (€190,000), and S is the annual savings.

Substituting the calculated values yields:

$$PB = \frac{190\ 000}{29\ 143.07} = 6.55 \text{ years}$$

The calculated payback period should be interpreted as an approximate value, as the analysis was performed under simplified assumptions and ideal operating conditions. Future changes in electricity prices, maintenance requirements and actual system performance may affect the economic viability of the proposed solution.

The economic analysis was based on the investment costs, electricity consumption and current electricity prices. The maintenance and servicing costs of the heat pump system were not included in the calculation, and therefore represent a limitation of the presented economic assessment. However, these costs are generally considerably lower than the achieved annual energy savings, and are not expected to affect the overall economic feasibility of the proposed solution significantly.

5 Discussion

The obtained results demonstrate that high-temperature heat pumps represent a technically feasible solution for greenhouse heating applications. The calculated peak heating demand of 91.31 kW confirms that the existing 80 kW electric heater is insufficient under extreme winter conditions, highlighting the need for a more efficient heating system.

The selected Thermeco2 HHR180 heat pump provides a substantial safety margin, while maintaining a high coefficient of performance. Similar findings have been reported, identifying high-temperature heat pumps as an effective technology for replacing conventional electric and fossil-fuel-based heating systems (Cox & T. L. J., 2023). The achieved COP value of 4.78 is consistent with the performance range reported for modern high-temperature heat pump systems (Sun et al., 2023). Such efficiency enables significant reductions in the electricity consumption and operating costs.

From an economic perspective, the calculated payback period of 6.55 years can be considered favourable given the expected service life of the equipment, which typically exceeds 20 years. After the payback period, the system continues generating considerable annual savings.

In addition to the economic benefits, the proposed solution contributes to environmental sustainability. The reduced electricity consumption lowers greenhouse gas emissions indirectly and supports the transition towards low-carbon agricultural production.

6 Conclusions

This study investigated the application of a geothermal high-temperature heat pump for greenhouse heating in northeastern Slovenia.

The heat loss calculations revealed that the greenhouse requires a maximum heating capacity of 91.31 kW during the coldest winter period. Replacement with a more efficient heating technology was considered, since the existing 80 kW electric heater cannot satisfy this demand.

A Thermeco2 HHR180 high-temperature heat pump was selected with a heating capacity of 130 kW and a COP of 4.78. The economic analysis demonstrated annual savings of €29,143.07 and a payback period of 6.55 years.

The results confirm that high-temperature heat pumps can provide reliable greenhouse heating while reducing operating costs and improving energy efficiency significantly. The technology therefore represents a promising solution for sustainable greenhouse production and broader agricultural decarbonisation efforts.

Future research could focus on a more detailed analysis of the seasonal performance of high-temperature heat pumps under varying operating conditions. Additionally, further studies could investigate the integration of greenhouse heating systems with nearby residential buildings and domestic hot water preparation, in order to improve the overall utilisation of the installed heating capacity and enhance the economic performance of the system.

References

Agencija Republike Slovenije za okolje. (2024). ARSO Meteo. https://meteo.arso.gov.si

Akripol. (2014). Zasteklitev s prekatnim polikarbonatom. https://www.akripol.si/wp-content/uploads/2019/09/katalog-polikarbonatne-plosce-si.pdf

Anifantis, A. S., Pascuzzi, S., & Scarascia-Mugnozza, G. (2016). Geothermal source heat pump performance for a greenhouse heating system: An experimental study. Journal of Agricultural Engineering, 47(3),164–170. https://doi.org/10.4081/jae.2016.544

Cox, S. B. G. C., & T. L. J. (2023). High-temperature heat pump model documentation and case studies. National Renewable Energy Laboratory. https://www.nrel.gov/docs/fy23osti/84560.pdf

Daibau International. (2024). Vrtanje vrtin: Cena – vrtina za vodo, vrtina za toplotno črpalko, https://www.mojmojster.net/cene/globinsko_vrtanje_vrtin

Engineering ToolBox. (2024). Solids, liquids and gases – Thermal conductivities. https://www.engineeringtoolbox.com/thermal-conductivity-d_429.html

ENGIE. (2024). CO_2 high-temperature heat pump Thermeco2 HHR180: Technical documentation. [Internal technical documentation]

GEN-I. (2023). Redni cenik električne energije za gospodinjske odjemalce. https://gen-i.si/dom/elektricna-energija/ceniki-in-akcije/redni-cenik-elektricne-energije-za-gospodinjske-odjemalce/

Nemali, K. (2021). Heating and cooling greenhouses. Purdue University. https://www.purdue.edu/hla/sites/cea/wp-content/uploads/sites/15/2021/01/Heating-and-Cooling-in-Greenhouses-1.pdf

Sun, J., Wang, Y., Qin, Y., Wang, G., Liu, R., & Yang, Y. (2023). A review of super-high-temperature heat pumps over 100 °C. Energies, 16(12), 4591, https://doi.org/10.3390/en16124591

Povzetek v slovenskem jeziku

Uporaba visokotemperaturne toplotne črpalke za ogrevanje rastlinjakov. Ogrevanje rastlinjakov je povezano z visoko porabo energije in visokimi obratovalnimi stroški, zlasti v zimskem obdobju. Prispevek obravnava uporabo geotermalne visokotemperaturne toplotne črpalke za ogrevanje rastlinjaka v severovzhodni Sloveniji. Analiziran je bil rastlinjak za gojenje vrtnic z namenom določitve toplotnih izgub, potreb po ogrevanju in ekonomske upravičenosti investicije. Izračuni toplotnih izgub so bili izvedeni na podlagi geometrije rastlinjaka, toplotnih lastnosti dvojnostenskih polikarbonatnih plošč ter najnižjih zunanjih temperatur, zabeleženih v obdobju od oktobra 2023 do aprila 2024. Rezultati so pokazali, da največja potrebna moč za ogrevanje znaša 91,31 kW, kar presega zmogljivost obstoječega električnega grelnika moči 80 kW. Zato je bila izbrana visokotemperaturna toplotna črpalka Thermeco2 HHR180 z grelno močjo 130 kW in grelnim številom (COP) 4,78. Ekonomska analiza je pokazala letni prihranek v višini 29.143,07 € in vračilno dobo investicije 6,55 leta. Ugotovitve potrjujejo, da visokotemperaturne toplotne črpalke predstavljajo tehnično izvedljivo in ekonomsko upravičeno rešitev za izboljšanje energetske učinkovitosti in trajnosti pri pridelavi v rastlinjakih.

JOURNAL OF ENERGY TECHNOLOGY
Vol. 19, No. 1, pp. 69–82, July 2026

Original Scientific Article

DESIGN AND ECONOMIC ASSESSMENT OF A 19-SEAT HYDROGEN FUEL CELL AIRCRAFT FOR REGIONAL AVIATION

Submitted
3. 6. 2026

Accepted
2. 7. 2026

Published
15. 7. 2026

ANITA PRAPOTNIK BRDNIK, MARŠENKA MARKSEL
University of Maribor, Faculty of Civil Engineering, Transport Engineering and Architecture, Maribor, Slovenia
anita.prapotnik@um.si, marsenka.marksel@um.si

CORRESPONDING AUTHOR
anita.prapotnik@um.si

Abstract This paper summarises the results from the MAHEPA project, which investigated the technological and economic feasibility of 19-seat hydrogen fuel cell aircraft and their potential deployment towards 2050. It assesses the key requirements necessary to enable their operation and long-term viability. The analysis is structured in three parts. First, it addresses the required infrastructure and safety measures for hydrogen-based regional aviation, including production and distribution. Second, it evaluates the development needs of critical technological components such as fuel cells, hydrogen storage systems and propulsion integration. Third, it examines the economic feasibility, where the direct operating costs are linked strongly to the aircraft mass characteristics. The economic results for the 2030–2050 horizon indicate potential cost competitiveness under favourable hydrogen pricing and continued technology development, supporting hydrogen fuel cell aircraft as a viable option for regional aviation.

Keywords
fuel cell aircraft, hydrogen aircraft, regional aviation, MTOM estimation, direct operating costs, 19-seat aircraft

https://doi.org/10.18690/jet.19.1.69-82.2026
CC-BY, text © Praprotnik Brdnik, Marksel, 2026
This work is licensed under the Creative Commons Attribution 4.0 International License.
This license allows reusers to distribute, remix, adapt, and build upon the material in any medium or format, so long as attribution is given to the creator. The license allows for commercial use. https://creativecommons.org/licenses/by/4.0

University of Maribor Press

1 Introducton

Due to the increasing environmental concerns associated with greenhouse gas emissions, significant efforts have been undertaken within the European Union in both the political and research domains to reduce dependence on combustion engines and transition towards alternative energy sources. This transformation spans multiple sectors, from energy production to energy consumption. One of the most critical sectors in this context is transportation, which contributes a substantial share of global greenhouse gas emissions. Consequently, strategies are being developed, both to reduce the transportation demand (e.g., car sharing and public transport), and to enable a transition towards alternative propulsion systems, particularly electrification.

A clear example of this transition can be observed already in the automotive industry, where coordinated EU-funded initiatives have supported the development of charging infrastructure, technological maturity of electric vehicles, and economic viability through subsidies. As a result, electric vehicles now offer a competitive range (typically 300–500 km), acceptable charging times via fast-charging networks, and increasingly comparable purchase and operating costs. Consequently, their market penetration is increasing steadily and rapidly (EEA, 2025).

The key question is whether other transport sectors can follow a similar trajectory. Among these, the aviation sector represents one of the greatest challenges, due to its rapid growth, high emissions and significant technological constraints (EASA, 2025). In particular, the high specific energy requirements of flight make battery-electric solutions feasible only for very small aircraft with limited passenger capacity. Unless substantial breakthroughs in battery energy density occur, batteries are unlikely to provide a viable solution for regional aviation (Prapotnik Brdnik et al, 2019).

Alternative pathways include hydrogen-based propulsion and sustainable aviation fuels (SAF), including synthetic fuels. While synthetic fuels, produced through carbon capture and fuel synthesis processes, offer compatibility with existing infrastructure, their current production costs remain high, limiting the near-term economic feasibility (Cabrera and de Sousa, 2022). Hydrogen, on the other hand, offers a high gravimetric energy density, making it a promising candidate for aviation applications. However, it introduces significant challenges, including low volumetric energy density, complex storage requirements and safety considerations due to flammability (Adolf et al, 2017).

This study investigates the potential of hydrogen-powered regional aviation, and evaluates whether such systems can become a feasible future solution. The analysis is structured around three key aspects: (i) ground infrastructure readiness, (ii) technological readiness, and (iii) economic feasibility.

2 Ground infrastructure and hydrogen supply chain

Hydrogen is a tasteless, colourless, odourless, non-toxic and highly flammable gas. It is found in its pure form in nature rarely, but can be produced from various energy sources, such as natural gas and electricity (Adolf et al, 2017). Therefore, hydrogen should not be considered a primary energy source, but rather an energy carrier and storage medium. Its main advantages are its low mass and the wide range of production pathways available. However, its high flammability and the fact that, as the lightest element, it can leak easily through materials and cause embrittlement of certain metals, represent significant challenges (ISO, 2015). The hydrogen supply chain consists of four main steps: (a) production, (b) compression or liquefaction, (c) transportation, and (d) storage.

2.1 Hydrogen production

As already mentioned, hydrogen can be produced in various ways (Adolf et al, 2017). Currently, the most common production method is steam methane reforming. Hydrogen produced by this process is referred to as *grey hydrogen*. If carbon capture and storage technologies are incorporated into the process, the resulting product is known as *blue hydrogen*. Alternatively, hydrogen produced through water electrolysis powered by electricity generated from renewable sources is referred to as *green hydrogen*. At present, the production cost of green hydrogen is significantly higher than that of blue or grey hydrogen. However, several studies suggest that green hydrogen will become the dominant production pathway by 2030 (IRENA, 2020). Therefore, this study considers only green hydrogen as the energy source.

2.2 Hydrogen preparation

Before distribution, the hydrogen is purified and either compressed or liquefied. Due to the high mass of pressurised storage tanks, only liquid hydrogen is considered suitable for aviation applications (Prapotnik Brdnik et al, 2019). Hydrogen liquefaction is typically achieved using the Linde cycle. Since liquefaction equipment is expensive, the process becomes economically viable only at large production scales. Consequently, liquefaction at centralised production facilities prior to delivery appears to be the most suitable solution (Marksel et al, 2019).

2.3 Hydrogen delivery

Hydrogen can be delivered in three principal ways: by truck in pressurised vessels, by cryogenic truck in liquid form, or through pipelines in gaseous form. Delivery using pressurised vessels is feasible only for short distances and relatively small quantities of hydrogen. Pipeline transport requires substantial initial investment, but offers very low transportation costs once the infrastructure is established. Therefore, for very large quantities and long transportation distances, pipelines represent the most suitable solution. Cryogenic truck transport is generally the most economical option for medium distances and moderate quantities of hydrogen (Yang and Ogden, 2007).

According to (Marksel et al, 2019), in 2017 there were approximately 150 European airports operating aircraft with capacities between 9 and 19 passengers. More than 90% of these airports handled three or fewer such aircraft movements per day, while the busiest airport operated approximately nine to ten aircraft of this category daily. Most of these flights covered distances between 100 and 500 km.

Assuming that the energy efficiency of a hybrid fuel-cell aircraft is comparable to that of a conventional aircraft, a 19-seat aircraft would require approximately 200 kg of hydrogen for a 500 km flight. This suggests that the hydrogen demand at regional airports would be relatively modest. Approximately 80% of all airports would require less than one tonne of hydrogen per day. If all regional aircraft with capacities of up to 70 passengers were powered by hydrogen, approximately 90% of airports would require less than 10 tonnes of hydrogen per day, while the largest airport would require approximately 40 tonnes per day (Marksel et al, 2019, Marksel et al, 2022).

Since a cryogenic truck can transport approximately 4 tonnes of liquid hydrogen, centralised liquefaction combined with cryogenic truck delivery appears to be the most suitable solution for regional aviation, at least during the initial phase of hydrogen adoption. In the longer term, if larger aircraft also transition to hydrogen propulsion, on-site hydrogen production at airports could become an attractive alternative.

2.4 Hydrogen storage

Based on the estimated hydrogen demand, dedicated long-term storage facilities at airports may not be necessary. Instead, direct aircraft refuelling from delivery trucks could represent the most efficient and cost-effective solution (Marksel et al, 2022).

2.5 Airport ground infrastructure

Although an extensive hydrogen storage infrastructure may not be required at airports, dedicated ground infrastructure is nevertheless necessary (Marksel et al, 2022). Due to the specific safety challenges associated with hydrogen handling, operational procedures must be defined clearly and followed strictly.

In this regard, the relevant ISO Standard, (ISO, 2004), although currently withdrawn, still provides useful guidance on the requirements for airport hydrogen infrastructure. Furthermore, the existing ISO Standards concerning hydrogen safety can be used as a reference for the development of operational procedures and safety measures (ISO, 2015).

According to these guidelines (ISO, 2004), the airport infrastructure should support several key operations, including: (a) warm refuelling (initial refuelling, or refuelling after an extended ground stay), (b) cold refuelling following a flight, (c) defuelling, and (d) boil-off gas management.

From a safety perspective (ISO, 2015), airport facilities should be equipped with appropriate warning signs and physical barriers to prevent unauthorised access to hydrogen-handling areas. Whenever possible, hydrogen-related operations should be conducted outdoors to minimise the accumulation of leaked hydrogen. In addition, hydrogen leak detection systems and flame detection equipment should be installed in all the relevant operational areas. Finally, all hydrogen-handling procedures should be performed exclusively by specially trained and qualified personnel in accordance with established safety protocols.

3 Technological readiness

Hydrogen fuel cell aircraft require the following new key technological components: electric propulsion motors, a fuel cell system and hydrogen storage tanks.

3.1 Electric motors

Electric motors represent one of the least challenging components in hydrogen fuel cell aircraft, as electric motor manufacturing for a wide range of applications is already a well-established and mature industry (Marksel et al, 2019). Electric motors for hydrogen fuel cell aircraft must ensure high reliability, compatibility with the propulsion system, economic viability, and, above all, high power density. Currently certified or flight-tested electric motors achieve a specific power of approximately 5 kW/kg. However, research and development indicate significant progress in the coming decades, with expected increases in the specific power to approximately 13 kW/kg by 2026, 23 kW/kg by 2035, and up to 25 kW/kg or more beyond 2050, alongside efficiencies of up to 99%.

The most promising manufacturers of electric motors for regional electric and hydrogen-powered aircraft are currently developing solutions that are already undergoing flight testing and enable appropriate integration with propeller systems. Development is focused on increasing both the absolute power and specific power of electric motors, with the current solutions already reaching power levels on the order of several hundred kilowatts.

The development of regional aviation between 2023 and 2026 includes several demonstration projects of electric, hybrid-electric and hydrogen-powered aircraft with a capacity of approximately 19 passengers. The expected propulsion motor power ranges from 350 kW to 1 MW. The hydrogen fuel cell aircraft development projects foresee replacing conventional engines with electric motors of approximately 600 kW, powered by fuel cell systems.

3.2 Fuel cells

Among the different types of fuel cells, solid oxide fuel cells (SOFC) and proton exchange membrane fuel cells (PEMFC) are considered for aviation applications (Marksel et al, 2019). PEMFC technology is currently the most technologically mature option for aerospace and space applications, due to its high power-to-weight ratio, which, today, reaches approximately 2.9 kW/kg at stack level, and is expected to increase up to 8 kW/kg in future developments. PEMFC systems operate at low temperatures (60–80 °C), enabling fast start-up and relatively simple system integration.

PEMFC technology is already applied widely in the automotive sector, and benefits from increasing production scale and decreasing costs (Thompson et al, 2018). Key challenges for aviation application remain the reduction of system mass while, simultaneously, improving the reliability, lifetime and power output under demanding operational conditions. Future cost reductions are expected primarily through economies of scale, industrial learning effects and increased production volumes. Two main development pathways are foreseen: the adaptation of automotive fuel cell systems for aviation use, and the development of aviation-specific fuel cells with higher specific power, longer lifetime and optimised lightweight materials.

3.2 Cryogenic tanks

Liquid hydrogen storage systems represent one of the least mature subsystems in hydrogen-powered aviation, primarily because the existing ground-based cryogenic tank designs are not transferable directly to aircraft applications. Conventional storage systems are designed to minimise boil-off over several days of storage, which results in heavy insulation and structural designs that are unsuitable for aviation due to excessive mass. Aircraft applications, in contrast, require dedicated tank designs optimised for short-duration storage, typically limited to the flight time and a short pre-flight ground period of one to two hours, where controlled boil-off is acceptable or managed actively.

Verstraete (Verstraete et al, 2010) investigated the design requirements for liquid hydrogen tanks in regional aircraft, and highlighted the strong dependence of tank mass, insulation thickness and boil-off behaviour on ground time and operational constraints. His results showed that the gravimetric index of a liquid hydrogen tank system (the ratio between the mass of the fuel content and total mass of the storage system) can be expected to reach values of approximately 60–70%, depending on the structural materials, insulation concept and allowable boil-off conditions. Achieving values towards the upper end of this range requires optimised lightweight structures and highly efficient thermal insulation systems.

4 Estimation of the direct operating cost

The economic perspective of hydrogen fuel cell aircraft is shaped primarily by the capital costs (CAPEX) and operating costs (OPEX). CAPEX includes aircraft development, certification, production and infrastructure investment, while OPEX refers to the recurring costs associated directly with operating the aircraft, such as hydrogen fuel, maintenance, insurance, etc…...Since aircraft development is expected to be supported largely by EU-funded programmes, the main economic challenge lies in reducing the direct operating costs. If these can be reduced to levels comparable to or lower than those of conventional aircraft, fuel cell aircraft could become a viable solution for future aviation applications.

The operating costs depend on several factors, the most important being aircraft mass. Therefore, before performing a cost analysis, an estimation is required of the fuel cell aircraft mass.

4.1 Estimation of the maximum take-off mass of the aircraft

In the literature several methods exist for estimating the maximum take-off mass (MTOM) of an aircraft, ranging from simple approaches requiring only basic input data such as passenger numbers and range, to highly detailed methods requiring full aircraft design specifications. Therefore, a dedicated model was developed that is sufficiently flexible to differentiate between aircraft with different performance characteristics, while remaining simple enough to estimate MTOM without detailed design data (Marksel and Prapotnik Brdnik, 2022).

Aircraft performance can be summarised by key parameters, such as passenger numbers, range, cruise speed, take-off and landing distance and manoeuvring capability (e.g., rate of climb). Most of these parameters, with the exception of range and passenger capacity, are influenced strongly by wing loading (wing area per unit of aircraft mass) and power loading (engine power per unit of aircraft mass). The developed model therefore incorporates the following input parameters: power loading, wing loading, range, passenger numbers and selected wing geometric parameters.

The model calculates the fuselage and wing dimensions using analytical relations, while other aircraft masses are estimated using a mass percentage breakdown approach (Kundu, 2010; Marksel and Prapotnik Brdnik, 2022). Validation has shown that the method provides good agreement with the existing conventional aircraft mass estimates. It has therefore been adapted for fuel cell aircraft applications.

In this adapted version, the electric motor mass is determined based on the required power, the fuel cell system mass is estimated using data from the automotive sector (Thompson et al, 2018), and the tank mass is derived using the Verstraete methodology for cryogenic hydrogen storage system estimation (Verstraete et al, 2010).

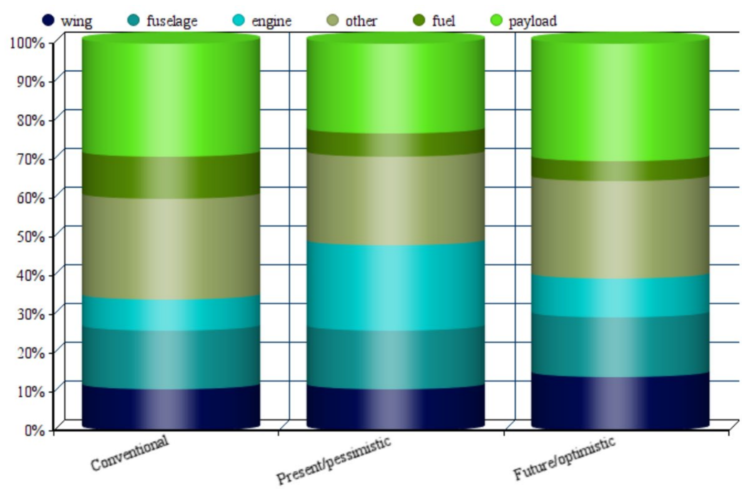

Figure 1: Breakdown of aircraft mass by subsystems
(Marksel and Prapotnik Brdnik, 2022)

4.2 Estimation of the maximum take-off mass of the aircraft

Currently in Europe, six 19-seat aircraft models are in operation: Aircraft Industries L410 NG, DHC-6 Twin Otter, Dornier 228 NG, Beechcraft 1900D, British Aerospace Jetstream, and Fairchild Swearingen Metroliner (Marksel and Prapotnik Brdnik, 2023). The first three models are still in production, while the latter three are no longer produced, although existing aircraft remain in service across Europe.

In total, 11 companies operate 19-seat aircraft fleets, ranging from 1 to 13 aircraft 19 seat aircraft per operator. The majority of these aircraft are used for domestic operations (without cross-border flights), with the exception of one operator providing services between the United Kingdom and France across the English Channel.

The annual utilisation of these aircraft varies significantly, ranging from approximately 200 to just over 1,300 flight hours per aircraft. The number of flights per year ranges from slightly above 400 to just below 8,000, corresponding to an average utilisation of approximately 1 to 22 flights per day per aircraft.

4.3 Estimation of the direct operating cost

The direct operating costs (DOC) are divided into annual depreciation, annual interest costs, annual insurance costs, annual fuel costs, annual maintenance costs, annual crew costs and annual airport and air navigation charges (Scholz, 2015). The detailed calculation is presented in (Marksel and Prapotnik Brdnik, 2023).

The annual depreciation, interest and insurance costs are estimated as a percentage of the aircraft purchase price. The purchase price is estimated using a mass-based cost model, in which the aircraft is decomposed into its major subsystems, the mass of each subsystem is determined, and the corresponding manufacturing and assembly costs are calculated. Depreciation is determined further by the expected operational lifetime of the aircraft.

The annual fuel costs depend on both the number of flights and the total distance flown. These costs are estimated by dividing each flight into its main phases–take-off, cruise and landing–and calculating the fuel consumption for each phase separately. Since the fuel consumption is strongly dependent on the aircraft mass, accurate mass estimation is an essential prerequisite for operating cost calculations.

The annual crew costs depend on the total flight hours, including block time, which accounts for ground manoeuvring before take-off and after landing. These costs are calculated using the hourly rates of the pilots and cabin crew.

The maintenance costs are determined by both the material costs and labour costs associated with the maintenance personnel and engineering specialists. For conventional kerosene-powered aircraft, detailed maintenance cost data are available from the existing operators (Aircraft Industries, 2023). For hydrogen fuel cell aircraft, the maintenance requirements for the airframe are assumed to be similar to those of conventional aircraft, while the propulsion system maintenance differs. In particular, maintenance is expected to focus on the fuel cell system and its periodic replacement, whereas electric motors and hydrogen tanks are anticipated to require mainly inspections and routine servicing (Thompson et al, 2018).

The airport-related costs include both air navigation charges paid to Eurocontrol and airport fees. These costs are among the most difficult to estimate, as charging schemes vary considerably between airports, both in terms of pricing and the services included.

The results indicate that the dominant cost category depends strongly on the aircraft`s utilisation. For operators with high annual flight activity, fuel costs represent the largest share of direct operating costs, whereas, for operators with low annual utilisation, depreciation becomes the dominant cost component. An example of the DOC breakdown for the Croatian airline Trade Air is presented in Figure 2.

The cost analysis shows further that hydrogen fuel cell aircraft are expected to have higher direct operating costs than conventional aircraft by around 2030. However, by 2050, the direct operating costs are projected to become lower than those of kerosene-powered aircraft. This trend is driven primarily by the expected increase in kerosene prices and the simultaneous decrease in hydrogen production costs. The projected evolution of the direct operating costs for the Croatian airline Trade Air is presented in Figure 3. The Figure shows that the annual direct operating costs of conventional aircraft are expected to increase substantially between 2030 and 2050, while the costs of fuel cell aircraft remain more stable. Although fuel cell aircraft may initially have comparable or slightly higher operating costs, they become increasingly cost-competitive over time. The widening gap between the two cost curves suggests that hydrogen fuel cell aircraft could offer long-term operational cost advantages, particularly if fossil fuel prices, carbon costs and environmental compliance costs continue to rise.

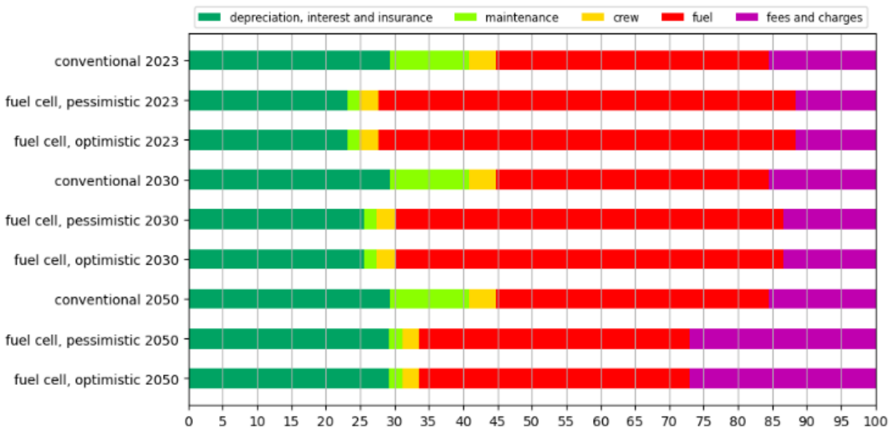

Figure 2: DOC breakdown for Croatian Trade Air airline
Source: (Marksel, 2023)

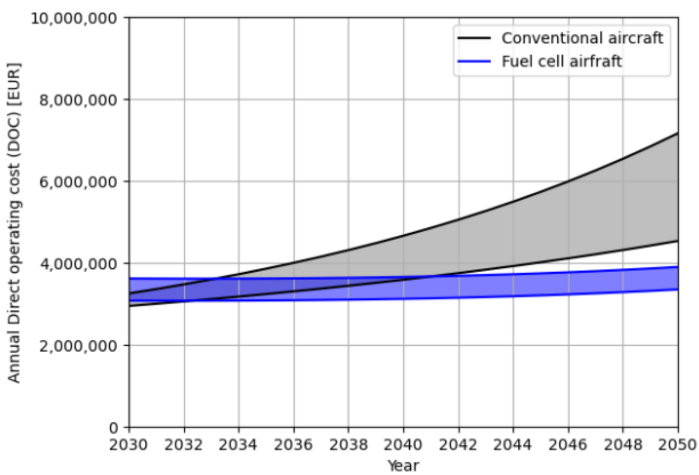

Figure 3: The projected evolution of direct operating costs for the Croatian airline Trade Air
Source: (Marksel, 2023)

5 Conclusion

Hydrogen fuel cell aircraft represent a promising alternative to conventional kerosene-powered aircraft, and have the potential to play an important role in the future decarbonisation of aviation. The analysis presented in this study indicates that ongoing technological developments in fuel cells, electric propulsion systems, and hydrogen storage technologies, could enable hydrogen-powered regional aircraft to become both technically and economically competitive in the coming decades.

Nevertheless, any long-term economic projections should be interpreted with caution. The large-scale adoption of alternative energy carriers, such as hydrogen, would likely influence global energy markets, and could affect the future prices of oil and petroleum-derived fuels significantly. As a result, the future evolution of both hydrogen and kerosene prices remains highly uncertain, making precise long-term predictions difficult.

Despite these uncertainties, the results suggest that hydrogen offers several important advantages, including the potential for low-emission operation, compatibility with renewable energy sources, and long-term sustainability. Consequently, hydrogen fuel cell technology appears to be a promising pathway towards more sustainable regional air transport.

References

Aircraft Industries (2023). *Direct operating costs (DOC) for L 410 NG.* https://let.cz/l410ng.

Adolf, J. et al (2017). Shell hydrogen study, energy of the future. Sustainable mobility through fuel cells and H2. https://epub.wupperinst.org/frontdoor/deliver/index/docId/6786/file/6786_Hydrogen_Study.pdf.

Cabrera, E., & de Sousa, J. M. M. (2022). Use of Sustainable Fuels in Aviation–A Review. *Energies*, *15*(7), 2440. https://doi.org/10.3390/en15072440.

European Environment Agency (2025). New registrations of electric cars in Europe, https://www.eea.europa.eu/en/analysis/indicators/new-registrations-of-electric-vehicles.

European Union Aviation Safety Agency (2025). European Aviation Environmental Report 2025, *https://www.easa.europa.eu/en/domains/environment/eaer*

IRENA (2020). Green Hydrogen Cost Reduction: Scaling up Electrolysers to Meet the 1.5^{0}C Climate Goal. https://www.irena.org/-/media/Files/IRENA/Agency/Publication/2020/Dec/IRENA_Green_hydrogen_cost_2020.pdf.

International Organization for Standardization (2004). *ISO/PAS 15594:2004: Airport hydrogen fuelling facility operations*. https://www.iso.org/standard/28327.html.

International Organization for Standardization (2015). *ISO/TR 15916:2015: Basic considerations for the safety of hydrogen systems*. https://www.iso.org/obp/ui/#iso:std:iso:tr:15916:ed-2:v1:en.

Kundu, A. K. (2010). *Aircraft design*. Cambridge University Press.

Marksel, M. et al. (2019), MAHEPA D10.1. Ground infrastructure investment plan, https://mahepa.eu/wp-content/uploads/2019/07/MAHEPA_D10.1-Ground-infrastructure-investment-plan_FINAL.pdf

Marksel, M., Kamnik, R., Božičnik, S., & Prapotnik Brdnik, A. (2022). Hydrogen infrastructure and logistics in airports. In C. Ö. Colpan & A. Kovač (Eds.), *Fuel cell and hydrogen technologies in aviation* (pp. 117–146). Springer. https://doi.org/10.1007/978-3-030-99018-3.

Marksel, M; Prapotnik Brdnik, A. (2022). Maximum Take-Off Mass Estimation of a 19-Seat Fuel Cell Aircraft Consuming Liquid Hydrogen, *2022*, 14, 8392. https://doi.org/10.3390/su14148392.

Marksel, M; Prapotnik Brdnik, A. (2023). Comparative Analysis of Direct Operating Costs: Conventional vs Fuel cell 19-seat Aircraft, *Sustainability*, 15, 11271. https://doi.org/10.3390/su15141127.

Prapotnik Brdnik, A., Kamnik, R., Marksel, M., & Božičnik, S. (2019). Market and Technological Perspectives for the New Generation of Regional Passenger Aircraft. *Energies*, *12*(10), 1864. https://doi.org/10.3390/en12101864.

Scholz, D. (2015). *Aircraft design: Lecture notes*. Hamburg University of Applied Sciences. http://LectureNotes.AircraftDesign.org.

Thompson, S. T., James, B. D., Huya-Kouadio, J. M., Houchins, C., DeSantis, D. A., Ahluwalia, R., Wilson, A. R., Kleen, G., & Papageorgopoulos, D. (2018). Direct hydrogen fuel cell electric vehicle cost analysis: System and high-volume manufacturing description, validation, and outlook. *Journal of Power Sources, 399*, 304–313. https://doi.org/10.1016/j.jpowsour.2018.07.100.

Verstraete, D., Hendrick, P., Pilidis, P., & Ramsden, K. (2010). Hydrogen fuel tanks for subsonic transport aircraft. *International Journal of Hydrogen Energy, 35*(20), 11085–11098. https://doi.org/10.1016/j.ijhydene.2010.06.060.

Yang, C., and Ogden, J.M. (2007). Determining the Lowest-Cost Hydrogen Delivery Mode. I*nt. J. Hydrogen Energy*, vol. 32, pp. 268–286, 2007. https://doi.org/10.1016/j.ijhydene.2006.05.009.

Povzetek v slovenskem jeziku

Načrtovanje in ekonomska analiza 19-sedežnega letala na vodikove gorivne celice za regionalni zračni promet. Prispevek povzema rezultate projekta MAHEPA, v okviru katerega so raziskovali tehnološko in ekonomsko izvedljivost 19-sedežnih letal na vodikove gorivne celice ter njihov potencial za uvedbo v uporabo do leta 2050. Obravnava ključne zahteve, potrebne za omogočanje njihovega obratovanja in dolgoročne vzdržnosti.

Analiza je razdeljena na tri sklope. Prvi obravnava potrebno infrastrukturo in varnostne ukrepe za regionalno letalstvo na vodik, vključno s proizvodnjo in distribucijo vodika. Drugi ocenjuje razvojne potrebe ključnih tehnoloških komponent, kot so gorivne celice, sistemi za shranjevanje vodika in integracija pogonskega sistema. Tretji sklop analizira ekonomsko izvedljivost, pri čemer so neposredni obratovalni stroški tesno povezani z masnimi značilnostmi letala.

Rezultati ekonomske analize za obdobje 2030–2050 kažejo, da bi lahko bila letala na vodikove gorivne celice stroškovno konkurenčna ob ugodnih cenah vodika in nadaljnjem tehnološkem razvoju, kar podpira njihov potencial kot izvedljivo rešitev za regionalno letalstvo.

JOURNAL OF ENERGY TECHNOLOGY
Vol. 19, No. 1, pp. 83–108, July 2026

Original Scientific Article

ASSESSING THE POTENTIAL OF ELECTROCHEMICAL IMPEDANCE SPECTROSCOPY AS A SUPPORTING TOOL FOR EQUIVALENT CIRCUIT MODELING IN BATTERY MANAGEMENT SYSTEMS

DENIS BATIUK,[1] IGOR MELE,[2] KLEMEN ZELIČ,[2]
MARTIN PEC,[3, 4] TOMAŽ KATRAŠNIK,[2]
AMOR CHOWDHURY[1, 2]

[1] University of Maribor, Faculty of Energy Technology, Krško, Slovenia
denis.batiuk1@um.si, amor.chowdhury@um.si
[2] University of Ljubljana, Faculty of Mechanical Engineering, Ljubljana, Slovenia
igor.mele@fs.uni-lj.si, klemen.zelic@fs.uni-lj.si, tomaz.katrasnik@fs.uni-lj.si, ameramor.chowdhuryhaque@fs.uni-lj.si
[3] University of Maribor, Faculty of Electrical Engineering and Computer Science, Maribor, Slovenia
martin.pec@um.si
[4] EMSISO d.o.o., Pesnica pri Mariboru, Slovenia
martin.pec@emsiso.com

CORRESPONDING AUTHOR
denis.batiuk1@um.si

Submitted
5. 2. 2026

Accepted
9. 4. 2026

Published
15. 7. 2026

Abstract Accurate yet computationally efficient battery models are essential for industrial battery management systems (BMS), which operate under strict constraints on sensing and processing power, as well as certification requirements. Electrical equivalent circuit models (ECMs) are therefore adopted widely in practice, while physics-based models (PBMs) provide detailed descriptions of transport, kinetic, and degradation processes, but are not yet adopted in embedded implementation. The present work assesses the potential of electrochemical impedance spectroscopy (EIS) as a supporting tool for equivalent circuit modeling in BMS applications, with an emphasis on its ability to provide frequency-resolved, process-level indications rather than direct parameter information. By separating the ohmic, charge-transfer, and diffusion-related contributions in the frequency domain, EIS offers complementary insights that are not accessible through time-domain measurements alone. The analysis addresses how such indications can guide ECM structure selection and parameter interpretation, the limitations imposed by measurement duration, noise, and temperature gradients, and the feasibility of EIS-supported modeling approaches under typical BMS constraints. The results delineate the scope within which frequency-informed modeling can enhance physical consistency and diagnostic interpretability while preserving the computational characteristics required for BMS implementation.

Keywords
electrochemical impedance spectroscopy, battery management system, equivalent circuit models, physics-based models, lithium-ion batteries, frequency-domain analysis, parameter identification, diagnostics

https://doi.org/10.18690/jet.19.1.83-108.2026
CC-BY, text © Batiuk et al., 2026
This work is licensed under the Creative Commons Attribution 4.0 International License.
This license allows reusers to distribute, remix, adapt, and build upon the material in any medium or format, so long as attribution is given to the creator. The license allows for commercial use. https://creativecommons.org/licenses/by/4.0
University of Maribor Press

1 Introducton

Lithium-ion batteries have become a key technology in electric mobility, stationary storage, and portable electronics, combining high energy density, cyclic stability, and adaptability to various applications (Larcher & Tarascon, 2015; Shen & Gao, 2019). The increasing requirements for energy, safety, and functionality, create the need for models that can be deployed in industrial BMSs, enabling the accurate assessment of internal states, safe operation, and real-time degradation diagnostics (Xu et al., 2022; Balasingam et al., 2020). In this context, battery cell models serve as a necessary bridge between the measurable quantities (voltage, current, temperature) and the hidden internal processes that determine the performance and lifetime of battery systems significantly. Two conceptually different modeling paradigms are established in the literature and industrial practice. Electrical equivalent models (ECMs) describe the voltage–current response with resistive and capacitive elements, often in Thevenin structures, with a historical development dating back to the early empirical formulations such as the Shepherd model (Shepherd, 1965). Physics-based models (PBMs) are based on the physical processes of diffusion, charge transfer, electrolyte transport, and electrochemical reaction kinetics. The foundational work is the Doyle-Fuller-Newman model (Doyle et al., 1993), with later extensions derived from the theory of porous electrodes and including detailed descriptions of material properties, electrode topology (Mele et al., 2020), modeling EIS spectra (Mele et al., 2024), and degradation mechanisms (Newman & Thomas-Alyea, 2004; Brosa Planella et al., 2022; Al-Zubaidi R-Smith et al., 2021) as well as safety (Katrašnik et al., 2021). Between these two classes, recent research has introduced physically consistent equivalent-circuit models (PC-ECM), which retain the structure of discretized electrochemical transport equations while remaining in a circuit-based ODE representation (Zelič et al., 2021; Tibaut et al., 2024).

The gap between the two approaches remains significant: ECMs are compatible with the embedded processor platforms due to their low computational complexity, while PBMs and PC-ECMs offer significantly more information, which, traditionally, exceeds the capabilities of real-time BMS implementation (Berger et al., 2024; Lucaferri et al., 2023), whereas recent advances of authors prove the applicability of computationally optimized models on advanced microchips (Rahmani et al., 2025). Therefore, industrial battery management systems are based almost exclusively on ECMs, while PBMs are used primarily in research environments and for digital twins. Recent comparative studies confirmed this widening divergence, showing that ECM parameterizations calibrated under controlled conditions fail to generalize across dynamic loads and temperature variations, while physics-based models maintain mechanistic consistency (Lagnoni et al., 2024).

Electrochemical impedance spectroscopy (EIS) offers frequency-resolved insights into the dynamic processes of battery cells (Geng et al., 2021). The impedance response across different frequency ranges reveals the ohmic, kinetic, and diffusion contributions, providing information that classical time-domain tests cannot (Barsoukov & Macdonald, 2018; Orazem & Tribollet, 2017; Meddings et al., 2020). EIS is an established validation tool in PBMs (Doyle et al., 1993), and a growing body of research is investigating which frequency information can be incorporated into the parametric identification of ECM (Sovljanski et al., 2025; Mathivanan et al., 2025; Belmajdoub et al., 2024).

The central research question of the article is not whether EIS can replace PBMs, but to what extent it can contribute to reducing the discrepancy between the phenomenological and physically based approaches. Therefore, the frequency ranges with the highest diagnostic value, the influence of disturbances and temperature gradients on impedance data are analyzed, and the feasibility of measurements in industrial environments, where sensor technology and time constraints are essential (Andre et al., 2011; Da Silva et al., 2024; Xu et al., 2024).

In this paper, we first discuss the conceptual foundations and the nature of the distinction between ECM and PBMs. We then present the limitations of the embedded processor architectures and sensor technology, as well as the reasons why PBMs are currently not suitable for widespread industrial implementation. We then analyze the information value of impedance measurements, the experimental requirements, and the possibilities of incorporating EIS into the identification procedures for ECMs. The conclusion summarizes opportunities to integrate EIS into future generations of BMS systems, and identifies areas where EIS can serve as a bridge between the conceptually distinct approaches (Belmajdoub et al., 2024).

2 Battery cell models

Battery cell models serve as the basis for analyzing, simulating, and managing lithium-ion systems (Larcher & Tarascon, 2015). The voltage–current response of a lithium-ion cell is nonlinearly dependent on temperature, state of charge, load history, and degradation rate; therefore, models enable understanding of the operation and development of algorithms for state assessment, diagnostics, and optimization of operation in BMS. Two main paradigms are established in the literature: equivalent electrical models (ECM) and PBMs (Doyle et al., 1993; Barsoukov & Macdonald, 2018). ECMs provide a computationally efficient description of the dynamic response, whereas PBMs are based on a physically grounded description of the transport, kinetic, and thermal processes.

2.1 Equivalent electrical circuits model ECM

ECMs are based on equivalent electrical circuits that approximate the internal electrochemical processes by using voltage sources, resistances, and capacitances. The main advantage of the approach is its simple linear structure, which enables implementation in embedded processing units and the direct application of standard control, observation, and filtering methods (Shepherd, 1965). ECMs will enable the simulation of voltage response with low computational complexity, which is why they have become the standard choice in industrial applications such as electric vehicles, energy storage, and transmission devices (Tran et al., 2021).

The historical development of ECMs began with semi-empirical voltage-driven models, among which Shepherd's approach is one of the first systematic formulations of the voltage response as a function of current and discharged capacitance (Shepherd, 1965). Over time, structural extensions were introduced, including an internal resistance to describe the ohmic drop and additional dynamic terms. This led to the Rint models, and, later, to the family of Thevenin models, with one or more RC branches, as shown in Figure 1.

The RC branches describe the polarization phenomena and stress relaxation after load changes, thereby enabling the matching of transient phenomena across different time scales.

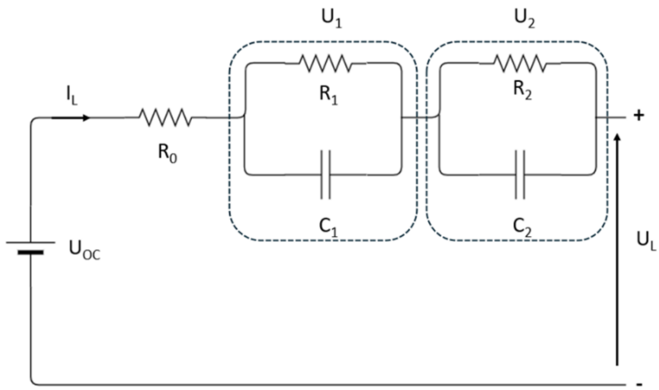

Figure 1: Second-order equivalent circuit (2nd-order RC Thevenin model) for a Li-ion cell

Over time, ECM development has progressed toward greater dynamic accuracy and flexibility. The structural extensions include multiple parallel RC branches, while the parametric extensions consider resistances and capacitances as functions of the state of charge, temperature, current, and aging. The parameters are determined from experimental data using identification methods that enable real-time adaptation of the model during operation. Such a formulation is compatible with extended and unscented Kalman filters, Luenberger observers, and online identification methods (Xu et al., 2022; Belmajdoub et al., 2024). The mathematical description of ECM is based on linear differential equations that relate the current, voltage, and voltage contributions of individual RC branches. The linear structure enables straightforward discretization and implementation in algorithms running on embedded processor platforms, ensuring real-time operation without excessive load on the processor resources.

ECMs allow for fast simulation, relatively easy parameter identification, and direct integration into BMS. Limitations arise from the aggregated nature of the parameters: the same parameter may capture contributions from multiple physical mechanisms, limiting interpretation to the phenomenological level. In addition, the model validity and predictive accuracy are typically restricted to the operating domain used for parameter identification, resulting in reduced reliability when extrapolating beyond the training conditions. Under extreme operating conditions–high currents, low temperatures, or advanced degradation–more pronounced deviations from realistic behavior may occur, requiring additional correction structures or model extensions (Belmajdoub et al., 2024).

2.2 Physics-based models PBM

PBM describes the operation of lithium-ion cells at the level of fundamental physical processes. They include the diffusion of lithium in the active particles, the charge and mass transport in the electrolyte, the kinetics of charge transfer at the electrode–electrolyte interface, double layer phenomena and thermal dynamics. The primary purpose of such models is to understand the influence of the material properties, electrode geometry, and operating conditions on the voltage response, efficiency, and degradation (Doyle et al., 1993; Newman & Thomas-Alyea, 2004). A breakthrough development is the DFN model, which combines solid-phase diffusion, electrolyte transport, and Butler–Volmer charge-transfer kinetics into a unified mathematical framework (Doyle et al., 1993). The Doyle–Fuller–Newman (DFN) model (often referred to as the pseudo-2D, P2D model) is a physics-based porous-electrode framework that links terminal voltage to the internal electrochemical processes. It represents transport in the electrolyte across the cell thickness and diffusion of the lithium within the active-material particles, coupled with charge conservation and interfacial reaction kinetics. As a result, DFN can reproduce the key dynamic and impedance features of Li-ion cells, but it is typically too computationally demanding for direct real-time use in embedded BMS hardware. (Figure 2). The structure of PBMs includes diffusion dynamics in particles (described by radial diffusion equations), transport in the electrolyte (described by Nernst–Planck or simplified transport equations), charge transfer kinetics at the interface (Butler–Volmer expression), and a thermal sub-model. Such a structure enables the simulation of local concentrations and potentials, the calculation of local heat generation, and the investigation of degradation mechanisms, including SEI growth, loss of active material, and electrolyte degradation.

The model consists of a system of nonlinear partial differential equations and algebraic equations that describe the concentrations, potentials, and current densities throughout the electrodes and electrolyte (Figure 3). Due to its computational complexity, the DFN model serves as a reference framework for analysis and development, while simplified versions have been developed for faster simulations.

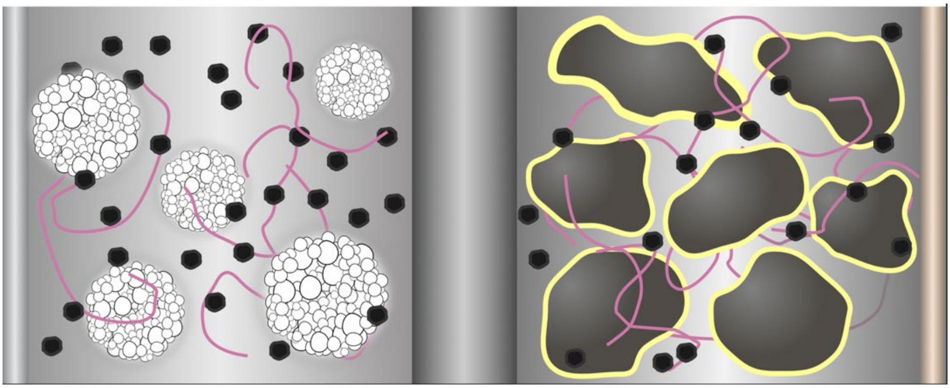

Figure 2: Conceptual DFN (P2D) porous-electrode model structure

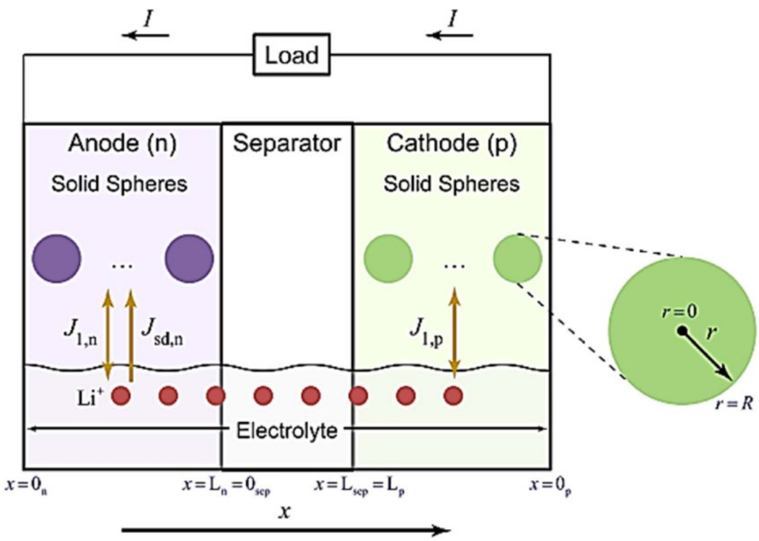

Figure 3: Diagram of the Doyle-Fuller-Newman (DFN) model (Pandey et al., 2023)

Simplifications are often based on the single-particle (SPM) approach (Rahmani et al., 2025), which preserves diffusion in the solid phase while neglecting gradients in the electrodes, and, hence, transport in the electrolyte, or replacing it with an efficient description (Newman & Thomas-Alyea, 2004; Brosa Planella et al., 2022). This reduces the number of states and equations, while retaining the crucial connection between diffusion in the active mass and the voltage response. Further extensions include models in which selected electrolytic processes are incorporated as correction terms or additional concentration states (Chapman et al., 2019).

The advantage of PBMs is the physical interpretability of parameters and the ability to separate the effects of individual mechanisms on the cell response. The models enable the analysis of the influence of materials, electrode thickness, porosity, diffusivity, and other design parameters on performance and lifetime. The limitations comprise challenging parameter determination and/or identification, which often requires advanced experimental equipment, and the higher computational demands of solving nonlinear partial differential and algebraic equations. Therefore, PBMs are used primarily in research environments and in the design of digital twins, materials, and structures.

2.3 Physically consistent equivalent-circuit models (PC-ECM)

Physically consistent equivalent-circuit models (PC-ECM; Zelič et al., 2021; Tibaut et al., 2024) constitute a class of circuit-based representations derived from the mathematical reduction of electrochemical partial differential equations (PDEs) into systems of ordinary differential equations (ODEs), followed by their transformation into equivalent electrical structures. Their development has been motivated by the need for model formulations that retain the key physical characteristics of ionic and electronic transport, interfacial reaction kinetics, and solid- and electrolyte-phase diffusion. If models are linearized, which makes them applicable for low current simulations, e.g. simulating EIS spectra, the system of equations is simplified to the ODE framework.

PC-ECM occupies a natural intermediary position between full PBMs and phenomenological ECM. They preserve the spatial structure of the underlying PDEs in a reduced, yet physically grounded form, which makes them suitable for resolving the contributions of individual processes, interpreting the origins of specific impedance features, and validating simplified or reduced-order models. The development of PC-ECM remains active, with a large number of variants proposed in the literature (Zelič et al., 2021; Geng et al., 2021; Von Srbik et al., 2016; Scipioni et al., 2017) that differ in the physical mechanisms captured, geometric assumptions, and numerical discretization strategies. Among these approaches, two representative examples are highlighted: a transmission line model (TLM) for porous electrodes derived from the concentrated-solution theory (Zelič et al., 2021), and a particle-level TLM obtained from the finite-volume discretization of Fick's diffusion equation in spherical geometry (Tibaut et al., 2024). These models illustrate typical PC-ECM formulations; detailed descriptions of their structure, parametrization, and validation are provided in the cited works. Because PC-ECM retains the spatial structure of the underlying PDE, it provides several advantages:

- transparent separation of processes such as ionic transport, charge-transfer kinetics, and solid-phase diffusion;
- the ability to reproduce impedance spectra across the full electrochemical frequency range;
- compatibility with standard circuit-based identification techniques; and
- computational tractability relative to the original PDE models.

In practice, PC-ECM is used primarily for research and diagnostic purposes, including the interpretation of impedance spectra, the extraction of transport and kinetic parameters, and the analysis of degradation mechanisms under controlled laboratory conditions.

3 Discrepancy between ECM and PBM

The different conceptual starting points of ECM and PBM result in significant differences in how they describe the behavior of Li-ion batteries. ECMs describe the battery cell as a macroscopic system in which the voltage response results from the sum of simplified, physically undetermined dynamic processes, combined into RC branches. PBMs describe the distributed processes that occur at the microscopic level within the active particles and in the electrolyte. This enables the direct analysis of the influence of diffusion in the solid phase, reaction kinetics at electrode surfaces, or charge transport in the electrolyte using a physical model (Brosa Planella et al., 2022). ECMs are based on a phenomenological approach, and describe the voltage response of a cell by a combination of an ohmic resistor and one or more RC branches, where the time constant of each branch is defined as (Tran et al., 2021):

$$\tau_i = R_i C_i. \tag{1}$$

Although these processes do not have a direct physical interpretation, they provide an effective approximation of different segments of the impedance spectrum of a battery cell. Typical time intervals covered by the RC branches of the ECM include the ohmic response (from 10 -5 to 10 -3 seconds), kinetic polarization processes (10 -2 to 1 second), and slower relaxation processes (1–20 seconds) (Barsoukov & Macdonald, 2018; Choi et al., 2020). Exact ranges vary with the cell design, temperature, and SoC; the intervals above indicate typical orders of magnitude. The Nyquist response of the ECM has the form of a sum of semicircular arcs:

$$Z_{ECM}(j\omega) = R_0 + \sum_{i=1}^{n} \frac{R_i}{1+j\omega\tau_i}, \quad (2)$$

which means that ECMs can describe the arc fairly accurately in the mid-frequency range, but cannot generate the diffusion tail resulting from transport limitations inherently (Tran et al., 2021; Ali et al., 2024), as shown in Figure 4 (Lazanas & Prodromidis, 2023).

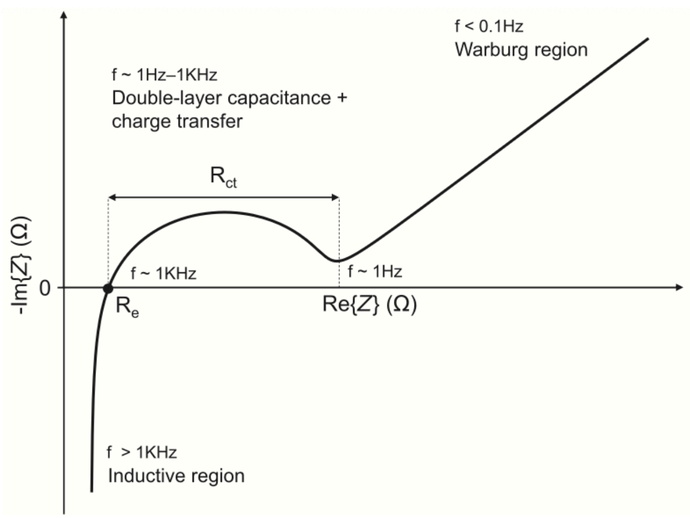

Figure 4: Idealized Nyquist diagram of a Li-ion cell with the ohmic, kinetic, and diffusion contributions (Lazanas & Prodromidis, 2023)

PBMs are derived by describing the processes at electrodes and in the electrolyte, where the cell behavior depends on a set of nonlinear transport and kinetic phenomena. For example, the Doyle–Fuller–Newman (DFN) model is derived by solving partial differential equations that describe the charge transport, ion diffusion in the solid phase, electrolyte diffusion, and reaction kinetics. A porous electrode model of the DFN type involves solving diffusion in the solid phase, concentration and potential transport in the electrolyte, double layer phenomena, and charge transfer kinetics simultaneously. The model does not generate a single time constant, but a continuum of eigentimes ranging from microseconds to several thousand seconds, leading to a dispersed frequency response (Drummond & Duncan, 2019). The slowest segment of the spectrum arises from the diffusion of lithium in the solid phase, which is determined by the time constant

$$\tau_{diff} = \frac{R_S^2}{D_S}, \tag{3}$$

where $R_S$is the radius of the active particle, $D_S$and is the diffusion coefficient in the solid phase. The mentioned time constant determines the rate of concentration equalization within the particles and in the graphite anodes, which occurs over approximately 10 to several hundred seconds. The faster part of the response is determined by the charge transfer kinetic processes, which are characterized by a time constant of

$$\tau_{\mathrm{ct}} = \frac{RT}{Fj_0}. \tag{4}$$

The equation includes the gas constant R and the Faraday constant F, $j_0$which is the exchange current density that describes the intensity of the electrochemical reaction at zero overpotential. Higher values of $j_0$mean shorter time constants, while the growth of interfacial layers and changes in the surface morphology reduce j_0, and thus prolong the kinetic response. Typical values of τ_{ct}range from a few milliseconds to about a tenth of a second. Diffusion in the electrolyte is described by the time constant

$$\tau_{\mathrm{elyte}} = \frac{L_e^2}{D_e}, \tag{5}$$

where $L_e$defines the characteristic transport length in the electrolyte, D_e, and is the diffusion coefficient of the lithium ions in the liquid phase. The time constant, which ranges from tenths of a second to a few seconds, has a significant impact on the system's behavior at medium frequencies.

The diffusion nature is captured by the Warburg impedance, which, in the case of semi-infinite diffusion, takes the form

$$Z_W = \sigma(1 - j)\,\omega^{-1/2}. \tag{6}$$

The coefficient σrepresents the Warburg diffusion resistance, and determines the amplitude of the diffusion impedance. It is a function of the diffusion coefficients, concentrations, active surface area, and geometry of the porous structure. A larger value σ indicates slower diffusion and a longer a 45-degree segment in the Nyquist plane.

For systems with finite diffusion, the Warburg impedance takes the form

$$Z_W = R_W \frac{\tanh(j\omega\tau_W)}{j\omega\tau_W}, \tag{7}$$

where $R_W$represents the diffusion resistance to equilibrium, $\tau_W$and the corresponding diffusion time constant. At high frequencies, the expression reproduces a 45-degree segment, while, at low frequencies, it transitions into a vertical, distinctly capacitive-like response.

The presented physical model enables direct analysis of the influence of solid-state diffusion, reaction kinetics at the electrode surfaces, or charge transport in the electrolyte. In contrast, ECMs capture these processes indirectly through the time constants of physically undefined processes. The difference leads to situations in which ECMs cannot capture the behavior of a battery cell when nonlinear interactions between the diffusion, kinetic, and thermal processes occur, especially at high currents, low temperatures, or advanced degradation (Ali et al., 2024; Drummond & Duncan, 2019).

The discrepancy continues at the temporal and spatial scales. Electrochemical processes co-occur in the active particles, electrolyte, porous electrodes, and interfacial layers, creating multi-layered dynamics distributed over a wide range of time constants, from a few milliseconds to a few hours. The ECMs combine these processes into a limited number of effective RC branches, meaning that several different physical processes contribute to the exact equivalent time constant. As a result, ECMs often fit the real response well in a limited frequency range, but deviate where separate physical mechanisms affect the voltage on different time scales. The gap between the two models is expressed most clearly when considering the degradation processes. PBMs enable the description of various aging mechanisms, including the growth of an interfacial solid layer, loss of active material, lithium plating, and the formation of microscopic cracks within the electrode structure. Each process can be represented in the model as a separate equation, or as an additional physical mechanism, enabling understanding of the impact of degradation on performance and lifetime. ECMs do not allow such differentiation; the degradation is reflected only as changes in the parameters, such as an increase in internal resistance or changes in the time constants. This limits the interpretation of long-term changes in ECMs, as it is impossible to separate the impact of the different aging mechanisms.

The discrepancy between the two approaches stems from the absence of a direct correlation between their parameters. As shown by Lagnoni et al. (2024), even when the ECM and PBMs are calibrated using identical datasets, the ECM structure collapses under dynamic load or thermal variation, confirming that the phenomenological model cannot preserve mechanistic fidelity. The ECM can be extended with additional RC branches or distributed elements to produce a very accurate fit of the impedance response. However, this does not improve the model's explanatory value, since the ECM parameters capture the aggregated consequences of multiple processes. The key methodological problem is that there is no mapping operator:

$$\mathcal{T}: \Theta_{\mathrm{ECM}} \rightarrow \Theta_{\mathrm{phys}}, \tag{8}$$

where Θ_{ECM} represents the space of resistances, capacitances, CPE parameters, and their derived time constants, while Θ_{phys}encompasses the diffusion coefficients, kinetic constants, porosities, and other physical quantities.

The discrepancy between the ECM parameters and physical processes becomes clearer when examining specific examples. First, different physical mechanisms can cause precisely the same changes in the ECM parameters. For example, an increase in the thickness of the SEI layer, a decrease in the electrolyte's ionic conductivity, an increase in electrode polarity, or an increase in contact resistance is reflected almost identically as an increase in the ohmic resistance R_0. Although these are four completely different physical causes, the ECM detects only the joint effect, so it is not possible to determine reliably from the change in R_0 which mechanism is responsible. The ECM thus describes the effect, not the cause, leading to inherent non-uniformity in interpretation.

Second, a single physical mechanism can affect multiple ECM parameters simultaneously. Diffusion limitation at the anode is a good example: the slowed diffusion of Li ions not only causes an increase in the resistance of a single RC branch, but also changes the CPE–α parameter, widens the Warburg segment, affects the phase angle, and changes the effective capacitance of the second RC branch. This means that a single physical process affects the entire set of ECM parameters, making it impossible to attribute the change to a single "electrical component." Again, we see that the ECM parameters represent aggregated indicators of multiple simultaneous processes, rather than direct physical quantities.

Both examples emphasize that the mapping between PBM and ECM parameters is neither unique, nor vice versa. Different physical mechanisms can cause identical changes in the ECM parameters, and a single physical mechanism can affect multiple ECM parameters simultaneously. Therefore, changes in the ECM parameters cannot be interpreted without additional physical context, while PBMs allow for a physical interpretation of the internal processes (Brosa Planella et al., 2022; Drummond & Duncan, 2019).

A PC-ECM does not alter the fundamental conclusions drawn in the preceding comparison between PBMs and classical ECM. PC-ECMs are aligned with PBMs conceptually and structurally, as its states, parameters, and topology arise from spatially resolved transport, interfacial kinetics, and diffusion processes, rather than from phenomenological aggregation (Zelič et al., 2021; Tibaut et al., 2024). Consequently, the relationship between PC-ECM and ECM exhibits the same structural limitations as the relationship between PBMs and ECM. When a PC-ECM is projected onto a low-order ECM structure–typically by collapsing the distributed resistive–capacitive pathways into a limited number of lumped time constants–the distinct contributions of transport and kinetic processes merge into aggregated parameters. This implies that different PC-ECM configurations, corresponding to distinct sets of physical properties and spatial distributions, can yield ECM parameter sets that are essentially identical. Similarly, a given ECM parameterization may be compatible with multiple, physically inequivalent PC-ECM configurations. The mapping remains inherently many-to-one.

As such, a PC-ECM does not provide a unique interpretative bridge between the ECM parameters and underlying physical mechanisms. Their primary contribution lies in offering a physically transparent intermediate representation, in which the individual processes remain separable and quantifiable, before they are ultimately collapsed into the simplified ECM structures required by embedded battery-management applications.

4 Industrial constraints on model-based BMS and SoX estimation

Battery management systems operate in an environment with limited processing power, a limited number of measurable quantities, and incomplete information about the cells' internal structure. Algorithms must operate within time frames defined by protection functions, communication protocols, and condition assessment procedures. Due to these limitations, electrical circuit models (ECMs) have been introduced in industrial practice to enable real-time implementation and parametric identification from the measurements available in service (Shen & Gao, 2019; Balasingam et al., 2020; Belmajdoub et al., 2024).

Three constraints determine the applicability of model approaches in BMS: the processor architecture, the set of available measurements, and the accessibility of the battery cell parameters. The combined impact of these constraints drives the development toward models with a limited number of states and low computational complexity (Berger et al., 2024).

4.1 Processor limitations and real-time execution

The embedded processing units in the BMS operate with a limited number of processing cycles and low power consumption. The calculations are performed at sampling rates between 1 and 10 kHz (Barsoukov & Macdonald, 2018), allowing sub-millisecond intervals to complete all the functions. PBMs comprise nonlinear differential equations that describe the transport, diffusion, and kinetic processes occurring at the electrodes and in the electrolyte (Lucaferri et al., 2023). Solving such equations requires iterative numerical methods, spatial discretization of distributed systems, and stable integration schemes, which increases the computational complexity of these models significantly compared to ECMs. Resultantly, ECMs allow for deterministic execution times and fewer arithmetic operations, making them more suitable for real-time BMS algorithms (Shen & Gao, 2019).

4.2 Limited sensors and the unavailability of parameters

BMSs have a limited set of measurements, such as cell voltage, current, and temperature. PBMs require information on electrode topology and material parameters, including the diffusion coefficients, kinetic constants, electrolyte transport properties, and maximum concentrations in the active materials, as well as the geometric parameters and electrode porosities. These data are not part of commercial data sheets, and experimental determination requires specialized equipment or destructive procedures (Balasingam et al., 2020). These parameters are determined most credibly using detailed analytical methods, such as microscopy, measurements of the open circuit potentials of electro materials… In-situ determination requires observable structures with a large number of states, which increases the sensitivity to errors, nonlinearity, and computational burden (Balasingam et al., 2020).

ECMs enable the identification of parameters from voltage, current, and impedance measurements, which are feasible under industrial conditions and do not require access to material data (Belmajdoub et al., 2024).

4.3 Industry consistency, safety requirements, and certification

The modeling approaches used in BMS must comply with Standards such as IEC, UL, ISO, and SAE. The Standards require deterministic responses, explainable deviations, repeatable diagnostic results, and numerical stability (Berger et al., 2024). PBMs exhibit a wide range of dynamics, due to their sensitivity to parameters and the variability of responses under different operating conditions, which increases the complexity of the validation. A comprehensive validation process is often beyond the capabilities of an industrial environment, due primarily to the large number of parameters and the need to validate across various operating scenarios (Balasingam et al., 2020; Lucaferri et al., 2023; Xu et al., 2024).

ECMs allow validation in a smaller number of test scenarios and have stable numerical properties. Due to their simpler verification and shorter certification time, they are suitable for environments where compliance with Standards and the predictability of performance meet the requirements for model accuracy (Shen & Gao, 2019; Berger et al., 2024).

4.4 Model-informed SoX estimation

Different battery models offer access to internal states with varying depth and fidelity, which determines the achievable accuracy and robustness of SoX estimators directly. Modern BMS implementations use a combination of sensing, data-driven, and physics-based approaches for state estimation and diagnostics (Rahmani et al., 2025). Simple ECMs offer a compact representation suitable for real-time SoC estimation; however, their empirical structure limits the identifiability of the transport and kinetic processes (Rahmani et al., 2025). PC-ECM, by preserving the spatial structure of the electrochemical transport, enables a more transparent mapping between the impedance features, time constants, and underlying mechanisms, supporting more reliable SoH and SoE estimation and physics-informed virtual sensing. High-fidelity PBMs (e.g., P2D) provide the richest set of internal variables, and are deployed increasingly as cloud-level digital twins for supervisory SoH and RUL estimation (Rahmani et al., 2025; Nguyen Van & Quang, 2023; Li et al., 2021). Together, these model families establish a hierarchy of achievable SoX capabilities, forming the basis for next-generation physics-enhanced BMS diagnostics (Rahmani et al., 2025).

5 Electrochemical impedance spectroscopy as an approach for connecting model structures

Electrochemical impedance spectroscopy (EIS) enables the measurement of complex impedance over a wide frequency range, revealing the dynamics arising from the ohmic, kinetic, and diffusion mechanisms. The frequency resolution of the processes allows the method to be used for model validation and for the synthesis of structures by ECM (Barsoukov & Macdonald, 2018; Orazem & Tribollet, 2017). The EIS data serve as the basis for identifying the transport properties, estimating time constants, and characterizing the degradation phenomena under various operating conditions (Belmajdoub et al., 2024; Andre et al., 2011).

5.1 Basic concept of electrochemical impedance spectroscopy

The method is based on the linear response of a cell to a small-amplitude sinusoidal excitation. Complex impedance

$$Z(j\omega) = Re[Z(j\omega)] + Im[Z(j\omega)], \tag{9}$$

describes the contributions of the resistive, capacitive, and diffusion processes. The interpretation of the spectrum is based on the separation of the frequency ranges, which is the fundamental starting point of electrochemical analysis (Barsoukov & Macdonald, 2018). The high-frequency part of the spectrum contains contributions from electrolyte conductivity and contact resistance. The mid-frequency part reflects the charge-transfer kinetics and double-layer response, while the low-frequency part reveals the diffusion mechanisms (Choi et al., 2020). This separation enables a comparison of the ECM paradigm with the physical parameters that are integral to PBMs (Sovljanski et al., 2025; Andre et al., 2011).

5.2 Connecting EIS, ECM, and PBMs

EIS provides an information link between the descriptive nature of the ECM and the physical design of PBMs. The electrochemical structures determine the spectral properties through diffusion coefficients, kinetic parameters, and electrolyte transport properties, which can be observed in the form of semicircular responses, Warburg impedance slopes, and characteristic high-frequency resistive segments (Barsoukov & Macdonald, 2018; Orazem & Tribollet, 2017).

The ECM parameters describe the aggregated effects of the same processes, but without a mapping operator that would relate the parameters to the physical properties directly (Andre et al., 2011). The frequency data allow the identification of the characteristic time constants, enabling a partial correspondence between the two model representations. Such an approach supports the development of model structures that combine the computational efficiency of the ECM with an aim to the information richness of PBMs (Geng et al., 2021; Belmajdoub et al., 2024).

5.3 Integrated EIS solutions for use in BMS

Embedded diagnostic platforms incorporate integrated circuits that enable EIS measurements during battery operation (Cicioni et al., 2023; Analog Devices, 2020). The integrated systems combine current injection blocks, precision voltage measurement circuits, and digital signal processors, enabling the generation of excitation signals and the calculation of real-time complex impedance. Such architectures reduce the need for external function generators and extensive analog filters (Xu et al., 2024).

The measurements are performed at low amplitudes, so they do not impact the cell's operation significantly. The typical frequency range spans from a few mHz to several tens of kHz, enabling the identification of resistive, kinetic, and diffusion processes. Integrated digital functions enable noise filtering and compensation for parasitic elements in the conductors (Belmajdoub et al., 2024). Such an approach opens the possibility of using EIS as a diagnostic tool for embedded BMS systems, where frequency information complements the ECM parameters, thereby enabling more reliable monitoring of the degradation processes (Xu et al., 2022; Xu et al., 2024).

6 Methodology for obtaining impedance data

The methodology provides a data basis for EIS-supported parametric synthesis of ECM structures and for the identification of the transport and kinetic properties. The impedance response of a lithium-ion cell depends on the temperature, state of charge, current history, and degradation rate. Therefore, the measurements must be designed to ensure repeatability, traceability, and data stability over the entire frequency range (Barsoukov & Macdonald, 2018; Meddings et al., 2020). Reliable data are a prerequisite for procedures that relate frequency characteristics to ECM parameters and LPV expansion, allowing the identification of time constants sensitive to the operating conditions (Belmajdoub et al., 2024).

The experimental framework comprises three interrelated components: measurement system design, calibration procedures, and data acquisition protocols in both laboratory and industrial environments. The consistency of these components determines the quality of the frequency information used in subsequent modeling.

6.1 Measurement system for impedance data acquisition

The measurement system must be capable of generating sinusoidal signals or pseudo-random excitations and measuring current and voltage simultaneously with the required resolution. Accuracy in the high-frequency range depends on controlling the parasitic wiring components, while low-frequency measurements require a stable measurement system and limiting the effects of temperature drift (Barsoukov & Macdonald, 2018). Amplifier blocks, reference sources, and isolation elements are standard building blocks that enable reliable data acquisition over an extended frequency range (Sovljanski et al., 2025).

EIS acquisition during battery cell operation requires amplitude-limited excitation to avoid influencing the voltage-stoichiometric state and thus the measurements. In industrial applications, the range of measurable quantities is limited, which requires the use of compact, energy-efficient, and BMS-compatible measurement modules. Embedded EIS platforms enable real-time measurements and complement standard diagnostics without the need for bulky external instruments (Mathivanan et al., 2025; Xu et al., 2024).

6.2 Calibration, verification, and quality assurance of measurements

The calibration of a measurement system determines the accuracy of the impedance data, and, thus, the reliability of further parameter identification. The procedures include the use of reference resistors, capacitances, and parallel combinations of elements, which allows verification of the linear response, phase accuracy, and amplitude stability over the entire frequency range (Barsoukov & Macdonald, 2018; Da Silva et al., 2024).

The reliability of the measurements is verified by repeating them at different temperatures, state-of-charge levels, and after selected loading sequences. This approach reveals the measurement system's variability and the influence of environmental conditions, enabling the identification of areas suitable for parametric synthesis and LPV identification. Special attention is paid to the low-frequency range, where the measurement time increases and the meter's stability becomes a limiting factor (Meddings et al., 2020; Sovljanski et al., 2025; Belmajdoub et al., 2024).

Impedance measurements performed at multiple state-of-charge levels improve the interpretability of frequency-dependent parameters further, and support the identification of SoC-dependent trends in ECM parameters (Wu et al., 2023).

6.3 Data acquisition under industrial conditions

Impedance data acquisition in an industrial environment requires adaptations that enable measurements under real operating conditions and with limited sensor resources. Frequency analyses are time-limited, so multifrequency excitations or pseudo-random signals are used when continuous sinusoidal excitations are not feasible (Mathivanan et al., 2025).

Environmental influences, temperature gradients, and dynamic load changes require additional procedures to filter out disturbances and verify the consistency of multiple consecutive measurements. The data obtained under these conditions allow for modeling that reflects operating conditions better, and therefore meets the diagnostic requirements in BMS systems better. Industrially oriented protocols thus contribute to the development of ECM structures and LPV models that are validated under conditions comparable to real-world applications.

7 Discussion and conclusions

The research examined the role of EIS in battery modeling for industrial BMS, with a focus on the conceptual and practical distinction between ECMs and PBMs. The analysis confirms that the discrepancy between these modeling paradigms is structural rather than parametric: ECM parameters capture the aggregated effects of multiple physical mechanisms, whereas PBMs describe the distributed transport and kinetic processes that cannot be mapped uniquely to low-order circuit elements. EIS does not eliminate this discrepancy, nor does it provide a direct mapping between the phenomenological and physical model parameters. Its primary contribution lies in offering frequency-resolved information that enables partial separation of the ohmic, kinetic, and diffusion-related dynamics, which are otherwise entangled in the time-domain responses. Integrating selected parts of the impedance spectrum into identification procedures enhances the precision with which the internal process contributions are separated. It enhances the diagnostic value of model structures, paving the way for advanced models with frequency-supported parameters (Sovljanski et al., 2025; Belmajdoub et al., 2024; Xu et al., 2024).

The effectiveness of the methodology depends on the reliability of the measurements, the repeatability of the EIS data, and the robustness of the measurement protocols. The industrial environment requires specially adapted procedures, due to limited sensors, interference, and time constraints. The advanced approaches can improve the assessment of SoC, SoH, and SoP significantly, as well as degradation mechanisms, but require well-defined parametric dependencies and validation across a wide range of operating conditions (Nguyen Van & Quang, 2023; Li et al., 2021).

The research efforts are focused on identifying the frequency ranges with the most significant diagnostic value, developing methods for processing EIS data under disturbances and temperature gradients, and designing models compatible with the processing limitations of BMS. By incorporating frequency information into linear model structures, the possibility of developing robust and computationally efficient models that capture the electrochemical dynamics of cells better is enhanced. EIS thus represents a relevant opportunity for further advancements in battery system modeling, and an essential step towards more advanced BMSs.

References

Larcher, D., & Tarascon, J.-M. (2015). Towards greener and more sustainable batteries for electrical energy storage. *Nature Chemistry*, *7*(1), 19–29. https://doi.org/10.1038/nchem.2085

Shen, M., & Gao, Q. (2019). A review on battery management system from the modeling efforts to its multiapplication and integration. *International Journal of Energy Research*, *43*(10), 5042–5075. https://doi.org/10.1002/er.4433

Xu, N., Xie, Y., Liu, Q., Yue, F., & Zhao, D. (2022). A Data-Driven Approach to State of Health Estimation and Prediction for a Lithium-Ion Battery Pack of Electric Buses Based on Real-World Data. *Sensors*, *22*(15), Article 5762. https://doi.org/10.3390/s22155762

Balasingam, B., Ahmed, M., & Pattipati, K. (2020). Battery Management Systems–Challenges and Some Solutions. *Energies*, *13*(11), Article 2825. https://doi.org/10.3390/en13112825

Shepherd, C. M. (1965). Design of Primary and Secondary Cells. *Journal of The Electrochemical Society*, *112*(7), 657. https://doi.org/10.1149/1.2423659

Doyle, M., Fuller, T. F., & Newman, J. (1993). Modeling of Galvanostatic Charge and Discharge of the Lithium/Polymer/Insertion Cell. *Journal of The Electrochemical Society*, *140*(6), 1526–1533. https://doi.org/10.1149/1.2221597

Mele, I., Pačnik, I., Zelič, K., Moškon, J., & Katrašnik, T. (2020). Advanced Porous Electrode Modelling Framework Based on More Consistent Virtual Representation of the Electrode Topology. *Journal of The Electrochemical Society*, *167*(6), Article 060531. https://doi.org/10.1149/1945-7111/ab84fb

Mele, I., Zelič, K., Firm, M., Moškon, J., Gaberšček, M., & Katrašnik, T. (2024). Enhanced Porous Electrode Theory Based Electrochemical Model for Higher Fidelity Modelling and Deciphering of the EIS Spectra. *Journal of The Electrochemical Society*, *171*(8), Article 080537. https://doi.org/10.1149/1945-7111/ad6eb9

Newman, J., & Thomas-Alyea, K. E. (2004). *Electrochemical systems* (3rd ed.). John Wiley & Sons.

Brosa Planella, F., Ai, W., Boyce, A. M., Ghosh, A., Korotkin, I., Sahu, S., Sulzer, V., Timms, R., Tranter, T. G., Zyskin, M., Cooper, S. J., Edge, J. S., Foster, J. M., Marinescu, M., Wu, B., & Richardson, G. (2022). A Continuum of Physics-Based Lithium-Ion Battery Models Reviewed. *Progress in Energy*, *4*(4), Article 042003. https://doi.org/10.1088/2516-1083/ac7d31

Al-Zubaidi R-Smith, N., Leitner, M., Alic, I., Toth, D., Kasper, M., Romio, M., Surace, Y., Jahn, M., Kienberger, F., Ebner, A., & Gramse, G. (2021). Assessment of lithium ion battery ageing by combined impedance spectroscopy, functional microscopy and finite element modelling. *Journal of Power Sources*, *512*, Article 230459. https://doi.org/10.1016/j.jpowsour.2021.230459

Katrašnik, T., Mele, I., & Zelič, K. (2021). Multi-scale modelling of Lithium-ion batteries: From transport phenomena to the outbreak of thermal runaway. *Energy Conversion and Management*, *236*, Article 114036. https://doi.org/10.1016/j.enconman.2021.114036

Zelič, K., Katrašnik, T., & Gaberšček, M. (2021). Derivation of Transmission Line Model from the Concentrated Solution Theory (CST) for Porous Electrodes. *Journal of The Electrochemical Society*, *168*(7), Article 070543. https://doi.org/10.1149/1945-7111/ac1314

Tibaut, T., Zelič, K., & Katrašnik, T. (2024). Transmission Line Model of Intercalation Electrode Particle in Lithium-Ion Batteries. *Journal of The Electrochemical Society*, *171*(2), Article 020515. https://doi.org/10.1149/1945-7111/ad24c4

Berger, F., Jöst, D., Barbers, E., Quade, K., Wu, Z., Sauer, D. U., & Dechent, P. (2024). Benchmarking battery management system algorithms - Requirements, scenarios and validation for automotive applications. *eTransportation*, *22*, Article 100355. https://doi.org/10.1016/j.etran.2024.100355

Lucaferri, V., Quercio, M., Laudani, A., & Riganti Fulginei, F. (2023). A Review on Battery Model-Based and Data-Driven Methods for Battery Management Systems. *Energies*, *16*(23), Article 7807. https://doi.org/10.3390/en16237807

Rahmani, P., Chakraborty, S., Mele, I., Katrašnik, T., Bernhard, S., Pruefling, S., Wilkins, S., & Hegazy, O. T. M. (2025). Driving the future: A comprehensive review of automotive battery management system technologies, and future trends. *Journal of Power Sources*, *629*, Article 235827. https://doi.org/10.1016/j.jpowsour.2024.235827

Lagnoni, M., Scarpelli, C., Lutzemberger, G., & Bertei, A. (2024). Critical comparison of equivalent circuit and physics-based models for lithium-ion batteries: A graphite/lithium-iron-phosphate case study. *Journal of Energy Storage*, *94*, Article 112326. https://doi.org/10.1016/j.est.2024.112326

Geng, Z., Wang, S., Lacey, M. J., Brandell, D., & Thiringer, T. (2021). Bridging physics-based and equivalent circuit models for lithium-ion batteries. *Electrochimica Acta*, *372*, Article 137829. https://doi.org/10.1016/j.electacta.2021.137829

Barsoukov, E., & Macdonald, J. R. (Eds.). (2018). *Impedance spectroscopy: Theory, experiment, and applications* (3rd ed.). John Wiley & Sons.

Orazem, M. E., & Tribollet, B. (2017). *Electrochemical impedance spectroscopy* (2nd ed.). Springer.

Meddings, N., Heinrich, M., Overney, F., Lee, J.-S., Ruiz, V., Napolitano, E., Seitz, S., Hinds, G., Raccichini, R., Gaberšček, M., & Park, J. (2020). Application of electrochemical impedance spectroscopy to commercial Li-ion cells: A review. *Journal of Power Sources*, *480*, Article 228742. https://doi.org/10.1016/j.jpowsour.2020.228742

Sovljanski, V., Paolone, M., Tant, S., & Sainflou, D. P. (2025). Optimizing Experiments for Accurate Battery Circuit Parameters Estimation: Reduction and Adjustment of Frequency Set Used in Electrochemical Impedance Spectroscopy. arXiv:2501.06112. https://doi.org/10.48550/arXiv.2501.06112

Mathivanan, S., Venkatesan, K., & Haribabu, P. (2025). Electrochemical Impedance Spectroscopy as a Diagnostic and Prognostic Tool for EV Batteries: A Review. *Journal of Electrochemical Science and Technology*, *16*(3), 267–286. https://doi.org/10.33961/jecst.2024.01060

Belmajdoub, N., Lajouad, R., El Magri, A., Boudoudouh, S., & Zaggaf, M. H. (2024). Review of battery models and experimental parameter identification for lithium-ion battery equivalent circuit models. *Indonesian Journal of Electrical Engineering and Computer Science*, *33*(3), 1336–1346. https://doi.org/10.11591/ijeecs.v33.i3.pp1336-1346

Andre, D., Meiler, M., Steiner, K., Wimmer, Ch., Soczka-Guth, T., & Sauer, D. U. (2011). Characterization of high-power lithium-ion batteries by electrochemical impedance spectroscopy. I. Experimental investigation. *Journal of Power Sources*, *196*(12), 5334–5341. https://doi.org/10.1016/j.jpowsour.2010.12.102

Da Silva, G. M. G., Faia, P. M., Mendes, S. R., & Araújo, E. S. (2024). A Review of Impedance Spectroscopy Technique: Applications, Modelling, and Case Study of Relative Humidity Sensors Development. *Applied Sciences*, *14*(13), Article 5754. https://doi.org/10.3390/app14135754

Xu, Y., Ge, X., Guo, R., & Shen, W. (2024). Recent Advances in Model-Based Fault Diagnosis for Lithium-Ion Batteries: A Comprehensive Review. arXiv:2401.16682. https://doi.org/10.48550/arXiv.2401.16682

Tran, M.-K., DaCosta, A., Mevawalla, A., Panchal, S., & Fowler, M. (2021). Comparative Study of Equivalent Circuit Models Performance in Four Common Lithium-Ion Batteries: LFP, NMC, LMO, NCA. *Batteries*, *7*(3), Article 51. https://doi.org/10.3390/batteries7030051

Pandey, S. V., Parikh, N., Prochowicz, D., Akin, S., Satapathi, S., Tavakoli, M. M., Kalam, A., & Yadav, P. (2023). Predicting the state parameters of lithium ion batteries: The race between filter-based and data driven approaches. *Sustainable Energy & Fuels*, *7*(3), 598–628. https://doi.org/10.1039/D2SE01209J

Chapman, S. J., Please, C. P., Marquis, S. G., Sulzer, V., & Timms, R. (2019). An asymptotic derivation of a single particle model with electrolyte. *Journal of The Electrochemical Society*, *166*(15), A3693–A3706. https://doi.org/10.1149/2.0341915jes

Von Srbik, M.-T., Marinescu, M., Martinez-Botas, R. F., & Offer, G. J. (2016). A physically meaningful equivalent circuit network model of a lithium-ion battery accounting for local electrochemical and thermal behaviour, variable double layer capacitance and degradation. *Journal of Power Sources*, *325*, 171–184. https://doi.org/10.1016/j.jpowsour.2016.05.051

Scipioni, R., Jørgensen, P. S., Graves, C., Hjelm, J., & Jensen, S. H. (2017). A Physically-Based Equivalent Circuit Model for the Impedance of a LiFePO4/Graphite 26650 Cylindrical Cell. *Journal of The Electrochemical Society*, *164*(9), A2017–A2030. https://doi.org/10.1149/2.1071709jes

Choi, W., Shin, H.-C., Kim, J. M., Choi, J.-Y., & Yoon, W.-S. (2020). Modeling and Applications of Electrochemical Impedance Spectroscopy (EIS) for Lithium-ion Batteries. *Journal of Electrochemical Science and Technology*, *11*(1), 1–13. https://doi.org/10.33961/jecst.2019.00528

Ali, H. A. A., Raijmakers, L. H. J., Chayambuka, K., Danilov, D. L., Notten, P. H. L., & Eichel, R.-A. (2024). A comparison between physics-based Li-ion battery models. *Electrochimica Acta*, *493*, Article 144360. https://doi.org/10.1016/j.electacta.2024.144360

Lazanas, A. Ch., & Prodromidis, M. I. (2023). Electrochemical Impedance Spectroscopy–A Tutorial. *ACS Measurement Science Au*, *3*(3), 162–193. https://doi.org/10.1021/acsmeasuresciau.2c00070

Drummond, R., & Duncan, S. R. (2019). Observer design for the Doyle–Fuller–Newman Li-ion battery model without electrolyte dynamics. *Journal of Energy Storage*, *23*, 250–257. https://doi.org/10.1016/j.est.2019.02.012

Nguyen Van, C., & Quang, D. T. (2023). State of charge estimation for Lithium-Ion battery cell considering the influence of aging parameters and operating temperature. *International Journal of Electrochemical Science*, *18*(12), Article 100379. https://doi.org/10.1016/j.ijoes.2023.100379

Li, M., Zhang, Y., Hu, Z., Zhang, Y., & Zhang, J. (2021). A Battery SOC Estimation Method Based on AFFRLS-EKF. *Sensors*, *21*(17), Article 5698. https://doi.org/10.3390/s21175698

Cicioni, G., De Angelis, A., Janeiro, F. M., Ramos, P. M., & Carbone, P. (2023). Battery Impedance Spectroscopy Embedded Measurement System. *Batteries*, *9*(12), Article 577. https://doi.org/10.3390/batteries9120577

Analog Devices (2020). CN-0510: Electrochemical Impedance Spectroscopy (EIS) Measurement System for Characterizing Lithium-Ion and Other Batteries. *Analog Devices*. https://www.analog.com/media/en/reference-design-documentation/reference-designs/cn0510.pdf

Wu, Y., Sundaresan, S., & Balasingam, B. (2023). Battery Parameter Analysis through Electrochemical Impedance Spectroscopy at Different State of Charge Levels. *Journal of Low Power Electronics and Applications*, *13*(2), Article 29. https://doi.org/10.3390/jlpea13020029

Povzetek v slovenskem jeziku

Ocena potenciala elektrokemijske impedančne spektroskopije kot podpornega orodja pri modeliranju z nadomestnimi vezji v sistemih za upravljanje baterij. Sistemi za upravljanje litij-ionskih baterij (BMS) temeljijo na modelih, ki povezujejo merljive električne količine z notranjim stanjem baterijske celice. Zaradi omejene procesne moči, omejenega nabora tipal in zahtev po determinističnem delovanju se v industrijski praksi večinoma uporabljajo električni nadomestni modeli (ECM), ki opisujejo napetostno-tokovni odziv z združenimi parametri (Larcher & Tarascon, 2015; Shen & Gao, 2019). Uporaba ECM omogoča implementacijo v realnem času, vendar le omejeno interpretacijo notranjih elektrokemijskih procesov in degradacijskih pojavov. Fizikalno utemeljeni modeli (PBM) temeljijo na opisih difuzije, prenosa naboja in reakcijske kinetike ter omogočajo neposredno obravnavo notranjih stanj, vendar numerična zahtevnost in zapletena identifikacija parametrov omejujeta uporabo v industrijskih sistemih. Članek obravnava vlogo elektrokemične impedančne spektroskopije (EIS) kot vira frekvenčno ločenih informacij o procesih v baterijski celici. Poudarek je na analizi informacij, ki jih je mogoče iz impedančnih meritev prenesti v strukturo in 107arameter ECM, ter na omejitvah, povezanih s trajanjem meritev, šumom in temperaturnimi nehomogenostmi. Obravnavani so tudi pristopi k razvoju hibridnih modelov, ki združujejo časovno in frekvenčno domeno ter so združljivi z omejitvami industrijskih BMS. Članek prispeva k razumevanju možnosti in omejitev uporabe EIS pri modeliranju baterijskih sistemov v realnih obratovalnih pogojih.

gen-i

PAMETNA ENERGIJA

Prihodnost je zelena, ustvarjamo jo skupaj

University of Maribor

Faculty of Energy Technology

https://journals.um.si/index.php/jet

jet@um.si

ISSN 2463-7815

JET